Quantification of glucose turnover and Cori cycling in AGTL-knockout mice by [U-$^{13}C_6$]glucose infusion and LC-MS/MS analysis of glucose ^{13}C-isotopomers

M.ª Margarida S. Coelho

2013

DEPARTAMENTO DE CIÊNCIAS DA VIDA

FACULDADE DE CIÊNCIAS E TECNOLOGIA
UNIVERSIDADE DE COIMBRA

Quantification of glucose turnover and Cori cycling in AGTL-knockout mice by [U-$^{13}C_6$]glucose infusion and LC-MS/MS analysis of glucose ^{13}C-isotopomers

Maria Margarida Serra Coelho

2013

DEPARTAMENTO DE CIÊNCIAS DA VIDA

FACULDADE DE CIÊNCIAS E TECNOLOGIA
UNIVERSIDADE DE COIMBRA

Quantification of glucose turnover and Cori cycling in ATGL-knockout mice by [U-$^{13}C_6$]glucose infusion and LC-MS/MS analysis of glucose ^{13}C-isotopomers

Dissertação apresentada à Universidade de Coimbra para cumprimento dos requisitos necessários à obtenção do grau de Mestre em Bioquímica, realizada sob a orientação científica do Professor Doutor Bruno Manadas (Centro de Neurociências e Biologia Celular, Universidade de Coimbra e Biocant) e do Professor Doutor Ângelo Tomé (Departamento de Ciências da Vida, Universidade de Coimbra)

Maria Margarida Serra Coelho

2013

TABLE OF CONTENTS

ACKNOLEDGEMENTS /AGRADECIMENTOS

First of all, I would like to thank Dr. John Jones, for introducing me into a research area I did not thought I would like as much as I do now. By its ideas and encouragement I have discovered a field that I really enjoy working on, and that makes me work harder every day. Em segundo lugar, gostaria de agradecer também ao Dr. Bruno Manadas por tudo o que aprendi, por exigir mais de mim, por poder fazer parte da sua equipa, mas acima de tudo por me ensinar a acreditar em mim e a valorizar-me. Um agradecimento sincero ainda ao Dr. Ângelo Tomé por possibilitar a realização desta tese e pela disponibilidade e compreensão. Gostaria ainda de agradecer à Vera Mendes pela paciência, pelos conselhos, pela confiança depositada em mim, pelas longas horas que dedicou a ensinar-me e por me ter acompanhado ao longo deste ano. Não poderia deixar de agradecer também à Alexandra Gonçalves, por me ter incentivado em todos os passos da minha tese, por ter passado infinidades de volta de fórmulas no Excel, por esclarecer todas as minhas dúvidas, por me ter ensinado sem rodeios tudo o que podia, mas acima de tudo por ser uma grande amiga.

Gostaria de agradecer também à Universidade de Maastricht (Holanda) e à Universidade de Graz (Áustria) (Dr. Rudolf Zechner), por terem fornecido as amostras dos ratinhos *wild-type* e $ATGL^{-/-}$, à Patrícia Nunes pela infusão dos animais e recolha das amostras, bem como à Dr. Margarida Carneiro (Universidade de Coimbra) que disponibilizou os ratinhos da estirpe B10.Q, usados na validação do método analítico.

Deixo a minha gratidão a todos os colegas e funcionários do Biocant, em particular, aos colegas da Unidade de Proteómica e Metabolómica, como a Joana Pinto, que tanto me aturou ao longo deste ano, por mais insuportável que eu estivesse; como a Sandra Anjo, a Cátia Santa e a Matilde Melo que sempre se preocuparam com o meu trabalho e mostraram vontade em ajudar, mesmo que nem soubessem o que lhes esperava; como a Liliana Loureiro, por aguentar as altas temperaturas do meu computador, e todos os papéis que eu espalho em cima do computador dela e a Lúcia Sabala pela amizade e boa disposição nas escapatórias para almoçar.

Gostaria de agradecer também a todos os meus amigos e familiares, que me apoiaram e que, mesmo por breves momentos, me fizeram esquecer o trabalho. Em especial à Teresa Lino e à Mafalda Costa, por serem a companhia de todo o meu percurso académico, por nunca terem deixado de estar ao meu lado, mesmo nos momentos mais difíceis. E por último, aos meus pais, sem os quais eu não seria a pessoa em que me tornei. Por me terem ajudado a crescer, por

terem aceitado e compreendido todas as minhas escolhas e pela confiança que depositam em mim. Obrigada à minha irmã e sobrinhos maravilhosos, por me darem todo o vosso amor.

Projecto executado mediante o financiamento dos projectos, PTDC/SAU-MET/11198/2009, PEst-C/SAU/LA0001/2013-2014 e RNEM (REDE/1506/REM/2005).

ABBREVIATIONS

α	Probability
%CV	Percentage of the Coefficient of Variation of the Mean
%RE	Percentage of Relative Error
^{12}C	Carbon 12
^{13}C	Carbon 13
$^{2}H_2O$	Deuterated Water
Akt/PKB	Protein Kinase B
APCI	Atmospheric-Pressure Chemical Ionization
ATGL	Adipose Triacylglyceride Lipase
$ATGL^{-/-}$	ATGL Knock-Out
ATP	Adenosine Triphosphate
cAMP	Cyclic Adenosine Monophosphate
CE	Collision Energy
CGI-58	Comparative Gene Identification - 58
CID	Collision-Induced Dissociation
CO_2	Carbon Dioxide
DAG	Diacylglycerol
DBS	Dry Blood Spot
EGP	Endogenous Glucose Production
ESI	Electrospray Ionization
EtOH	Ethanol
FA	Fatty Acid
FFA	Free Fatty Acid
G6P	Glucose-6-Phosphate
GC	Gas Chromatography
GC-MS	Gas Chromatography Coupled to Mass Spectrometry
GK	Glucokinase
GSK-3	Glycogen Synthase Kinase-3
H_2O	Water
HK	Hexokinase
HPLC	High Pressure Liquid Chromatography

HSL	Hormone Sensitive Lipase
$HSL^{-/-}$	HSL Knock-Out
IMTG	Intramyocellular Triglycerides
IRS	Insulin Receptor Substrate
IS	Internal Standard
Km	Michaelis Constant
KO	Knock-Out
LC	Liquid Chromatography
LC-MS	Liquid Chromatography Coupled To Mass Spectrometry
LC-MS/MS	Liquid Chromatography Coupled to Tandem Mass Spectrometry
LOD	Limit of Detection
LOQ	Limit of Quantification
m/z	Mass to Charge Ratio
MRM	Multiple Reaction Monitoring
mRNA	Messenger RNA
MS	Mass Spectrometry
MS/MS	Tandem Mass Spectrometry
NAD^+	Oxidized Nicotinamide Adenine Dinucleotide
NADH	Reduced Nicotinamide Adenine Dinucleotide
NMR	Nuclear Magnetic Resonance
O_2	Oxygen
PDH	Pyruvate Dehydrogenase
PDK	Pyruvate Dehydrogenase Kinase
PDK-1	Phosphoinositide Dependent Protein Kinase-1
PEDF	Pigment Epithelium-Derived Factor
PI3K	Phosphatidylinositol-3 Kinase
PIP_3	Phosphatidylinositol-3,4,5-Triphosphate
PKA	Protein Kinase A
PPAR	Peroxisome Proliferator Activated Receptor
Q1	First Quadrupole
q2	Second Quadrupole (Collision Cell)
Q3	Third Quadrupole
QC	Quality Control

R	Correlation Coefficient
R^2	Coefficient of Determination
Rd	Rate of Disposal
Ra	Rate of Appearance
RT	Retention Time
S/N	Signal-To-Noise Ratio
SD	Standard Deviation
SPE	Solid Phase Extraction
T2DM	Type II *Diabetes mellitus*
TAG	Triacylglycerol
WADA	World Anti-Doping Agency
WAT	White Adipose Tissue
WT	Wild-Type

SUMMARY

The pathophysiology of metabolic diseases such as type II *diabetes mellitus* (T2DM) is characterized by a loss of synchrony between triacylglycerols (TAG) synthesis and catabolism. The adipose triacylglyceride lipase (ATGL), an enzyme involved in TAGs hydrolysis, has been the target of several studies in order to understand its role in insulin resistance. The reason for this increasing interest is the fact that ATGL knock-outs ($ATGL^{-/-}$) have demonstrated to be more insulin sensitive and glucose tolerant in comparison to wild-types. Even though they do not resort to stored fatty acids (FAs) as energy fuel, these characteristics make $ATGL^{-/-}$ mice a unique model for the better understanding of the relationship between TAGs metabolism and insulin resistance.

The rate of glucose turnover and recycling via the Cori cycle is highly susceptible to both insulin sensitivity and nutrient availability. Under normal fasting conditions, the majority of glucose is recycled via the Cori cycle. However, in the case of $ATGL^{-/-}$ mice, since they are more dependent on glucose, it was hypothesized that these mice would be more dependent on endogenous glucose production (EGP) to meet this demand and that glucose would be disposed mainly through oxidation, resulting in less recycling via the Cori cycle.

To study this hypothesis, glucose enrichments from $ATGL^{-/-}$ mice and wild-type mice, infused with [U-$^{13}C_6$]glucose, were quantified by liquid chromatography coupled to tandem mass spectrometry (LC-MS/MS) analysis of dried blood spots (DBS). After method development and validation, the quantification of the parent [U-$^{13}C_6$]glucose enrichment allowed the determination of the rate of EGP, while the quantification of the partially labelled isotopomers [1,2-$^{13}C_2$]glucose and [1,2,3-$^{13}C_3$]glucose, provided a measure of the Cori cycle.

Analysis of EGP and Cori cycle metabolism between $ATGL^{-/-}$ and wild-type mice revealed that EGP rates tended to be lower for $ATGL^{-/-}$ mice compared to wild-types and that the Cori cycle contributed quantitatively to EGP in both groups. Therefore, these data do not support the hypothesis of higher glucose oxidation and reduced Cori cycling in $ATGL^{-/-}$ mice.

Key-words: ATGL; Glucose isotopomers; Gluconeogenesis; Cori cycle; Validation of analytical methods.

RESUMO

A patofisiologia de doenças metabólicas como a *diabetes mellitus* tipo II (T2DM) é caracterizada pela perda de sincronia entre a síntese e catabolismo de triacilgliceróis (TAG). A lipase adiposa de triacilglicerídeos (ATGL), uma enzima envolvida na hidrólise de TAGs, tem sido alvo de vários estudos de forma a compreender o seu papel na resistência à insulina. A razão para este aumento de interesse é o fato de os ATGL *knock-outs* ($ATGL^{-/-}$) terem demonstrado maior sensibilidade à insulina e tolerancia à glucose em comparação com ratinhos sem a delecção (WT). Apesar de eles não recorrerem a ácidos gordos armazenados como fonte de energia, estas características fazem dos ratinhos $ATGL^{-/-}$ um modelo único para a melhor compreensão da relação entre o metabolismo de TAGs e a resistência à insulina.

A taxa do turnover de glucose e reciclagem pelo ciclo de Cori é altamente suscetível tanto à sensibilidade a insulina como à disponibilidade de nutrientes. Sob condições normais de jejum, a maioria da glucose é reciclada pelo ciclo de Cori. No entanto, a maior dependência de glucose por parte dos ratinhos $ATGL^{-/-}$, levou-nos a colocar a hipótese de que estes ratinhos seriam mais dependentes da produção de glucose endógena (EGP) para fazer face a esta necessidade e que a glucose seria eliminada principalmente através da oxidação, resultando em menor reciclagem através do ciclo de Cori.

Para estudar esta hipótese, os enriquecimentos de glucose de ratinhos $ATGL^{-/-}$ e WT, infundidos com [U-$^{13}C_6$]glucose, foram quantificados por análise de gotas de sangue (DBS) por cromatografia líquida acoplada à espectrometria de massa (LC-MS/MS). Após o desenvolvimento e validação do método, a quantificação do enriquecimento da [U-$^{13}C_6$]glucose precursora permitiu a determinação da taxa de EGP, enquanto a quantificação dos isotopómeros parcialmente marcados [1,2-$^{13}C_2$]glucose e [1,2,3-$^{13}C_3$]glucose, forneceram uma avaliação do ciclo de Cori.

A análise da EGP e do metabolismo do ciclo de Cori entre ratinhos $ATGL^{-/-}$ e *wild-type*, revelou que as taxas de EGP eram tendencialmente mais baixas para ratinhos $ATGL^{-/-}$, quando comparados com ratinhos *wild-type* e que o ciclo de Cori contribuía quantitativamente para a EGP em ambos os grupos. Assim, estes dados não confirmam a hipótese de maior oxidação de glucose e ciclo de Cori reduzido em ratinhos $ATGL^{-/-}$.

Palavras-chave: ATGL; Isotopómeros de glucose; Gluconeogénese; Ciclo de Cori; Validação de métodos analíticos.

1. INTRODUCTION

1. INTRODUCTION

1.1. Diabetes mellitus

According to the World Health Organization (WHO), by the year 2025, there will be approximately 300 million individuals affected by type II *diabetes mellitus* (T2DM) worldwide, with the highest incidence in developed countries [1]. This increase in the incidence of T2DM is directly related with increasing obesity rates and lifestyle westernization [2][3][4].

Diabetes is a metabolic disease characterized by hyperglycemia (abnormal high levels of glucose in the blood), which results from defects in insulin secretion, insulin action, or both. Excessive thirst and frequent urination are characteristic, which lead to the intake of large volumes of water. These symptoms are due to the excretion of large amounts of glucose in the urine, a condition known as glucosuria. If it becomes chronic, hyperglycemia can then be associated with long-term damage, dysfunction, and failure of different organs, especially the eyes, kidneys, nerves, heart, and blood vessels, leading therefore to cardiovascular disorders, blindness, end-stage renal failure and amputations [5].

For T2DM, previously referred to as non-insulin-dependent diabetes, the cause of the disease is a combination of resistance to insulin action and an inadequate compensatory insulin secretory response, which leads to increased hepatic glucose production. T2DM is slow to develop and initially it does not present obvious symptoms. Most patients with this form of diabetes are obese, and obesity itself can be responsible for some degree of insulin resistance [6][7][8]. T2DM is caused by a combination of genetic and environmental influences. The genetic contribution to T2DM is not well understood, but at least 6 genetic loci in different chromosomes have been identified with abnormalities, which might contribute to this multi-genetic disease [5]. Although the precise mechanisms to explain diabetes are uncertain, it has been suggested that the final common pathway responsible for the development of T2DM is the failure of the pancreatic β-cell to compensate for insulin resistance [9].

In the fasting state of a diabetic patient, hyperglycemia is directly related to increased hepatic glucose production, while, in the postprandial state, hyperglycemia results also from defective insulin stimulation for glucose disposal in target tissues (mainly the skeletal muscles). When a diabetic patient ingests a meal containing carbohydrates, glucose accumulates in the blood. Unable to take up glucose, muscle and fat tissue use the fatty acids (FA) of stored triacylglycerols (TAG) as their main fuel instead. Acetyl-CoA derived from FA breakdown is

converted in the liver to ketone bodies – acetoacetate and β-hydroxybutirate – which are exported and carried to other tissues to also serve as fuel. Since FA cannot pass through the blood-brain barrier, the brain uses ketone bodies as alternative fuel when glucose is not available. However, the accumulation of these compounds leads to ketoacidosis, a life-threatening condition. Only an insulin injection reverses this sequence of events: Insulin will promote the movement of GLUT-4 into the plasma membranes of hepatocytes and adipocytes, allowing glucose to be taken up and phosphorylated in the cells. This way, blood glucose levels fall, greatly reducing the production of ketone bodies.

Normally, as glucose levels increase, insulin release would increase proportionately, to maintain normal glucose tolerance. However, insulin resistance develops with the progress of diabetes, causing an even higher increase in insulin secretion to compensate for the lack of insulin effect. On the other hand, with rising levels of glycemia, hormonal release by the β-cells becomes compromised, leading to higher glycemic levels [10].

1.2. Hepatic Glucose Metabolism

Glucose is considered the nearly universal fuel of higher organisms. In the human brain and nervous system, as well as the erythrocytes, testes, renal medulla, and embryonic tissues, glucose from the blood is the sole or major fuel source. By storing glucose as a high molecular weight polymer, such as starch or glycogen, a cell can stockpile large quantities of hexose units while maintaining a relatively low cytosolic osmolarity. When energy demands increase, glucose can be released from these intracellular storage polymers and it is used to produce ATP either aerobically or anaerobically. Glucose can act not only as a fuel, but also as a versatile precursor, capable of supplying a large array of metabolic intermediates for several biosynthetic reactions.

Hepatic metabolism can regulate blood glucose concentrations within a narrow range, either preventing hyperglycemia in the postprandial state or avoiding hypoglycaemia in the fasting state, under the appropriate regulation of hormones, which include glucagon and insulin. This is achieved by rapid transformation of plasma glucose to hepatic glycogen in the presence of insulin (postprandial response), and the reverse reaction in the presence of glucagon (fasting response). After the ingestion of a meal, the absorbed nutrients stimulate the secretion of insulin and, to a less extent, of glucagon, resulting in a rise in the portal vein of the insulin:glucagon ratio, which is further amplified by signals from the central nervous system. Under these conditions, the liver rapidly suppresses endogenous glucose production (EGP) and

starts to take up and temporarily store glucose. Together with the insulin stimulated increase in glucose uptake by peripheral tissues, such as skeletal muscle, these actions minimize the postprandial rise in plasma glucose concentrations following a meal. Changes in the uptake and release of other metabolites, such as lactate and alanine, can also affect postprandial glucose fluxes. On the other hand, under fasting conditions, although FA oxidation becomes the major source of energy supply, the body continues to consume glucose (≈7-10g/hour), with the brain taking its share (≈4g/hour). Given the small pool of circulating free glucose in fasting conditions, the liver switches from glucose storage to glucose production and contributes up to 90% of EGP (≈7-10g/hour), the rest being accounted by the kidneys. The liver contribution to glucose homeostasis is ensured by the release of glucose resulting from glycogenolysis and gluconeogenesis [11].

Hepatocytes take up glucose independently of insulin by the low-affinity high-capacity glucose transporter, GLUT-2, which mediates the diffusion of glucose across the plasma membrane. This transporter is so effective, that the concentration of glucose within an hepatocyte is essentially the same as the glucose concentration in the blood. When glucose enters the hepatocyte through this facilitated diffusion mechanism, it is retained through phosphorylation by the hepatic hexokinase IV (HK) isoform, glucokinase (GK), being transformed to glucose-6-phosphate (G6P). GK has a higher Km for glucose than the HK isozymes in other cells. The presence of GK allows hepatocytes to continue phosphorylating glucose even when the glucose concentrations rise above levels that would overwhelm other HKs. The high Km of GK also ensures that phosphorylation of glucose in hepatocytes is minimal when the glucose concentration is low, preventing the liver from consuming glucose as fuel via glycolysis [11][12].

Fructose, galactose and mannose, all absorbed from the small intestine, are also converted to G6P. From G6P, the glucose flux can be directed into glycogen via uridine diphosphate glucose (UDPG) (direct pathway of glycogen synthesis), the pentose phosphate pathway, resulting in the production of ribose-5-phosphate, or into glycolysis, yielding carbon-3 compounds such as pyruvate and lactate, as well as ATP and NADH. By the action of various allosterically regulated enzymes, and through hormonal regulation of enzyme synthesis and activity, the liver directs the flow of glucose into one or more of these pathways (Fig. 1.1) [11].

G6P can be dephosphorylated by glucose-6-phosphatase to yield free glucose, which is used to replenish blood glucose. When glucose levels are low in the blood, glucose is exported, to maintain the brain's blood glucose concentration high enough. However, G6P which is not immediately needed for blood glucose is converted to liver glycogen, or it has one of several other fates. After G6P breakdown by glycolysis and decarboxylation of pyruvate (by the pyruvate dehydrogenase reaction), the acetyl-CoA thereby formed can be oxidized by the Krebs cycle, yielding ATP by electron transfer and oxidative phosphorylation in the mitochondria. However, usually, FAs are the preferred fuel for energy production in hepatocytes. Acetyl-CoA can also serve as a FA precursor, which can then be incorporated into TAG, phospholipids, and cholesterol. Many of the lipids synthesized in the liver are then transported to other tissues by blood lipoproteins. Finally, G6P can enter the pentose phosphate pathway, yielding both reducing power (NADPH), and D-ribose 5-phosphate, a precursor for nucleotide biosynthesis [13][14].

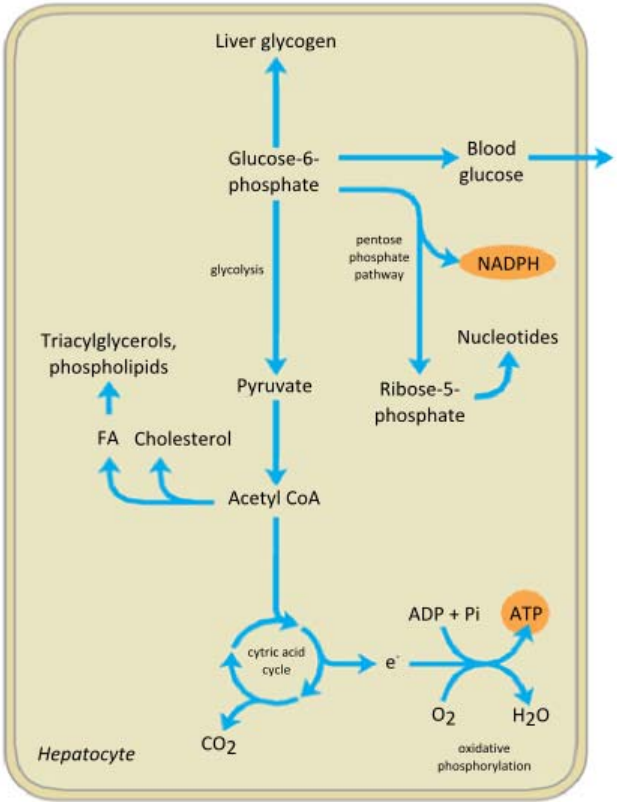

Fig. 1.1| Metabolic pathways for G6P in the liver. Anabolic pathways are shown leading upward, catabolic pathways leading downward, and distribution to other organs horizontally. The numbered processes in this figure are described in the text Adapted from [13].

1.2.1. Hormonal regulation of hepatic glucose metabolism

The concentration of glucose in the plasma is subject to tight regulation. The brain has a constant need for glucose and the liver is responsible for maintaining the blood glucose range within 60 to 90mg/dL. Among the most important regulators of blood glucose are the hormones insulin, glucagon, and epinephrine. Since the aim of this thesis is of a better understanding of the hepatic metabolic pathways, insulin will be majorly focused on this thesis, due to its importance in the regulation of glucose metabolism.

Insulin is produced by clusters of specialized pancreatic cells, the islets of Langerhans. Each cell type of the islets produces a single hormone: α-cells produce glucagon; β-cells, insulin; and δ-cells, somatostatin. What happens in the Langerhans cells when the rate of glucose catabolism increases, is that the raise in ATP concentration, causes the closing of ATP-gated K^+ channels in the plasma membrane (Fig. 1.2). Reduced efflux of K^+ depolarizes the membrane, thereby opening voltage-sensitive Ca^{2+} channels in the plasma membrane and releasing insulin by exocytosis. Stimuli from the parasympathetic and sympathetic nervous systems also stimulate and inhibit insulin release, respectively. A simple feedback loop limits hormone release: insulin lowers blood glucose by stimulating glucose uptake by the tissues; the reduced blood glucose is detected by the β-cells as a diminished flux through the HK reaction and this slows or stops the release of insulin [13].

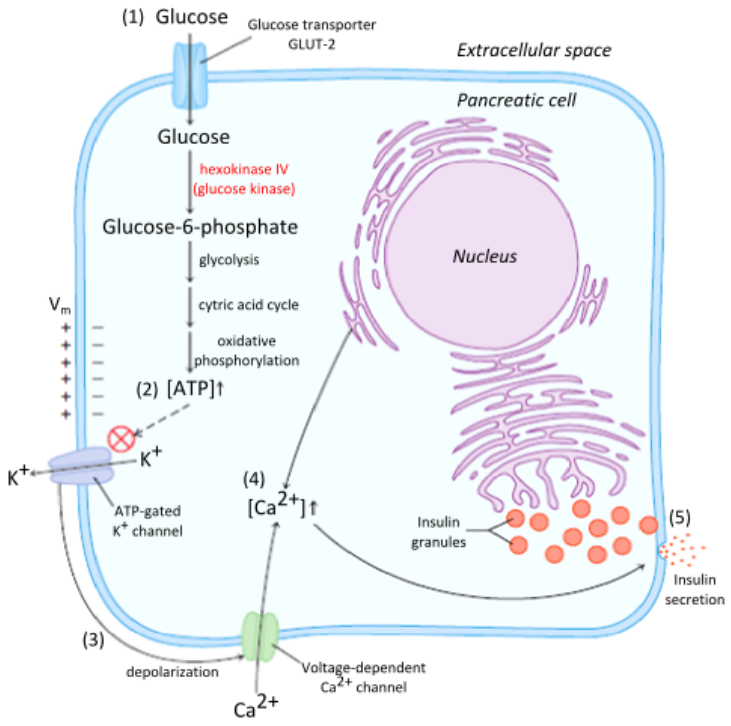

Fig. 1.2| Glucose regulation of insulin secretion by pancreatic β-cells. When the blood glucose level is high (1), active metabolism of glucose in the β-cells raises intracellular [ATP] (2), which leads to closing of the K^+ channels in the plasma membrane, depolarizing the membrane (3). In response to the change in membrane potential, voltage-gated Ca^{2+} channels in the plasma membrane open, allowing Ca^{2+} to flow into the cell; this raises cytosolic [Ca^{2+}] (4) enough to trigger insulin release by exocytosis (5) [13].

Insulin signals many body tissues, in particular liver, muscles and adipose tissue, indicating high blood glucose levels; as a result, cells take up excess glucose from the blood and convert it to the storage compounds, glycogen and TAG. To do so, insulin binds to the extracellular α-subunit of the insulin receptor in target cells and increases intrinsic tyrosine kinase activity of the intracellular β-subunit. The critical substrates for the hepatic insulin

receptor kinase that mediate the metabolic activity of insulin are insulin receptor substrate 1 (IRS-1) and IRS-2 (Fig. 1.3). Tyrosine phosphorylation of these subunits initiates their association with phosphatidylinositol-3 kinase (PI3K) and activates the PI3K catalytic subunit. PI3K product, phosphatidylinositol-3,4,5-triphosphate (PIP_3) causes translocation of the pleckstrin homology (PH) domain-containing kinases, pyruvate dehydrogenase kinase 1 (PDK-1) and protein kinase B (Akt/PKB) to the plasma membrane where they are activated. Activated Akt/PKB inhibits the activity of glycogen synthase kinase-3 (GSK-3) by phosphorylation. Since GSK-3 inhibits glycogen synthase (GS) by phosphorylation, suppression of GSK-3 leads to activation of glycogen synthesis promoting glycogenesis. Insulin activates GS and inactivates glycogen phosphorylase, so that much of the G6P is channelled into glycogen. Insulin also promotes the docking and fusion of GLUT-4-containing vesicles to the plasma membrane and stimulates the storage of excess fuel as fat. In the liver, insulin activates both the oxidation of glucose-6-phosphatase to pyruvate via glycolysis and the oxidation of pyruvate to acetyl-CoA. If not oxidized further for energy production, acetyl-CoA is used for FA synthesis in the liver, and the FA are exported as TAG of very-low density lipoproteins (VLDLs), to the adipose tissue [12][13].

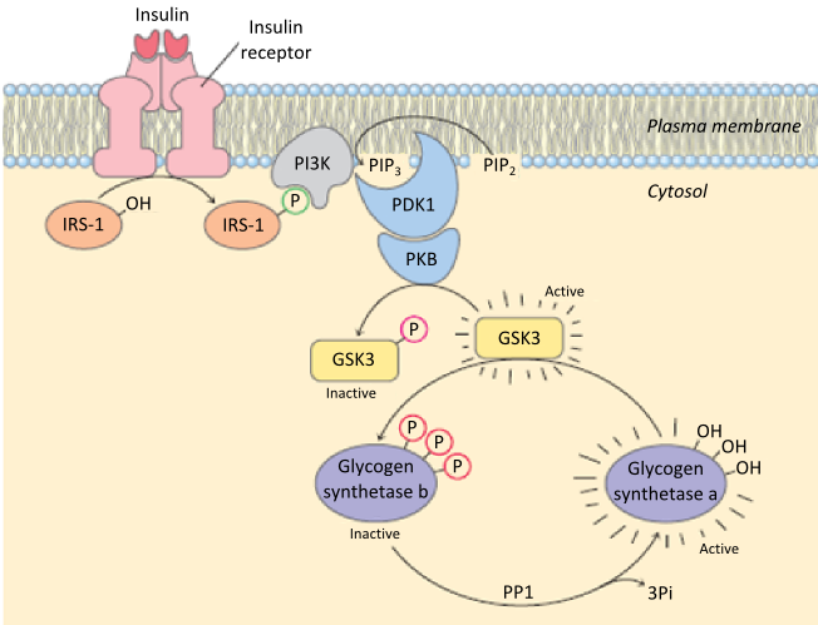

Fig. 1.3| The path from insulin to GSK-3 and glycogen synthase. Insulin binding to its receptor activates a tyrosine protein kinase domain in the receptor, which phosphorylates IRS-1. The phosphotyrosine in this protein activates PI3K, which converts PIP_2 to PIP_3. When bound to PIP_3, the PDK-1, that is activated, activates a second protein kinase, Akt also named PKB, which phosphorylates GSK-3. The inactivation of GSK-3 allows PP1 to dephosphorylate glycogen synthase, converting it to its active form. This way, insulin stimulates glycogen synthesis. GSK-3 = glycogen synthase kinase-3; IRS-1 = Insulin Receptor Substrate – 1; PDK-1 = phosphoinositide dependent protein kinase-1; PI3K = phosphatidylinositol-3 kinase; PIP_2 = phosphatidylinositol 4,5 – biphosphate; PIP_3 = phosphatidylinositol-3,4,5-triphosphate; PKB = Protein Kinase B; PP1 = phosphoprotein phosphatase 1 [13].

Insulin also regulates lipid metabolism by increasing FA synthesis, increasing esterification of free FAs (FFAs) and decreasing lipolysis. In addition, insulin exerts its anabolic effects on protein metabolism by increasing DNA replication and protein synthesis via control of amino acid uptake and decreased proteolysis. Moreover, it can control several other important processes such as cell growth, cell proliferation, survival and differentiation [15].

1.2.2. Reuse and recycle - Anaerobic respiration and Cori cycle

Glucose can be oxidized to pyruvate via glycolysis to provide ATP and metabolic intermediates (Fig. 1.4) or via the pentose phosphate pathway. In glycolysis, a molecule of glucose is degraded in a series of enzyme-catalyzed reactions to yield two molecules of pyruvate. During these sequential reactions, ATP is formed through substrate-level phosphorylation and NADH through oxidation and phosphorylation. A key step for these reaction to occur is the availability of NAD^+, because unless NADH is oxidized back to NAD^+, glycolysis cannot proceed and ATP is no longer produced [13].

To obtain energy, most vertebrates utilize aerobiosis as their prime mechanism, expending oxygen in the process. However, in situations where O_2 is scarce, such as in active skeletal muscle, due to physical exercise or a stressful situation, or in the case of submerse vegetal tissues, solid tumours or fermenting bacteria, NADH generated by glycolysis cannot be reoxidized by oxygen. The first cells that existed in our planet lived in an atmosphere almost devoid of oxygen, and had to develop strategies to extract energy. Most modern organisms still hold the ability of continuously generating NAD^+ during anaerobic glycolysis, by transferring electrons from NADH, producing reduced products such as lactate or ethanol. Thus, while NAD^+ regeneration is not coupled to ATP synthesis under these conditions, glycolytic carbon flux is maintained and ATP generated by substrate-level phosphorylation. This process, designated fermentation, is defined as the extraction of energy without oxygen consumption or alterations in NAD^+ or NADH concentrations. Some tissues and cells (such as erythrocytes, which do not possess mitochondria) can produce lactate from glucose even under aerobic conditions [13].

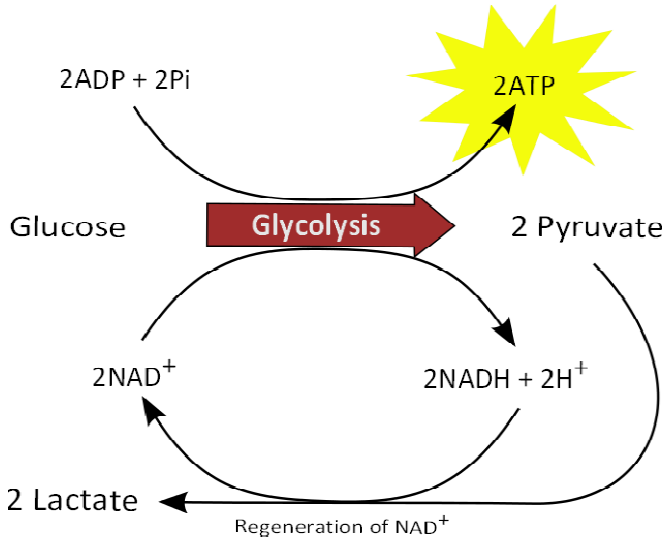

Fig. 1.4| Schematic representation of lactic fermentation, with glucose transformation into lactic acid. In this reaction, 2 ATP and 2 NADH are formed during the production of pyruvate, which is an intermediate for lactic acid formation. With formation of lactic acid, NAD^+ is regenerated without oxidative phosphorylation. This mechanism, present in most vertebrates, allows the organism to obtain energy when there is not enough oxygen available.

In myocytes, the cells of skeletal muscle, their metabolism is specialized in generating ATP as the immediate source of energy for contraction. To do so, these cells can use FAs, ketone bodies or glucose. Moreover, the skeletal muscle is adapted to do its mechanical work in an intermittent fashion, on demand. At rest, skeletal muscle prefers FAs from the adipose tissue and ketone bodies from the liver. These are oxidized and degraded to yield acetyl-CoA, which enters the Krebs cycle for oxidation to CO_2. The transfer of electrons to O_2 provides energy for ATP synthesis by oxidative phosphorylation. In a moderately active state, skeletal muscles use glucose in addition to FA and ketone bodies. Glucose is phosphorylated and degraded by glycolysis to pyruvate, which is converted to acetyl-CoA and oxidized via the Krebs cycle and oxidative phosphorylation. But if muscles are maximally active, the demand for ATP is so great that the blood flow cannot provide oxygen and fuels fast enough to supply sufficient ATP by aerobic respiration alone. Under these conditions, they degrade glycogen and resort to fermentation with the consequent formation of lactate, because NADH cannot be reoxidized to NAD^+, but NAD^+ is required as an electron acceptor for further oxidation of pyruvate. Therefore, pyruvate is reduced to lactate, accepting electrons from NADH and thereby regenerating the NAD^+ necessary for glycolysis to continue (Fig. 1.4). Glycolysis of glycogen, also yields 2 ATP per hexose, since glycogen phosphorilase uses inorganic phosphate rather than ATP for generating G6P [13].

When lactate is produced in great amounts, during a vigorous muscular contraction, acidification resulting from lactic acid fermentation is originated. It is the acidification in the muscles and blood as well as the relative small amount of glycogen in skeletal muscles that limits the period of vigorous activity. Nevertheless, lactate produced by superactivated skeletal

muscles can be recycled, being transported by the blood to the liver where it is converted to glucose by gluconeogenesis during the recovery from physical activity. Phosphocreatine, present in 10-30mM concentrations, is another temporary energy source in skeletal muscle. Through the actions of creatine kinase, it can phosphorylate ADP to yield ATP [13].

In humans, a muscle at rest extracts 50% of arterial oxygen, while during exercise this percentage increases up to 90%. Upon cessation of exercise, oxygen extraction does not immediately revert to basal values, reflecting the oxidation of accumulated lactate and the replenishment of glycogen stores. To the cycle of reactions which include the conversion of glucose to lactate in the muscles and the conversion of lactate to glucose in the liver, was first referred to by Carl F. Cori and Gerty T. Cori [16], reason why is now called the Cori cycle (Fig. 1.5). The glucose formed in the liver, returns to the muscles to replenish their glycogen stores, completing the Cori cycle. Glucose turnover rates (synthesis followed by degradation) and recycling by the Cori cycle are highly sensitive to insulin as to nutrients availability [13].

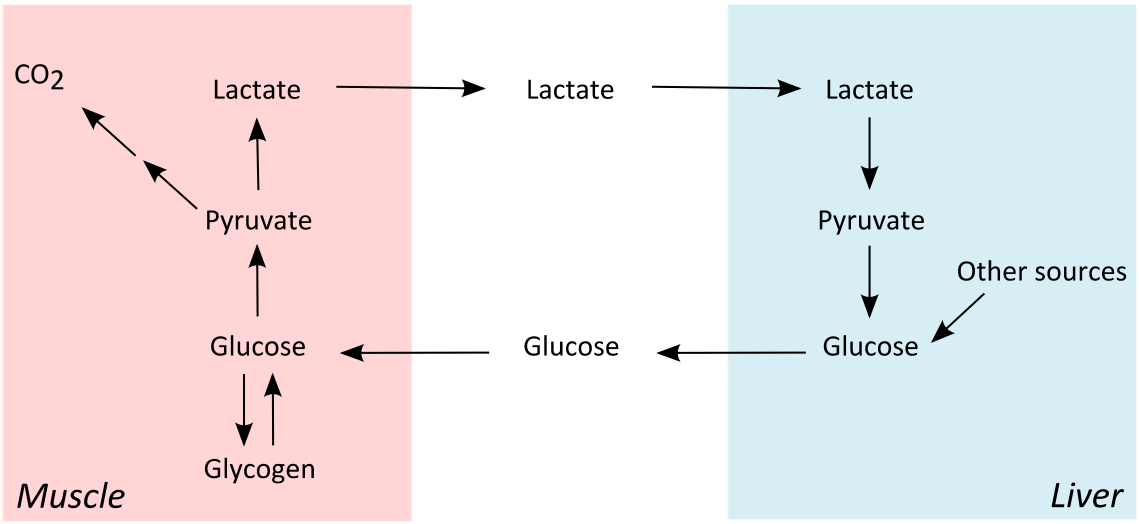

Fig. 1.5| Metabolic cycling between skeletal muscle and liver. Extremely active muscles use glycogen as their energy source, generating lactate via glycolysis. During the recovery state, part of this lactate is transported to the liver and converted to glucose via gluconeogenesis. This glucose is released to the blood and returns to the muscles to replenish their glycogen stores. The overall pathway (glucose → lactate → glucose) constitutes the Cori cycle.

1.2.3. Deregulation of hepatic glucose metabolism - insulin resistance

Insulin resistance is defined as a pathophysiological condition in which normal insulin concentration does not adequately produce a normal insulin response in target tissues such as

adipose tissue, muscle and liver. Under normal conditions, pancreatic β-cells secrete more insulin to overcome hyperglycemia, but besides the regulation of glucose metabolism, insulin is also responsible for the regulation of lipid metabolism by increasing FA synthesis and esterification of FFAs, and decreasing lipolysis.

It is now well established that both plasma and cellular FA concentrations correlate positively with increased insulin resistance [6][17][18]. In fact, people with enlarged subcutaneous adipocytes have shown to be more hyperinsulinemic and glucose intolerant, making them individuals at risk of developing T2DM, compared to those with similar degrees of adiposity but smaller adipocytes. However, it is also recognized that lipodystrophy with lack of adipose tissue can be associated with insulin resistance and increased risk for development of T2DM, as well [19]. In 2000, Shulman hypothesized that insulin resistance develops due to alterations in the partitioning of fat between adipose tissue and muscle or liver [20]. In addition, several factors linked to the development of T2DM might be involved directly or indirectly in the regulation of adipogenic genes [21]. It was even proposed that impaired adipocyte proliferation and differentiation may cause the progressive filling of existing adipocytes, leading to overflow of excess calories as fat into other tissues and insulin resistance [22]. Nowadays, the mechanisms underlying insulin resistance are poorly understood, but it is clear that a relation between deregulation of lypolysis, deregulation of glucose metabolism and insulin sensitivity exists.

1.2.3.1. Molecular mechanisms of insulin resistance

Several mechanisms, including abnormal insulin production, mutations in insulin receptor and its substrates, and insulin antagonists have been proposed, but it appears that defects in post-receptor signalling are the major cause of insulin resistance in target tissues [23]. In fact, a reduced expression and/or diminished phosphorylation of early insulin signalling molecules has been observed in insulin target tissues of obese and T2DM patients [24][25]. Several lipid metabolites that are products of TAG hydrolysis (i.e. DAGs, FAs, fatty acyl-CoAs (FACoA) and ceramides) have been shown to directly or indirectly interfere with insulin signalling and glucose transport. The most common pathways are the increase in serine/threonine phosphorylation of IRS-1, decrease in IRS-1-associated PI3K activity and Akt/PKB activity, and decrease in GLUT-4 translocation [20][26][27][28].

1.2.3.2. Athletes paradox

Even though TAG deposition is positively associated with insulin resistance, it is not currently known whether intramyocellular triglycerides (IMTGs) cause insulin resistance. First, despite the positive association between IMTG and insulin resistance in obesity and T2DM, endurance trained athletes are highly insulin sensitive even though they present elevated IMTG deposition [29][30]. The reason for this "athletes paradox" is unknown, but may be due to an increase in lipid droplet-to-mitochondria contact [31] and an enhanced oxidative capacity of athletes to oxidize TAG-derived FA [29], thereby preventing the accumulation of insulin-inducing FA metabolites. Second, studies that have altered IMTG levels have concomitantly changed other lipid metabolites, such as DAG, ceramides and long chain FACoA (LCFACoA), making it impossible to discern specific effects of IMTG.

1.3. Lipolysis

FAs are essential components to every organism. They are important substrates for oxidation and cellular energy production, more specifically to membrane biosynthesis, as signalling intermediaries and to ATP production through β-oxidation and acetyl-coA flux through the Krebs cycle. Cells can obtain FA to use as fuel from three sources: fats consumed in the diet, fats stored in cells as lipid droplets, and fats synthesized in one organ for export to another. The ability to store and release this energy in response to the energetic needs is advantageous to survival and requires a regulated balance of the TAG synthesis and its hydrolysis [13].

Despite being of physiological importance, an oversupply of FA is highly detrimental. Increased concentrations of nonesterified FAs disrupt the integrity of biological membranes, alter cellular acid-base homeostasis, and make possible the generation of harmful bioactive lipids. These effects, in turn, impair membrane function and induce endoplasmic reticulum (ER) stress, mitochondrial dysfunction, inflammation, and cell death. As a countermeasure, cells are able to detoxify nonesterified FAs by esterification with glycerol to yield inert TAG. Higher organisms can also store FA in a specialized organ, the adipose tissue, which supplies FA to other high-demand tissues such as liver and muscle (exogenous FA), only when required. It is this regulated balance of FA esterification and TAG hydrolysis, which creates an efficient buffer system [18].

The first hormone induced enzyme to be discovered, which was responsible for the catabolism of TAG, was the hormone sensitive lipase (HSL) [32]. Because HSL was shown to hydrolyze both TAG and DAG substrates, it was believed that the enzyme represented the only lipase activated by hormonal stimulation. However, although HSL knock-outs ($HSL^{-/-}$) male mice presented infertility, owing to a defect in sperm maturation from alterations in lipid and energy metabolism, they were normal in most regards, but they accumulated abnormally high amounts of DAG [33][34]. Surprisingly, these mice were not overweight or obese. By the contrary, with increased age, they showed reduced white adipose tissue (WAT) weight [35] and were resistant to genetically or diet-induced obesity [36]. These results lead to the search of a second enzyme with TAG hydrolase function and hormone sensibility. As a result, in 2004 three groups independently published the discovery of an enzyme capable of hydrolysing TAG and named it adipose triacylglyceride lipase (ATGL) [35], desnutrin [37] and calcium-independent phospholipase A2z (iPLA2z) [38], respectively.

Whole-body lipolysis occurs in three principal sites: gastrointestinal lipolysis, which mediates the catabolism of dietary fat; vascular lipolysis, which is responsible for the hydrolysis of lipoprotein-associated TAG in the blood; and intracellular lipolysis. Intracellular lipolysis catalyzes the breakdown of TAG stored in intracellular lipid droplets (LD) for subsequent export of FA (from adipose tissue) or their metabolism (in nonadipose tissue). This thesis is focused on the intracellular lipolysis which involves neutral pH (optimum around pH 7) and acid lipases present in lysosomes (optimum pH range: 4-5). Among the well-characterized neutral TAG hydrolases, there is ATGL and HSL, whereas lysosomal acid lipase (LAL) is the most important lipase in lysosomes [18].

1.3.1. Adipose triacylglyceride lipase (ATGL) expression and function

ATGL is an enzyme with transacylase and phospholipase activity [35][38][39], which was shown to be actually lower than its TAG hydrolase activity [35][38]. Interestingly, ATGL increases hydrolysis of TAG but not of other substrates, whereas HSL has broad substrate specificity [35][37][38]. mRNA for ATGL is expressed at high levels in murine WAT and brown adipose tissue (BAT) and to a lesser degree in testes, cardiac muscle and skeletal muscle. WAT's contribution to the regulation of energy homeostasis is due to both the enormous lipid storage capacity as well as its function as an endocrine organ, secreting numerous hormones and adipo-cytokines [40]. In humans, the highest ATGL expression was also found in the adipose tissue [35]. Inclusively, it

was found that during adipocyte differentiation, ATGL expression increases progressively [37], revealing its importance for this tissue.

Insulin and insulin-like growth factors (Il-GF) represent the most potent inhibitory hormones in lipolysis, so, as expected, ATGL mRNA concentrations are markedly affected by the nutritional status, increasing therefore during fasting and decreasing during food intake. Thus, ATGL gene expression might contribute to elevated FA mobilization under conditions of defective insulin signalling [41]. ATGL mRNA expression is also elevated by peroxisome proliferator activated receptor (PPAR) agonists and glucocorticoids [18], and recently, several groups reported that pigment epithelium-derived factor (PEDF) induces TAG hydrolysis in adipose tissue, muscle, and liver, via ATGL [42][43].

1.3.2. Regulated lipolysis by HSL and ATGL

Most of the body's energy reserves are stored in the WAT, which implies that the supply of muscles with energy during a prolonged physical activity is largely dependent on lipolysis. The emerging view on lipolysis is that ATGL has a combined action with HSL for the regulation of lipid degradation (Fig. 1.6) [44]. In basal conditions, perilipin A and comparative gene identification (CGI-58) form lipid droplet complexes, while ATGL and HSL are found mainly in the cytoplasm. Lipolysis rate under this condition is low, being FA resynthesized into TAG (futile cycle) or directed towards oxidation in mitochondria [44]. In human adipose tissue, only β1 and β2 receptors induce lipolysis. Some hormones, bind to these receptors and stimulatory G_S proteins activate adenylate cyclase, causing a rise in cAMP levels and elevated activity of cAMP-dependent protein kinase-A (PKA). When lipolysis is stimulated, PKA activation results in HSL phosphorylation at Ser^{563}, Ser^{659} and Ser^{660} residues and also perilipin's phosphorylation at other six serine residues. Perilipin's phosphorylation results in the release of CGI-58, which binds to ATGL. CGI-58 then acts as a coactivator protein, promoting full hydrolase activity of ATGL to initiate lipolysis and TAG breakdown. HSL is translocated to lipid droplets and associates with the phosphorylated perilipin to degrade diacylglycerols (DAG) into monoacylglycerols (MAG). Ultimately, a monoacylglicerol lipase (MGL) cleaves final FA to form glycerol [18][44][45].

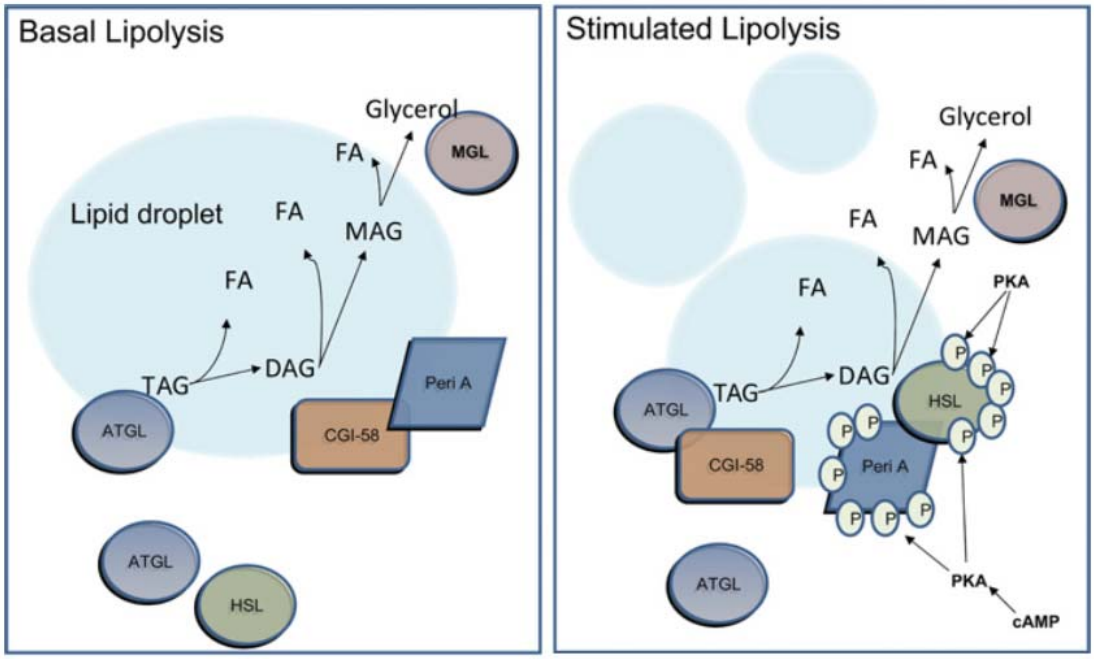

Fig. 1.6| Schematics of regulated intracellular lipolysis. Basal lipolysis: Perilipin A and CGI-58 form a complex on the lipid droplet. ATGL is localized partially in the lipid droplet and HSL is mostly in the cytoplasm. The rate of lipolysis (i.e. the production of FA and glycerol) is very low under these conditions, with released FA being resynthesized back into lipids (futile cycling) or directed towards oxidation in mitochondria. Stimulated lipolysis: PKA activation results in phosphorylation of HSL and perilipin's serine residues (denoted by P). Phosphorylation of perilipin releases CGI-58, which binds ATGL to initiate lipolysis and the breakdown of TAG. HSL translocates to the lipid droplet, associates with phosphorylated perilipin A and degrades DAG. MGL cleaves the final FA to produce glycerol. The production of FA and glycerol is much higher than in the basal state [44].

ATGL and HSL are responsible for more than 90% of TAG hydrolysis [46]. In non-adipose tissues with high FA oxidation rates, such as muscle and liver, ATGL-mediated TAG hydrolysis, follows another mechanism, where another perilipin is responsible for recruiting ATGL and CGI-58 to the lipid droplets. Although most non-adipose tissues also express ATGL and HSL, expression levels are low in some of these tissues, raising the question of whether other lipases are additionally required for efficient lipolysis [18].

A role for neutral lipid metabolism in signalling gained substantial interest when it was noted that both these hormones were regulated by insulin [47] and that increased cellular TAG concentrations were strongly associated with insulin resistance in skeletal muscle and liver [48][49]. However, the relative inert nature of TAG makes it unlikely that they interfere directly with insulin signalling [18].

1.3.3. ATGL knock-outs ($ATGL^{-/-}$)

ATGL knock-out ($ATGL^{-/-}$) mice present a severe "lipid" phenotype. They exhibit low lipolysis with consequent reduction of FAs release from WAT by more than 75% and an augment in adipose tissue mass, with an increase in TAG deposition in non-adipose tissues, such as heart, pancreas, kidneys and skeletal muscle, making them mildly obese [41]. Defective TAG mobilization and massive accumulation, causes severe cardiomyopathy due to myocardial fibrosis and a defect in contractile performance that ultimately reduces their life span [50]. They also present defective thermogenesis in brown adipose tissue (BAT) and an overall defect in energy homeostasis [41]. Circulating FFAs are reduced in $ATGL^{-/-}$ mice, which is thought to contribute to their impaired capacity for thermogenesis. Since FFAs are considered to be key fuels for sustaining the endotermic conversion of gluconeogenic precursors to glucose, it would be expected that hepatic gluconeogenesis might be limited in these animals. In fact, gluconeogenesis rates were normal in $ATGL^{-/-}$ mice [51], but it is not known if there were changes in gluconeogenic precursors or alternative selection of energy-generating substrates.

It was observed that the increase in plasma levels of FAs and glycerol that is usually induced during physical exercise was diminished in both $ATGL^{-/-}$ as $HSL^{-/-}$. However, exercise performance was only compromised in $ATGL^{-/-}$ mice, but unaffected in $HSL^{-/-}$. The diminished exercise performance in older $ATGL^{-/-}$ mice would be most likely related to cardiac lipid deposition, aberrant cardiac function, and impaired blood flow. But on the other hand, further experiments in young $ATGL^{-/-}$ mice that did not display cardiac lipid accumulation revealed that endurance treadmill running was also compromised, suggesting that potential cardiovascular responses do not fully explain the reduced exercise tolerance [52]. Actually, these mice cannot adjust circulating FAs to the increased energy consumption of the body during exercise [52][53], because the ATGL deletion compromised the mice's ability to alternate from a carbohydrate metabolism to a FA metabolism during fasting [52].

Besides increased glucose uptake and utilization, $ATGL^{-/-}$ mice exhibit increased glucose tolerance and insulin sensitivity, a metabolic pattern opposite to that of diabetic and/or obese individuals [50][54]. This increased insulin sensitivity is observed even despite the fact that ATGL deficiency leads to an insulin secretion defect in the pancreatic islets [55]. However, insulin signalling can be different for each tissue, being increased in skeletal muscle, unchanged or possibly increased in WAT, and decreased in brown adipose tissue and liver, though, the key tissue in mediating insulin sensitivity in these mice is the skeletal muscles [54].

It is clear that a relation between ATGL and insulin sensitivity exists, however, the mechanisms behind it are still unclear. Reduced TAG hydrolysis and FAs delivery would be expected to decrease (or at least not increase) other lipid metabolites as observed for FA-CoA and ceramides. But interestingly, DAGs are unexpectedly increased in skeletal muscle of $ATGL^{-/-}$ mice. Also, in $ATGL^{-/-}$ mice, insulin stimulated PI3K and Akt/PKB activities as well as phosphorylation of critical residues of IRS-1 (Tyr(P)-612) and Akt/PKB (Ser(P)-473) are increased in skeletal muscle [54]. One hypothesis is that PEDF, which induces TAG hydrolysis via ATGL, has a role on insulin resistance. PEDF exhibits a large spectrum of bioactivities, including anti-angiogenic, antitumorigenic, neuroprotective, antioxidative, and anti-inflammatory effects. Although the mechanism remains to be clarified, ATGL activation by PEDF may be involved in the pathogenesis of insulin resistance and the development of hepatosteatosis [56].

ATGL and HSL are responsible for more than 90% of the lipolytic activity in WAT and cultured adipocytes [46]. As expected, ATGL-deficient mice develop hepatosteatosis, but it is better tolerated metabolically than hepatosteatosis of diabetes and obesity [51], indicating an alternative pathway for TAG hydrolysis. The pronounced remaining activity of hepatic TAG hydrolase(s) indicates that other lipases might contribute to the highly dynamic turnover of TAG [18].

Humans with ATGL mutations also present a tendency to accumulate fat in multiple tissues [57][58], however, in contrast to mice, human patients with ATGL or CGI-58 deficiency are not as overweight or obese. This has been used as argument that ATGL mediated lipolysis in human WAT is less important than that of mouse WAT [41]. However, even though ATGL deficient humans are not overweight or obese, they do present neutral lipid storage disease with myopathy (NLSDM) [59]. Conversely, in the livers of insulin-resistant patients with non-alcoholic fatty liver disease (NAFLD), levels of ATGL and CGI-58 protein are reduced [60], and genetic variations within the ATGL gene have already been associated with T2DM and alterations in plasma TAGs and FFAs [61].

1.3.4. Randle Cycle

In 1963, Philip Randle, proposed a “glucose – FA cycle” to describe fuel flux between tissues and fuel selection (Fig. 1.7) [62]. The glucose – FA cycle is a biochemical mechanism that adapts substrate supply and demand in normal tissues in coordination with hormones, which control substrate concentrations in the circulation.

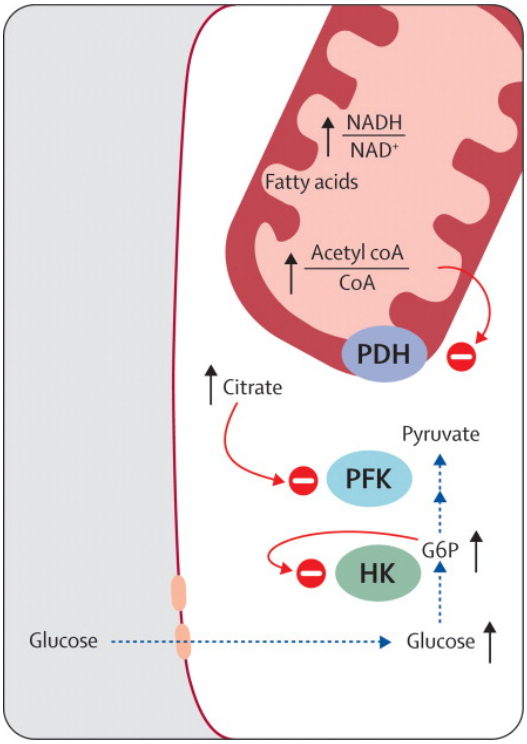

Fig. 1.7| Glucose-FA cycle proposed by Randle and colleagues. Red circle with minus sign represents inhibition. Black line with arrowhead represents increase or accumulation of substrate. Blue dotted line with arrowhead indicates a pathway that is inhibited (see text for details) [7].

Randle demonstrated that impairment of glucose metabolism by FAs (or ketone bodies) oxidation was mediated by a short-term inhibition of several glycolytic steps, namely inhibition of phosphofructo-1-kinase (PFK-1) and pyruvate dehydrogenase (PDH). The extent of inhibition is graded and increases along the glycolytic pathway, being most severe at the level of PDH and less severe at the level of glucose uptake and PFK. This sequence occurs because the initial event, triggered by FA oxidation, is an increase in the ratios of [acetyl-CoA]/[CoA] and [NADH]/[NAD^+], both of which inhibit PDH activity and leads to increasing concentrations of intracellular citrate. The citrate accumulation would inhibit PFK, increasing intracellular G6P concentrations and inhibiting HK activity. The inhibition of HK activity would result in an increase in intracellular glucose concentration and decreased muscle glucose uptake. In contrast, upregulation of pyruvate dehydrogenase kinase (PDK) either by response to high-fat tissue, starvation, or insulin deficiency, keeps glucose oxidation at a low level, whereas FA oxidation is increased. In this situation, metabolism fails to adapt to transitions of a fasted-to-fed state, which is a feature of insulin resistance. On the other hand, certain FA can bind to PPARs, a class of transcription factors, which regulate lipid and glucose homeostasis through their long-term transcriptional effects. Increases in plasma FA concentrations initially induce insulin resistance by inhibiting glucose transport and/or phosphorylation activity, only then the reduction in muscle glycogen synthesis and glucose oxidation occurs [7][17][63].

2. TECHNICAL STRATEGIES

2. TECHNICAL STRATEGIES

2.1. Metabolomics

The technological advances made in the past few years have led to the development of the field of systems biology. It has become evident that the research in areas of the "omics cascade", such as genomics, transcriptomics, proteomics, and metabolomics is, nowadays, of great importance (Fig. 2.1). Metabolomics is defined as a large-scale, qualitative and quantitative study of all metabolites in a given biological system [64], representing a wide variety of compound classes, such as amino acids, peptides, lipids, organic acids and nucleotides. Metabonomics is a subset of metabolomics and is defined as the quantitative measurement of the multiparametric metabolic responses of living systems [65].

One of the first metabolite profiling experiments was reported by Pauling and colleagues in 1971. They analyzed the metabolite content of human urine vapor and breath of patients subjected to a defined diet, using gas chromatography (GC) [66]. Unlike transcripts and proteins, the molecular identity of metabolites cannot be deduced from genomic information, which means that the identification and quantification of metabolites must rely on techniques such as mass spectrometry (MS) and nuclear magnetic resonance (NMR) spectroscopy [64]. The advantages of NMR include its high selectivity, non-destructiveness and minimal sample preparation. However, it is not sensitive enough to low concentrations of metabolites and the identification and quantification of individual metabolites might be challenging in complex mixtures. For these reasons, NMR is normally used for profiling of high-abundance metabolites (> 100 μmol). On the other hand, MS offers quantitative analysis with high selectivity as well as the potential to identify metabolites from complex mixtures. Incorporation of state-of-the-art micro liquid chromatography (LC) separation techniques coupled with discrete MS sampling of the chromatographic outflow provides a controlled stream of relatively few analytes that can be comprehensively characterized by the mass spectrometer at any given time, resulting in the optimal combination of sensitivity and selectivity. However, MS usually requires a sample cleaning step (i.e. to remove salts or macromolecules that compromise the function of both LC and MS components). This procedure may result in metabolite losses, and sampling of some metabolites may be discriminated over others [64][67].

Metabolomics can yield new biomarkers that can reach the clinic as tools to diagnose health status, disease, or outcome of pharmacological treatment [67][68]. However, the problem in this area is the lack of standardized databases, therefore the widespread application

of metabonomics (the quantitative study of the metabolites), in the clinical setting is going to be dependent on the development of central standardized databases for multivariate metabolomic data [67][69]. In 2007 the Human Metabolome Database (HMDB) was presented to the scientific community as being the most complete and comprehensive collection of human metabolite and human metabolism data in the world, having compiled hundreds of MS and NMR metabolomic analyses [70].

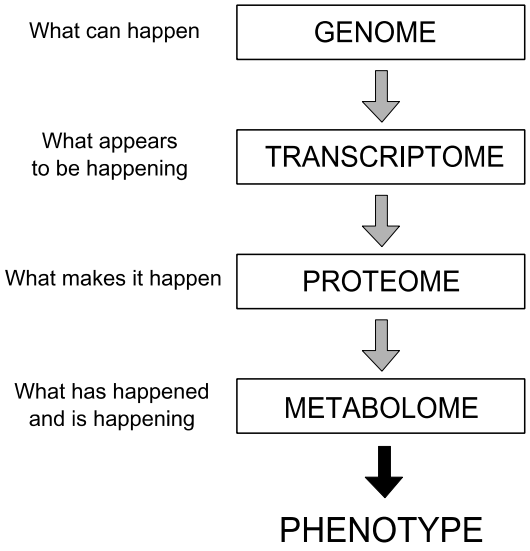

Fig. 2.1| The "omics cascade" comprises a series of levels of the systems biology. The genome refers to the organism's hereditary information, which includes both genes and non-coding sequences of DNA or RNA. The transcriptome comprises all RNA molecules, which include mRNA, rRNA and tRNA. Proteomics is the entire set of proteins expressed by a genome. The metabolome includes all metabolites such as metabolic intermediates, hormones and other signalling molecules, and therefore, since it is at the end of the "omics cascade" it is the most predictive of the phenotype. Adapted from [67].

2.2. Stable isotope tracers in metabolic studies

Tracer-based metabolomics is a form of targeted metabolomics in which the distribution of ^{13}C from a labelled precursor among various metabolic intermediates is determined [71]. When administered, ^{13}C propagates through the metabolic network as a function of the metabolic activity. Over time, characteristic ^{13}C-patterns are produced in the carbon backbone of metabolic intermediates, end-products, or biomass components. These labelling patterns can be recorded by either NMR or MS. In vivo fluxes can be back-calculated from the isotopologue patterns and physiological rates, by using mathematical models that are able to describe the scrambling of ^{12}C and ^{13}C atoms [72]. The use of stable isotope tracers and mass isotopomer analysis helps to define the metabolic intermediates relevant to the objective of the study, the known metabolic pathways allow interpretation of precursor-product relationship of compounds, and the distribution of ^{13}C, the determination of a quantitative relationship between precursor and product [71].

Isotopes that are radioactive, spontaneously disintegrate to form another element, releasing radiation as a by-product of the decay. Stable isotopes, on the other hand, also differ in the number of neutrons present but do not decay spontaneously and therefore do not emit radiation [73]. In the case of metabolic studies, stable isotope and mass isotopomer analysis has largely replaced radioactive tracers. One advantage of stable isotope application is the generation of positional and mass isotopomers from ^{13}C-labelled precursors which can be determined without purification and chemical degradation. The formation of positional mass isotopomers in metabolic intermediates from the distribution of ^{13}C of a specifically labelled precursor depends on the biosynthetic pathway and the relative dilution of intermediates, providing therefore important information on metabolic pathways and relative abundance of intermediates [71].

The use of a substance (tracer) that can be used to follow another substrate (tracee) requires that such substance experiences the identical metabolic fate as the tracee. The ideal tracer should be detected with such precision that could be administered in tracer amounts, thereby avoiding any alteration in the metabolism of the tracee. Tracers used for the purpose of metabolic research are usually identical to the tracee, except that one or more atoms differ from the more abundant naturally occurring form of that atom. To be of use in metabolic research, the natural abundance of a given isotope (and the presence of multiple other isotopes) needs to be low [73], and even so, contributions from its isotopic natural abundance must be factored out [74]. The presence of naturally occurring stable isotopes within the body prior to tracer infusion means that the tracer (merely) enriches the amount of this isotope. Knowledge of the background abundance of the isotope is therefore necessary to determine the degree of enrichment required [73].

In the case of blood glucose levels, rate of appearance (Ra) represents the rate by which glucose enters the organism via dietary absorption and via endogenous glucose production (EGP), and rate of disposal (Rd), the rate of oxidative disposal and non-oxidative disposal (glycogen synthesis) of glucose. At the simplest level, glucose metabolism in the fasting state can be looked at as a single compartment represented by a bathtub where water enters via a

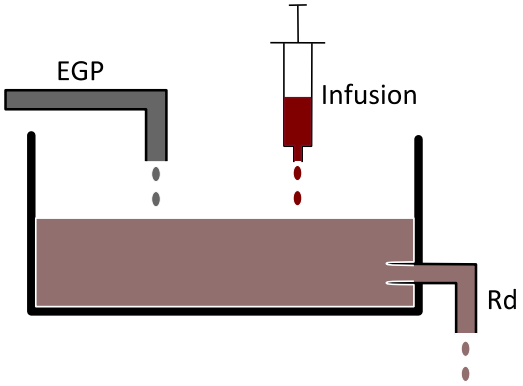

Fig. 2.2| Diagram illustrating the pool concept in tracer dilution studies. EGP – Endogenous glucose production; Rd – Rate of disposal. Adapted from [73].

faucet (EGP) and leaves via the drain (Rd) (Fig. 2.2). The water level rises if EGP > Rd, falls if EGP < Rd, and remains constant when EGP = Rd, as happens when peripheral glucose concentrations are kept constant. If a dye could be added to the water in such a way that it is instantaneously and uniformly distributed throughout the bathtub, subsequent water loss via the drain will not change the resulting dye concentration in the bathtub. In contrast, water entering from the faucet has no dye and over time will dilute the dye concentration. This underlies the basis of the tracer dilution technique, commonly used to measure EGP where unlabeled glucose dilutes the tracer. In fact, tracers used to measure metabolic fluxes are usually infused at a (constant) rate so that after a period of time the tracer will be removed at the same rate as it appears. The time to reach that equilibrium (assuming a one compartment system with constant tracer infusion) depends on the tracer's infusion rate relative to the tracer's clearance (removal from the pool). Assuming that the tracer and tracee are cleared at the same rate, the concentration of tracer and tracee in the body pool will reflect their respective rates of infusion/appearance [73].

The unit of measure used in tracer-based metabolomics is expressed in terms of isotopomer molar fraction (or ratios), and isotopic enrichment per molecule (or per carbon atom) of metabolites rather than relative concentrations (activities) of metabolites in a sample as in many metabolomics studies [71].

2.3. Dry Blood Spots (DBS)

Dry blood spots (DBS) were first described in 1913 for the estimation of blood glucose concentration [75], and became established in the 1960s by Robert Guthrie, who was able to develop a cost-effective screening test for newborns for the detection of phenylketonuria [76]. Since then, the DBS methodology has become more and more common, and is now used in the widespread screening of newborns for the detection of metabolic diseases. DBS possibilities continue to expand in terms of scientific investigation, including the measurement of antibodies [77][78], viruses [79][80] and indicators of endocrine, immune, reproductive and metabolic function, as well as measures of nutritional status and infectious disease [81]. The introduction of liquid chromatography coupled to tandem mass spectrometry (LC-MS/MS) instrumentation has enabled the development of assays using micro quantities of blood and serum with good sensitivity and precision. However, there are still insufficient reports on the potential routine use of LC-MS/MS applications, even though the specificity of LC-MS/MS should theoretically greatly improve the analysis of DBS samples [82].

In the case of rodents, blood samples should be taken from the tail vein after a short period of time in a warming chamber [83]. The general procedure is that the well formed blood drop should be applied to the printed side of the filter paper/card to allow a sufficient quantity of blood to soak through and completely fill a pre-printed circle. After collection, the filter paper/card should be allowed to air dry thoroughly on a non-absorbent surface for a minimum of 3hours in an open space at room temperature (15-22°C) away from direct sunlight [82]. Samples should not be heated, stacked or allowed to touch other surfaces [84]. The reason why blood spots should dry at least 3hours at room temperature is to ensure there is not any remaining moisture before shipment, which could induce bacterial growth and could alter elution properties, or facilitate degradation of unstable analytes [82][84]. However, the drying time depends on the type of paper/card and the blood volume applied [84]. Within 24hours of collection, the dried blood collection card should be prepared for shipment [82]. DBS samples should therefore be protected from humidity and moisture by covering them with a paper overlay and packing them in low gas-permeable zip-closure bags with desiccant packages and humidity indicator cards. DBS samples protected in this manner may be stored at room temperature for many weeks, months or years. However, samples that contain unstable compounds should be stored at a lower temperature (2-8°C, ≤-15°C or ≤-60°C) [84].

Collection paper/card used for human sampling is manufactured from high-purity cotton linters and is certified to meet performance standards for sample absorption and lot-to-lot consistency set by the Clinical and Laboratory Standards Institute [81]. The vast majority of reported methods for DBS analysis have standardised on Whatman 903 paper because of its well characterised performance [84]. Some properties of the DBS paper/card like particle retention, pore size and thickness determine the loading capacity and spreadability of blood sample, uniformity and absorption characteristics. Usually, 3.2mm or 6mm disks are punched out for analysis [84]. The filter paper/card matrix stabilizes most analytes in dried blood spots, but the rate of sample degradation will vary by analyte. Stability should be evaluated prior to sample collection because this has direct implications for sample handling and storage [81]. DBS as proven to prevent the stability of most samples during large periods of time [82]. Although refrigerating or freezing samples promptly after drying is always advisable to minimize the chances of degradation, the stability of most analytes in DBS provides flexibility in the collection of samples in field settings. For long-term storage, samples should be packed with desiccant and frozen in a reliable laboratory-grade freezer to ensure sample integrity [81].

DBS offers a series of advantages in comparison to whole blood, plasma or serum sample collection. In the case of rodents, the maximum blood volume permissible to take from an individual animal is limited [85]. If a smaller volume of blood is taken from the rodents, on one hand, the animal does not have to be sacrificed, meaning that the costs associated per animal use are decreased and on the other hand, several samples can be collected from the same animal, allowing serial exposure profiling at multiple occasions and monitoring of the effect of a drug over time in the same animal. In addition, the usual sampling route is by an orbital sinus puncture, however this technique is potentially harmful when is not performed by skilled technicians. Ocular damage due to poor practice of this technique would eventually require the termination of the animal. The tail vein sampling method is relatively less technically challenging and the risk to the animal is minimal. Pediatric clinical studies have driven a particular increase in the use of juvenile animals. Depending on the age of the animal, there are some limitations in the total circulating blood volume, which may render the standard sampling techniques unfeasible, resulting in the usage of terminal blood sampling techniques, thereby increasing the number of animals required to generate data. Even by pooling samples of different young animals to obtain a sufficient plasma volume for analysis, variability or mean exposure in groups cannot be assessed. Given the emergent use of transgenic mice, the costs per animal have become an important parameter to take into consideration when choosing the sampling technique [83][84].

In terms of storage and transport, DBS offers a simpler storage and easier transfer because there is no need for freezers or dry ice in most applications, unlike prepared plasma and blood samples. Because blood is spotted onto specially designed filter paper/card, an even spreading is promoted and the samples present a potentially increased stability. In terms of sample processing for LC-MS/MS analysis, the DBS method presents advantages over the plasma methods because of smaller volume of blood required, no centrifugation for plasma separation and no freezing temperature for sample storage and shipment is needed [83][84]. Due to the stability of DBS samples in laboratory freezers for long periods of time, samples can be analysed at the scientists convenience, and reanalysed as new biomarkers of interest and techniques emerge [81]. A typical drop of blood will contain approximately 50µL of whole blood and will result in a DBS sample approximately 12mm in diameter. Such a spot will yield approximately seven 3.2mm discs of blood [81]. However, this method also presents disadvantages. The capillary blood obtained through skin puncture differs from blood obtained through venipuncture, because the capillaries contain neither venous nor arterial blood. Capillary blood is actually more similar to arterial than to venous blood and because of the local trauma created

when the skin is punctured, capillary blood is usually contaminated with interstitial and intracellular fluids. The degree of contamination is affected by the amount of pressure exerted around the puncture site in order to increase blood flow. Excess squeezing can therefore influence the analytic values obtained from these samples [82]. However, the utilization of heating pads, allows not only to increase blood flow, which decreases the amount of squeezing needed, but also the arterialization of venous blood in superficial veins [86][87]. Also, due to the collection of surface blood, the most apparent limitation of this technique is the potential for surface contamination; however, this is minimized by the sanitation of the site prior to sampling, which is also common to other sampling techniques [83]. Different blood volumes spotted onto DBS paper/card may result in different measured analyte concentrations from a fixed punch size and hematocrit value. Accurate pipetting using a calibrated pipette, followed by cutting the whole spot from the paper/card appears to be the only option for accurate and precise absolute quantification of the analyte of interest [84]. Many routine clinical tests require a serum matrix and DBS may cause reduction in sample integrity or interference. Also, most modern clinical laboratories are highly automated and this investment in automation is planned around venous blood [82]. Therefore assay protocols must be developed for DBS and validated for accuracy, precision, reliability and limits of detection. DBS results may not be directly comparable with those derived from serum or plasma. Assays of DBS samples provide results that represent the concentration of an analyte in whole blood. For serum and plasma samples, the cellular fraction of whole blood is removed following centrifugation, therefore the concentration of analytes in these samples, is higher relative to whole blood. Corrections for data comparison are important because the established clinical cut-points are typically based on serum/plasma samples collected via venipuncture. The relatively small quantity of sample collected with DBS may also be an insurmountable limitation for some analytes that require large volumes of blood, particularly in the early stages of research before more-sensitive protocols become available. Few labs have direct experience with DBS analytic method. Therefore, finding a collaborating lab for sample analysis can be a challenge, although this situation is likely to improve as interest in DBS sampling grows [81].

2.4. High pressure liquid chromatography coupled to mass spectrometry (HPLC-MS)

A variety of methods have been used to measure the isotope enrichment of several metabolites, such as glucose. Most of these methods are based on the technique of gas chromatography coupled to mass spectrometry (GC-MS). However, in this case, the sample requires an extensive pre-treatment and derivatization before being injected into the system. The greatest advantage of LC-MS over GC-MS is the fact that the sample preparation is substantially reduced, and no derivatization is needed [88].

LC-MS has been used in many of the "omics" areas, such as proteomics, lipidomics and metabolomics. This technique offers greater sensitivity and selectivity, minimizing the occurrence of false negatives and false positives; it is capable of analysing a broad range of molecules, and detecting unique biomarkers within a complex sample; and its faster than other techniques [89]. While chromatography alone cannot resolve different analytes with the same retention times (RT), when coupled to MS they can be easily differentiated, since MS is able to resolve analytes according to their mass/charge ratio (m/z). Hence it is the combination of both techniques that has made LC-MS such a powerful technique.

2.4.1. High Pressure Liquid Chromatography (HPLC)

High pressure liquid chromatography (HPLC) is by far the best technique for the separation of metabolites by RT, separating high- and low- concentration metabolites as well as concentrating individual metabolites during the chromatography. The basis of a liquid chromatography is that it separates molecules according to their mechanism of interaction with the stationary phase after the sample has been inserted into the column (Fig. 2.3). The mobile phase is a liquid delivered under high pressure to ensure a constant flow rate and thus make the chromatography reproducible, while the stationary phase is packed into a column capable of withstanding high pressures. A chromatographic separation occurs if the components of a mixture interact to different extents with the mobile and/or stationary phase and therefore take different time to move from the position of sample introduction to the position at which they are detected. Among the different interactions between solute and stationary phase, there are i) adsorption chromatography; ii) partition chromatography; iii) ion exchange chromatography; iv) size exclusion chromatography; and v) affinity chromatography [89].

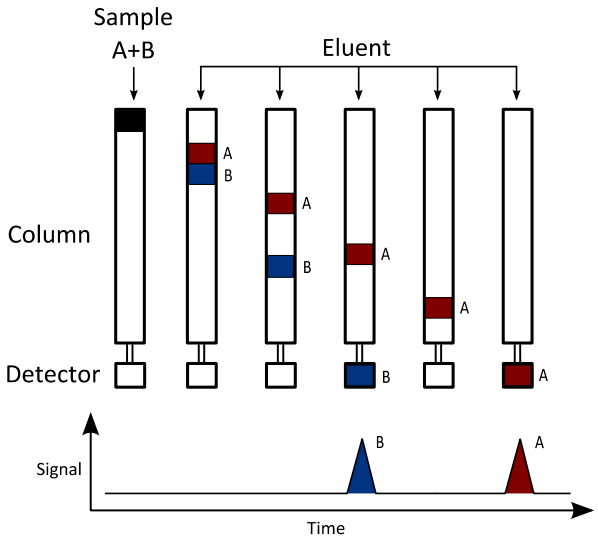

Fig. 2.3| Schematic illustration of the separation of two components (A and B) by chromatography. The sample is placed in the column, and depending on the velocity by which different molecules pass through, they can be separated and consequently detected at different times. The stationary phase (matrix) will determine the different interaction of the molecules, thereby determining their velocity Adapted from [144].

2.4.2. Mass Spectrometry (MS)

MS provides both qualitative (structure) and quantitative (molecular mass and/or concentration) information of analyte molecules after their conversion to ions. These ions are then attributed a positive or negative charge, separated by charges in a magnetic or electrostatic field in vacuum, and their mass analysed, based on their m/z.

2.4.2.1. Ionization

Once the sample components have been separated in the LC system, analytes must be converted into ion species. In the early years of the LC-MS technique, sample ionization constituted a problem, since it caused analyte destruction. Since then, considerable progress has been made regarding the ionization, that together with the research and development of the LC-MS technique, lead to the introduction of soft ionization techniques [90]. Nowadays, the most used ionization methods in LC-MS include electrospray (ESI) and atmospheric-pressure chemical ionization (APCI) [67][89].

Due to its ease of use, low solvent consumption, capability of being used for large analytes, wide polarity range and ability to be applied to thermally labile compounds, ESI is most commonly employed for LC-MS based metabonomics (Fig. 2.4). Generally, ESI is ideal for semi polar and polar compounds, whereas APCI is more suitable for neutral or less polar compounds [64]. ESI is a soft ionization method that offers excellent quantitative analysis and high selectivity [68]. The solvent emerging from the needle breaks into fine threads which subsequently divide

into small droplets when subjected to ionization in positive or negative mode. These charged droplets shrink due to liquid evaporation, and as a result, the distance between the charges on the surface becomes smaller and smaller, leading to a field-induced electrohydrodynamic droplet disintegration or Coulomb explosion. This results in the formation of highly-charged microdroplets, further resulting in ions appearing in the gas phase, either due to emission or desorption of pre-formed ions from the droplet surface or due to soft desolvation of pre-formed ions [91]. Because ions are generated directly from the liquid phase into the gas phase, this technique is established as a convenient mass analysis platform for connecting both interfaces, the LC and the MS analysis.

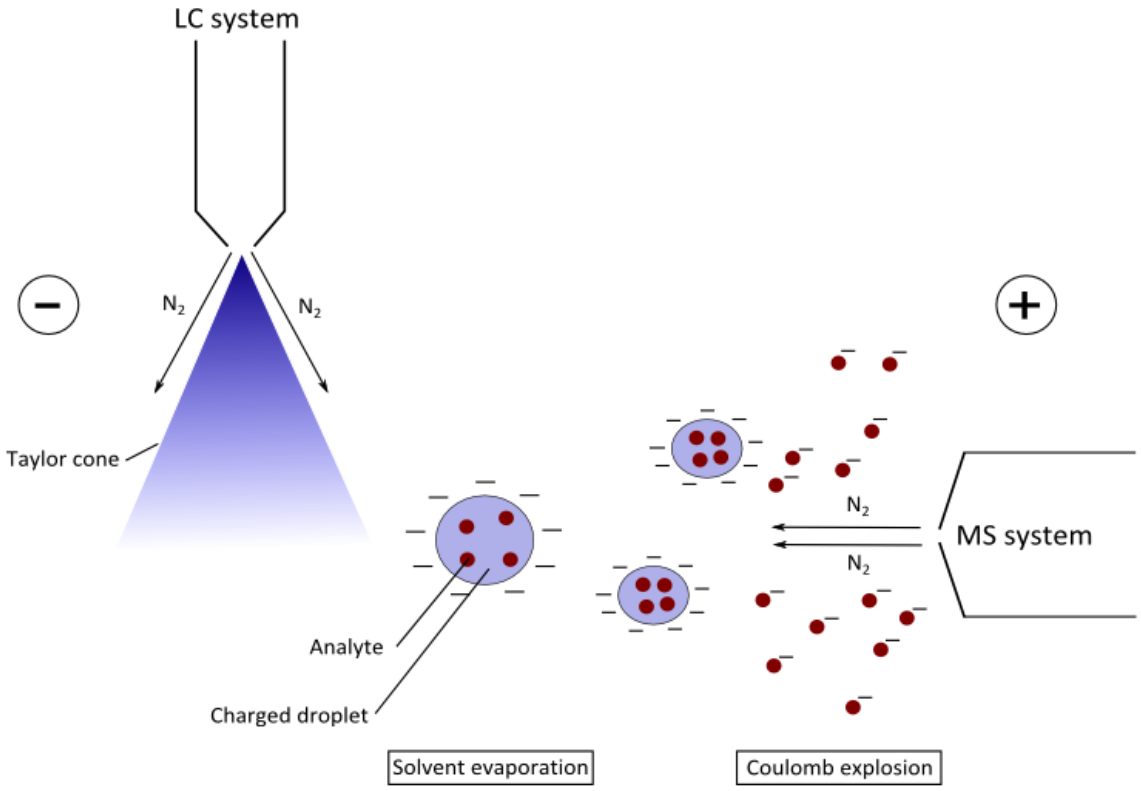

Fig. 2.4|Sequence of events leading to ion formation in electrospray ionization (ESI). After leaving the capillary and before the droplets go into a series of divisions, there is the formation of a Taylor cone for brief moments, as the charged droplets enter the evaporation chamber. In the evaporation chamber the droplets will gradually evaporate, and nitrogen gas will increase this evaporation and force the molecules within the droplets to be closer. Since all droplets have the same charge, they will repulse amongst each other, leading to the Coulomb explosion.

2.4.2.2. Tandem MS – Quadrupole System

After producing the ions, it is necessary to separate them into different m/z ratios, determine these m/z values and then measure the relative intensities of each group of ions [89]. The most common mass analyzers are the quadrupole and the time-of-flight (TOF) based analyzers [68].

As the name suggests, a quadrupole consists of four rods (Fig. 2.5). The opposite pairs of these rods are connected electrically and a voltage, consisting of both radiofrequency (RF) and direct-current (DC) components, is applied, being the RF components on the two pairs of rods 180° out-of-phase. At a specific value of these voltages, ions of a particular m/z follow a stable trajectory through the rods until they reach the detector, as for the other ions, they become unstable and collide with the quadrupoles. The mass spectrum can therefore be produced by varying RF and DC voltages in a systematic way to bring ions of increasing or decreasing m/z ratios to the detector. The quadrupole analyser is used in LC-MS because of a fast scanning mass analyzer, and use of low voltages, which make it tolerant to relatively high operating pressures such as those encountered in the LC-MS system [89].

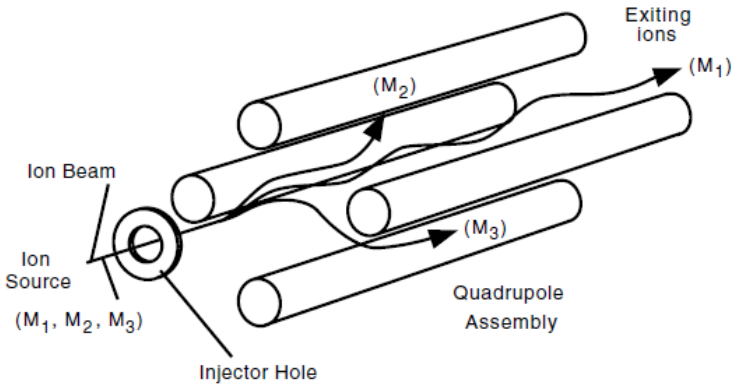

Fig. 2.5| Schematic of a quadrupole mass analyser. By selecting the voltages of the quadrupole rods, it is possible to select ions according to their m/z values. Only the ions with a stable trajectory will go through the quadrupole analyser and reach the detector (M1), while other (M2, M3) are deflected to the rods [92].

Tandem mass spectrometry (MS/MS) is a term which covers a number of techniques in which one stage of MS is used to isolate an ion of interest, and a second stage is then used to probe the relationship of this ion with others, from which it may have been generated [89].

To perform tandem mass analysis with a linear QqTrap instrument, three quadrupoles are placed in series. The second set of rods is not used as a mass separation device but as a

collision cell (q2), where fragmentation of ions transmitted by the first set of quadrupole rods (Q1) is carried out, and as a device for focussing any product ions into the third set of quadrupole rods (Q3). Both sets of rods may be controlled to allow the transmission of ions of a single m/z ratio or a range of m/z values to give the desired analytical information [89]. Quadrupole-time-of-flight (Q-TOF) analyzers offer significantly higher sensitivity and accuracy over tandem quadrupole instruments when acquiring full fragment mass spectra. But the quadrupole ion trap mass analyzer however, can be used for both MS scanning and MS/MS studies, because it allows the isolation of one ion species [68].

2.4.2.3. Scan Modes

There are several scan mode techniques for tandem mass spectrometry, such as product-ion scan, and multiple reaction monitoring (MRM). The most commonly used scan mode in metabonomics is the MRM for targeted analysis and in metabolomics, is the product-ion scan for non-targeted screenings and identification of metabolites.

In the MRM, the scan is carried out by setting each of the stages of MS to transmit a single ion (Fig. 2.6). Each quadrupole has a separate function: the first quadrupole (Q1) filters a preset m/z to select an ion of interest (precursor ion), which is then fragmented in the second quadrupole (q2), a collision cell, which can use argon, helium or nitrogen as the collision gas. As for the third quadrupole (Q3), it analyses the fragment ions (product ion) generated in q2 [68][93]. By fragmenting the analyte and monitoring both parent and one or more product ions simultaneously, greater specificity is achieved for the targeted analysis [94].

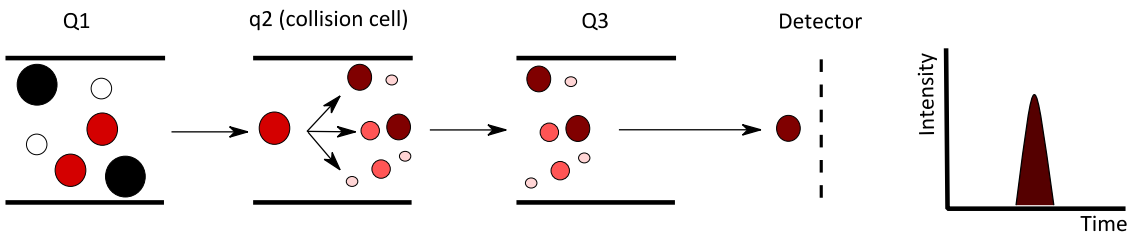

Fig. 2.6| Schematic of the multiple reaction monitoring (MRM) on a triple quadrupole mass spectrometer. In the MRM the targeted parent ion is selected in the first quadrupole (Q1) and enters the second quadrupole (q2) where it undergoes collision-induced dissociation (CID). One or more fragment ions are then selected according to the predefined transitions and the signal provides the spectral counts for quantification.

2.5. Data Processing

The data processing step consists in transforming raw data into a format that is easy to use in the subsequent data analysis steps. There are several parameters one needs to take into consideration when acquiring. Sensitivity is defined as the slope of a plot of analyte amount vs. signal strength, which in the case of MS, refers to the electric charge of the analyzed ion species reaching the detector per mass of analyte used. The parameter of sensitivity is dependent not only on the ionization efficiency, but also on the extraction of ions from the ion source, the mass range set to be acquired, and the transmission of the mass analyzer. The signal-to-noise ratio (S/N) provides a quantitative measure of the signal's quality by quantifying the ratio of intensity of a signal relative to noise, being the latter dependent from the electronics of the mass spectrometer. The resolution of the peaks is also important to perceive, because it gives the smallest difference in m/z that can be separated for a given signal, allowing to increase the systems accuracy [89][95].

Very rarely is a single mass spectrum able to provide complete analytical information of a sample. The mass spectrometer is therefore set up to scan, repetitively, over a selected m/z range for an appropriate period of time. At the end of each scan, the mass spectrum obtained is stored for subsequent manipulation before the next spectrum is acquired [89]. A typical processing pipeline of a spectrum goes through filtering, feature detection, alignment and normalization. Filtering processes the raw data with the purpose of removing chemical noise (caused by molecules within buffers and solvents, being especially strong at the beginning and end of the elution), random noise (attributed to the detector) or a baseline. Feature detection is used to detect signals caused by true ions from the raw signal and avoid detection of false positives. There is always some variation in RTs of a metabolite across different sample runs, hence alignment is responsible for clustering measurements across different runs and combining data from different samples to correct for RT. And finally, normalization is able to remove systematic variations between samples, while retaining interesting biological variation [96].

2.6. Method Validation

To ascertain if the quantification results are reliable, consistent and reproducible, the method used needs to be validated first. In scientific studies it is important to ascertain data quality, since unreliable results may lead to over- or underestimation of effects, false

interpretations and misguided conclusions. Unless contested, these errors will likely multiply within the scientific community, or become part of the accepted general knowledge and lead to further misinterpretations [97]. Since laboratory results may be used for case-report interpretation, by judicial authorities for implementation of legal measures or by medical doctors for patient treatment, it is of far most importance to certify the quality of the method developed for analysis. For these reasons, peer-reviewed scientific journals have high demands for the validation of newly developed methods [98].

An analytical method needs to be validated whenever implementing a bioanalytical method for the first time. However, there is not a consensus of which parameters should be evaluated, of the experimental set-up, the choice of appropriate decision criteria and statistic tests, which is due to the existence of so many different guidelines regarding method validation. For example, some international guidelines as the International Union of Pure and Applied Chemistry (IUPAC), the United States Food and Drug Administration (FDA), the World Health Organization (WHO), the International Organization for Standardization (ISO) are the most commonly used, however they all differ amongst each other, for that reason it is important that the laboratory standardizes its criteria. The essential parameters for method validation defined by the Food and Drug Administration (FDA) Guidance are: selectivity, sensitivity, accuracy, precision, reproducibility, and stability [99]. Although these parameters are important in method validation, they are only guidelines, depending on the analyst to determine how to do the validation according to costs, risks and technical possibilities.

Method validation should consist in: system qualifications, sampling, sample preparation, analysis and data evaluation. A system qualification refers to the suitability of the instrument and materials for the intended analysis, the analysts qualifications and the established protocols. The sampling step consists in choosing a sample representative of the material as a whole. Sample preparation is where some time should be spent on the selection of a proper sample preparation procedure. The analysis is related to the certainty level of the instrument. And finally, data evaluation refers to the summary and analysis of data by using mathematical and statistical tests.

3. OBJECTIVE

3. OBJECTIVE

Given that a key enzyme for TAG hydrolysis is absent in ATGL$^{-/-}$ mice, the skeletal muscles of these animals should be more dependent on other energy sources, such as glucose, resulting in increased oxidative glucose disposal. The increase in glucose oxidative disposal, may lead to an increased production of glucose from gluconeogenesis by the skeletal muscles, therefore EGP will be determined in order to elucidate these mechanisms. If glucose oxidation is increased in AGTL$^{-/-}$, the difference between glycolytic and glucose oxidation fluxes will be smaller, resulting in less net lactate production from glycolysis and smaller efflux of lactate into the liver for re-synthesis into glucose. Thus, this hypothesis will be addressed by evaluating Cori cycle activity comparing ATGL$^{-/-}$ mice with wild-type mice.

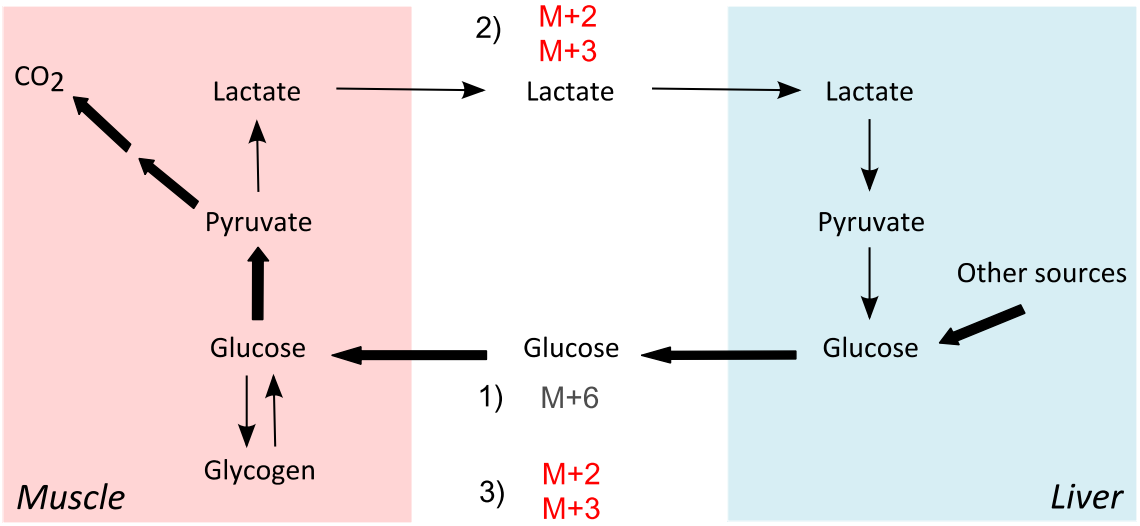

Fig. 3.1| Glucose and lactate inter-conversion between liver and muscle. In ATGL$^{-/-}$, the glucose requirement for oxidation is increased due to a reduced availability of FAs. Therefore, it is expected that glucose production and muscle oxidation fluxes, shown by the heavy arrows, will dominate. Glucose turnover will be evaluated through dilution of the infused [U-$^{13}C_6$]glucose (M+6 enrichment of plasma glucose). In turn, assessment of partially labelled glucoses [1,2-$^{13}C_2$]glucose and [1,2,3-$^{13}C_3$]glucose (M+2 or M+3) via recycling through lactate formation, in relation to the amount of [U-$^{13}C_6$]glucose precursor, (i.e. the ratio of M+2 and M+3 to M+6) will allow the evaluation of the Cori cycle.

Stable isotope tracers are commonly used for metabolic studies, in order to follow the products of metabolism derived from that tracer. In this case, to study EGP and the turnover of glucose by the Cori cycle, [U-$^{13}C_6$]glucose (M+6) was used as a stable isotope tracer. Quantification of the enrichment of the [U-$^{13}C_6$]glucose precursor will allow the assessment of EGP rate. On the other hand, quantification of partially labelled glucoses [1,2-$^{13}C_2$]glucose (M+2) and [1,2,3-$^{13}C_3$]glucose (M+3) enrichment of will allow the measurement of Cori cycles activity.

DBS are commonly applied for sampling blood for analysis of metabolic diseases in infants, however, the scientific interest in this sampling technique as increased due to the improvement on the analysis sensitivity with instruments like LC-MS. Because of the limited sample volume of mice, and in particular, for $ATGL^{-/-}$ mice, where low plasma glucose levels are expected, whole blood samples for the project were sampled in filter paper and analysed by LC-MS/MS.

In summary, plasma glucose enrichments from $ATGL^{-/-}$ mice and wild-type mice infused with [U-$^{13}C_6$]glucose were quantified by LC-MS/MS. Before quantifying the samples, method development and validation are necessary to certify the consistency of the results. EGP quantification and evaluation of the Cori cycle activity of the $ATGL^{-/-}$ mice will allow a better understanding of their metabolism, which in turn might lead to the development of new therapies for the control of FA release and other lipolytic products involved in the development of insulin resistance and T2DM.

4. MATERIALS AND METHODS

4. MATERIALS AND METHODS

4.1. Instrumentation

The LC system used for all analysis was an Ultimate™ 3000 LC system (LC Packings, Dionex). The MS used was a hybrid triple quadrupole/linear ion trap 4000 QTRAP® LC-MS/MS system equipped with an ESI Turbo V ion spray™ source (AB Sciex). The software operating the LC system was the Chromeleon® 6.80 (Dionex) and operating the MS system was the Analyst® 1.5.1 (ABSciex).

4.1.1. Equipments

- Analytical balance CP 224S (Sartorius)
- Bench-top centrifuge Minispin® (Eppendorf)
- Concentrator Plus (Eppendorf)
- Microcentrifuge QS 7000 (Edward Co.)
- Sonicator VibraCell™ 75041 (Sonics®)
- Ultrasonic bath Sonorex™ (Bandelin)
- Vortex MS3 basic (IKA®)

4.1.2. Materials

- Column Luna NH_2 (3µm, 100Å, 150×2.00mm)
- Combiptip® (Eppendorf)
- Microcentrifuge tubes: 500µL; 1.5mL; 2mL
- Micropipettes Research® plus (Eppendorf)
- Multipipette® Plus (Eppendorf)
- OMIX C18 pipette tips, 100µL (Agilent Technologies)
- Vials, 500µL (Cronus®)

4.1.3. Standards and Reagents

- [U-$^{12}C_6$]glucose, 1-^{13}C 99% (Cambridge Isotope Laboratories, Inc.)
- [1,2-$^{13}C_2$]glucose, 99atom% (Omicron Biochemicals, Inc.)
- [1,2,3-$^{13}C_3$]glucose, 99atom% (Omicron Biochemicals, Inc.)
- [U-$^{13}C_6$]glucose, ^{13}C 99% (Cambridge Isotope Laboratories, Inc.)
- [U-$^{13}C_6$, U-$^{2}H_7$]glucose, ^{13}C 99%; 1,2,3,4,5,6,6-$^{2}H_7$, 97-98% (Cambridge Isotope Laboratories, Inc.)
- [U-$^{12}C_6$]fructose, ≥99% (Sigma Aldrich®)
- Acetonitrile LC-MS (Biosolve)
- Ethanol absolute UV-IR-HPLC (Panreac)
- Water HiPerSolv CHROMANORM® for HPLC (VWR®)

4.1.4. Solutions preparation

Due to the instability of glucose analytes, solutions had to be prepared periodically. Therefore, in this section is only presented how they were prepared in general terms.

Individual stock solutions of the analytes [U-$^{12}C_6$]glucose, [1,2-$^{13}C_2$]glucose, [1,2,3-$^{13}C_3$]glucose, [U-$^{13}C_6$]glucose, [U-$^{13}C_6$, U-$^{2}H_7$]glucose and fructose were prepared by weighting 1-3mg and adding 1mL of H_2O. Stock solutions were stored at -20°C.

Mixed stock solution of [U-$^{12}C_6$]glucose/[1,2,3-$^{13}C_3$]glucose and [1,2-$^{13}C_2$]glucose/[U-$^{13}C_6$]glucose were prepared by diluting the respective individual stock solutions in water at a concentration of 1mM. From the mixed stock solution at 1mM, every working solution was prepared by dilutions with water.

4.2. Analytical method development

Fragmentation spectra of each analyte was obtained by injecting each one into the MS by direct infusion with a 1mL syringe at a flow of 10µL/min, where 200µM solutions of [U-$^{12}C_6$]glucose, [1,2-$^{13}C_2$]glucose, [1,2,3-$^{13}C_3$]glucose, [U-$^{13}C_6$]glucose, and [U-$^{13}C_6$, U-$^{2}H_7$]glucose were analyzed individually. A collision energy (CE) ramping was obtained for each of the analytes, to acquire the fragments produced by each of them. Moreover, declustering potential

(DP) was evaluated to see which potentials best separated clusters of the analytes studied in this project. Analysis of the fragmentation spectra was performed on the Peak View™ 1.1.1.2 software (ABSciex).

4.2.1. Chromatographic settings

Chromatographic separation was performed on a Luna NH_2 (3µm, 100Å, 150×2.00mm) column, for better monosaccharide separation at ambient temperature. Retention time for all glucose analytes is approximately 8min. Flow rate was 150µL/min and running time for each sample was 15min. After sample injection, one blank (H_2O) of 4 min running and afterwards a second blank (H_2O) with an 8min running program are injected. Elution gradients of the three LC programs are represented on Table 4.1 Injection volume for a sample was 1µL, while for the blank programs were injected 19µL.

Table 4.1| Elution gradients used on each LC program.

Running program	Time gradient (min)	Mobile phase	
		H_2O (%)	ACN (%)
Sample (15min)	0	20	80
	1	20	80
	5	40	60
	15	80	20
Blank - 1 (4min)	Isocratic	95	5
Blank - 2 (8min)	0	95	5
	1	20	80
	8	20	80

4.2.2. Mass spectrometry settings

The mass spectrometer was controlled by Analyst® 1.5.1 (ABSciex). Samples were injected at 150µL/min by ESI, and the source was operated in the negative ionization mode. The study of glucose in the negative ionization mode is more advantageous, because of the low level of formation of cationic adducts with ubiquitous ions such as Na^+, which in the positive mode would deteriorate the signal from the protonated molecule [100][101]. The ionization source

operated in the negative mode at an ion spray voltage of 4500V, the nebulizer gas 1 (GS1) was 35psi, the nebulizer gas 2 (GS2) was 30psi and the temperature was at 450°C. In the blank programs, the 4min blank was operated in the positive mode, while the 8min blank program was operated in the negative mode. Glucose enrichments were quantified using the multiple reaction monitoring (MRM) triple quadrupole scan mode. To define the MRM transitions, and the ideal MS parameters for the different analytes, 200µM standard solutions of each analyte were analysed as described on 4.2. MS parameters were the same for all transitions: collision gas (CAD) 6psi, curtain gas (CUR) 30psi, collision cell exit potential (CXP) -8eV, entrance potential (EP) -4eV, dwell time 100ms, declustering potential (DP) -50eV, except collision energy (CE), which differs amongst transitions as represented on Table 4.2. MRM transitions for monitoring [U-$^{12}C_6$]glucose were 179/89 and 179/119, for [1,2-$^{13}C_2$]glucose, 181/89, 181/91 and 181/119, for [1,2,3-$^{13}C_3$]glucose, 182/89, 182/92 and 182/120, for [U-$^{13}C_6$]glucose, 185/92, 185/123 and 185/61 and for the internal standard (IS) [U-$^{13}C_6$, U-$^{2}H_7$]glucose were 192/94 and 192/128. Peak areas were integrated using the Multiquant™ 2.1.1 software (ABSciex).

Table 4.2| MRM method with the m/z values selected in Q1 and Q3 and the CE used for each transition.

Analyte	Transition	Q1 (m/z)	Q3 (m/z)	CE (eV)
[U-$^{12}C_6$]glucose	179/89	179.1	89.1	-11
	179/119	179.1	119.1	-11
[1,2-$^{13}C_2$]glucose	181/89	181.1	89.1	-12
	181/91	181.1	91.1	-12
	181/119	181.1	119.1	-12
[1,2,3-$^{13}C_3$]glucose	182/89	182.1	89.1	-11
	182/92	182.1	92.1	-11
	182/120	182.1	120.1	-11
[U-$^{13}C_6$]glucose	185/92	185.1	92.1	-11
	185/123	185.1	123.0	-11
	185/61	185.1	61.0	-24
[U-$^{13}C_6$, U-$^{2}H_7$]glucose	192/94	192.1	94.1	-13
	192/128	192.1	128.1	-13

4.3. Animal model

The animals used in this project were part of a collaboration with the Maastricht University (Netherlands) and the Graz University (Austria). Fourteen wild-type mices and 10 whole-body $ATGL^{-/-}$ mice were used, and both belonged to a C57BI6 strain, with the same genetic background. Breeding was performed amongst heterozygotic mice in the Maastricht University, where they were given a standard chow diet and were kept in cycles of 12h/12h with and without light.

Table 4.3| General characteristics of the $ATGL^{-/-}$ (knock-outs) and wild-type groups.

Group	n	Age (Mean±SD) (weeks)	Weight (Mean±SD) (g)
Knock-out	10	8.5±1.6	23.4±3.7
Wild-type	14	9.1±1	26.3±4.2

Animals were fasted for 6 hours and anesthetized with 1.5% isofluorane given by a gas mixture (2:1 O_2/N_2O) through a facial mask. Then, they were given a primed-constant infusion of [U-$^{13}C_6$]glucose (6.25µmol/kg prime, at a constant velocity of 5µmol/kg/min). Infusion was performed for 120min.

Bloodspots were collected, with the mice under anaesthesia, directly on to a filter paper at 105, 110 and 115min. At the end of the 120min infusion, plasma was recovered and frozen. For a subgroup of animals, bloodspots were collected before the start of tracer infusion (0min) in order to obtain background ^{13}C levels. Besides the blood spots, the infusate was also harvested on to a filter paper (IM 1, 2 and 3), in order to control the different enrichments, because the infusion was not always made with the same stock solution, since the animals received it in different days/weeks.

For the preliminary tests and validation studies, other mice samples were used. Blood was drawn from 6 different mice of the B10.Q strain. Breeding was performed amongst heterozygotic mice in the University of Coimbra, where they were given a standard chow diet and were kept in cycles of 12h/12h with and without light. Bloodspots were collected, with the mice under isofluorane anaesthesia as well.

4.4. Calibration curves

Calibration curves express the relationship between instrument response and known concentrations of analyte. The concentrations of the calibrants should be evenly spaced and the number of calibrants used in the calibration curve's construction should be six or more (including a blank or calibration standard with a concentration close to zero), being this number defined by the expected range of analytical sample values [97][98], which means that interpolation of the results is required, rather than extrapolation. A calibration curve should be generated for each analyte of interest, and it is important to define the correct form of the "curve" of the calibration data, to ensure that data obeys a linear relationship, before using linear regression [89][97].

One of the problems in the construction of calibration curves is that standard solutions usually are made up in pure solvents and the obtained signal intensities will not reflect the effect of the matrix present in the "unknown" samples with the analyte or the IS or the effect the matrix might have on the mass spectrometer [64][89]. One approach to the matrix effects problem is to do a clean-up prior to analysis and/or apply chromatographic separation. However it is not always possible to develop a simple procedure to solve this problem, especially if the matrix is quite complex. Calibration standards can be made up in a matrix extract rather than in a pure solvent, but there is no guarantee that the composition of that extract is identical to the matrix in which the analytes of the study are in. Calibration could be based on the method of standard additions, which involves the addition of known amounts of each of the analytes of interest to a sample, being the signal increase related to the amount of analyte added and to the amount originally present in the sample, meaning that for each sample, several standards would have to be analyzed. Another approach is to use internal standards within pure solvent calibrants, which would improve precision [89][97]. Most authors advice that for bioanalytical methods, calibrators should be prepared by spiking blank matrixes [97]. But in some cases, that approach may not be the best given the analytes in question. First, the matrix effect in ion suppression or enhancement should always be considered, especially in LC-MS methods using ESI, which means that the relationship between peak area and actual concentration could be compromised [102], however there is no guarantee that the blank matrix would behave precisely as the sample matrices. Another factor that should be considered is that, in the case of glucose, because it is an endogenous metabolite, and so it is not possible to use animal blank matrixes, the best course of action would be to either use the method of standard additions, which involves the preparation of a large number of samples [89], use surrogate matrixes, which

would not mimic the matrixes studied [103], or to use pure standard solutions containing an internal standard [104]. The utilization of a proper IS will overcome these issues, because since it should behave as the analytes of study, a ratio between the studied analyte and the IS will correct for any changes in manipulation, transport, degradation and ion suppression [89][102].

When performing pure standard solutions, they are usually prepared in the mobile phase of the LC system. Several studies have demonstrated the solubility of glucose with organic solvents, and throughout the literature, the best solvent to dissolve glucose as been water [105][106][107]. Therefore, pure water was the solvent chosen to solubilise the glucose analytes. Furthermore, formic acid is commonly used in small percentages within the mobile phase to improve peak resolution. However, in the case of glucose this monocarboxylic acid, degrades glucose [108], which is the reason why formic acid was not used in this project.

Analytes of interest were quantified using calibration curves with different known concentrations of standards. Stock solutions at the concentration of 1mM, containing [U-$^{12}C_6$]glucose and [1,2,3-$^{13}C_3$]glucose and another with [1,2-$^{13}C_2$]glucose and [U-$^{13}C_6$]glucose were prepared, and from this stock solutions, so did the 500µM, 30µM and 3µM solutions. Then, from these solutions, the other calibrant solutions were prepared. Fifty microliters of each calibrant solution were mixed with 50µL of the IS (30µM [U-$^{13}C_6$, U-$^{2}H_7$]glucose), diluting the calibrant solutions by half. Three replicates of two different calibration curves were prepared with a wide concentration range (0.15; 0.3; 0.45; 0.6; 1.2; 1.5; 2.1; 3; 6; 15; 30; 50; 100; 150; 250µM). The reason why two calibration curves were made instead of four (one for each analyte), is that given the results of the abundance of the different glucose isotopes for each analyte (section 5.2.2), it is possible to prepare the calibration curves together, as long as they do not influence one another. Therefore, the [U-$^{12}C_6$]glucose and [1,2,3-$^{13}C_3$]glucose were prepared together, as well as the [1,2-$^{13}C_2$]glucose and [U-$^{13}C_6$]glucose. The reason why such a wide range of calibrants was prepared is because of the different concentrations within different samples detected in the preliminary tests. Therefore, a wide calibration curve is built, to select the calibrants of interest according to the samples.

The FDA guideline recommends that randomization of samples should be avoided, as it could make the detection of carry-over problems more difficult [99]. In practice, to prevent these problems, it is recommended that following a blank sample, calibration samples should be analyzed from low concentration to high [98]. This recommendation was followed throughout this project for every calibration curve.

4.5. Sample treatment

The general process to extract analytes from the DBS samples is referred in the literature as an extraction with an organic solvent and gentle shaking or vortexing. After centrifugation, the resulting extracts are transferred to new tubes. These extracts can then be directly injected onto the LC-MS/MS system or dried for reconstitution with an MS-friendly solvent prior to analysis [84][109][110].

To prepare the samples for analysis in this project, 6.0mm DBS disks were punched, then added 50µL of IS solution (30µM [U-$^{13}C_6$, U-$^{2}H_7$]glucose), and 450µL of EtOH. The samples are, at this stage, within a 9:1 EtOH:H_2O solution. Samples were processed using an ultrasonic bath for 45min at room temperature and were centrifuged for 5min at 13,900×g [84][104][109]. Supernatant was transferred to a new micro centrifuge tube, evaporated at 60°C and resuspended in 50µL of H_2O [84][104][111]. Samples were sonicated with a cup-horn at 40%, for 2min, with pulses of 1sec and pauses of 1sec. After vortex and spin, samples cleaned up by solid phase extraction (SPE) using reversed phase packed zip-tips. This reversed phase process allows the binding of mostly hydrophobic compounds, and as glucose is hydrophilic, glucose will not be adsorbed and will be clean up from hydrophobic compounds, such as lipids. The first step in this SPE process is to activate the stationary phase with 40µL of 50%ACN:H_2O. Then, the C18 SPE zip tip is equilibrated with 120µL of 2%ACN:H_2O. Afterwards, 50 µL of sample pass through the C18 SPE zip tip and are harvested in a microcentrifuge tube. The same volume of 2%ACN:H_2O is added to elute any glucose that might be left behind and harvested with the sample, diluting it. The great advantage of these tips is that they are less time consuming than a chromatography and are able to remove contaminants in a single step. After new vortex and spin, samples were transferred to a vial for analysis.

4.6. Quantification

Quantification of analytes in metabonomics is critical in understanding biological processes. Therefore to assess the amount of analyte present on a given sample, the construction of a calibration curve is needed, but the most adequate features to build the calibration curves must be chosen.

An external standard is applied when a number of standards containing unknown amounts of the analyte of interest are analysed and the signal intensity of these standards is

plotted against the known concentration of the analyte of interest. The problem with external standardization is that it takes no account of matrix effects on the analytical signal or losses of analyte from the "unknown" standards during sampling, manipulation or storage. Standard additions, on the other hand, address the influence of matrix effects. An analytical measurement is made on the "unknown" standard, then a known amount of analyte is added, and a second analytical measurement is made. From the increase in analytical signal, is possible to calculate the analytes concentration by dividing the signal by the response factor, i.e. the signal per unit concentration. This method assumes the matrix has the same effect on the added analyte as on the analyte of the "unknown" standard, and also, does not account for analyte losses between sampling, manipulation or storage. The internal standard is designed to overcome these problems. An IS is a compound, which ideally should be an isotopically labelled analogue of the analyte that is added to the sample as early as possible in the analytical procedure, that compensates for any variability that might occur to the sample during sample preparation, manipulation and measurement, but still being differentiated from the analyte in study [97]. Analytical signals from both the analyte and the IS are measured for the standard calibrants and the "unknown" samples, and it is the ratio of these two signal intensities that is used to generate the calibration curve and determine the amount of analyte present in the "unknown" samples [89]. It is clear that stable isotope standards are critical for absolute quantification in metabonomics. However, the availability of commercial isotope-labelled standards is limited and the costs can become excessive to use in large scale. However the major obstacle in metabolite quantification is that the metabolite's signal intensity is not only dependent on its concentration, but also on its chemical structure and matrix [64]. In the case of this project, the IS used was the [U-$^{13}C_6$, U-$^{2}H_7$]glucose. This is an isotope analogue of glucose, so it can be used for all the analytes of this project as an IS, since all of them are glucose analogues as well.

After analysing the results of method validation, one transition for each analyte was selected for the quantification of samples. For [U-$^{12}C_6$]glucose, the transition 179/89 was selected, for [1,2-^{13}C] was the 181/91, for [1,2,3-$^{13}C_3$]glucose was the 182/92 and for [U-$^{13}C_6$]glucose was the 185/92. These transitions should belong to the analogue fragment among analytes, therefore, the transition used for the IS [U-$^{13}C_6$, U-$^{2}H_7$]glucose was the 192/94.

The regression model chosen for the calculi of the calibration curves equation was 1/x as determined on section 5.3.2.3. Using data from the calibration curves, the percentage of isotopic abundance was calculated to eliminate the amount of isotopic abundance that might be contributing to the analytes abundance within the samples. Isotopic abundance of [1,2-

$^{13}C_2$]glucose was given by its abundance on [U-$^{12}C_6$]glucose, calculated as described on equation (1) . In turn, to calculate the amount of [1,2,3-$^{13}C_3$]glucose given by [1,2-$^{13}C_2$]glucose, the amount of [1,2,3-$^{13}C_3$]glucose obtained from the [1,2-$^{13}C_2$]glucose/[U-$^{13}C_6$]glucose was calculated as described on equation (2) [112]. After obtaining the mean isotopic abundance, that contribution is removed from the peak area values by subtracting the amount of isotopic abundance [U-$^{12}C_6$]glucose adds to [1,2-$^{13}C_2$]glucose and the amount [1,2-$^{13}C_2$]glucose adds to [1,2,3-$^{13}C_2$]glucose.

$$\%[1,2-{}^{13}C_2]glucose\ isot.ab. = \frac{Amount\ of\ [1,2-{}^{13}C_2]glucose\ from\ [U-{}^{12}C_6]glucose}{Amount\ of\ [U-{}^{12}C_6]glucose} \times 100 \quad (1)$$

$$\%[1,2,3-{}^{13}C_3]glucose\ isot.ab. = \frac{Amount\ of\ [1,2,3-{}^{13}C_3]glucose\ from\ [1,2-{}^{13}C_2]glucose}{Amount\ of\ [1,2-{}^{13}C_2]glucose} \times 100 \quad (2)$$

After subtracting the isotopic abundance, the concentration of each analyte within the DBS sample was calculated using the equations of the calibration curves. With the concentration values, the enrichment of each analyte was calculated. Any problems that might have occurred with the chosen IS, can be overcome by this calculi, because it is expected that ^{13}C labelled glucose analytes, will have greater similarities with the other analytes than [U-$^{13}C_6$, U-$^{2}H_7$]glucose, which is deuterated. The enrichment, Ra and EGP were calculated as described on equations (3), (4) and (5) respectively.

$$Enrichment = \frac{C_{tracer}}{C_{tracer} + C_{tracee}} \quad (3)$$

C_{tracer} - concentration of tracer

C_{tracee} - concentration of tracee

$$Ra = \frac{E_{tracer}}{E_{tracee}} \times F \quad (4)$$

E_{tracer} - enrichment of tracer

E_{tracee} - enrichment of tracee

F - rate of tracer infusion

$$EGP = Ra - F \quad (5)$$

Ra - rate of appearance

F - rate of tracer infusion

Data which could not be interpolated from the calibration curves was eliminated and to eliminate outliers, a Grubbs test was preformed. Normalization of the distribution of the data was analysed by the Kolmogorov-Smirnov test. In turn, to the normal distributions the unpaired t-test was applied, while as a non-parametric test, the Mann-Whitney test was used.

4.7. Method and sample treatment optimization

4.7.1. Differentiation of fructose from glucose with the MRM method

Due to the structural similarity between fructose and glucose, they are often determined by LC-MS/MS together, because their parent ions and fragment ions present the same m/z [101].

Fructose MRM method was determined by injecting 200µM solution of [U-$^{12}C_6$]fructose by direct infusion with a 1mL syringe at a flow of 10µL/min as described for the glucose isotopes method development on section 4.2. Solutions of 1µM solution of fructose and 1µM solution of [U-$^{12}C_6$]fructose and [U-$^{12}C_6$]glucose were prepared and analysed by LC-MS/MS system using the same column as for the glucose analysis, as described on section 4.2.1.

4.7.2. Abundance of the different glucose isotopes

Because of the natural isotopic abundance of ^{13}C of 1.109% and impurities within the glucose isotopes analysed in this project, the abundance of all the glucose analytes studied under this project was assessed for each of the isotopes. Solutions of 250µM of each glucose isotope were prepared as a pure standard solution, and analyzed individually in the LC-MS/MS.

Additionally, 6 control DBS sample were processed and the natural abundance of the glucose isotopes assessed for biological samples as well. To every sample, 500µL were added of 9:1 EtOH:H_2O. Samples were processed using an ultrasonic bath for 45 min, then centrifuged for 5min at 13,900×g. The supernatant was transferred to another micro centrifuge tube and evaporated at 60°C under vacuum. Samples were resuspended in 50µL of H_2O and sonicated with the cup-horn at 40% for 2min with pulses of 1sec and pauses of 1sec. After vortex and spin, samples were cleaned up using a C18 SPE zip tip. To activate the stationary phase, 40µL of 50%ACN:H_2O were added to the zip tip, and then 120µL of 2%ACN:H_2O for equilibration. Afterwards, 50 µL of sample passed through the C18 SPE zip tip and were harvested. The same volume of 50%ACN:H_2O was added to elute any glucose that might be left behind and harvested with the sample, diluting it. Also vortex and spin were performed before transferring the samples into a vial for analysis. No IS was added to these samples.

4.7.3. Evaluation of the influence of C18 SPE clean-up in glucose analysis

The best percentage of ACN for elution that is used at the final stage of the C18 SPE step, after the sample has passed the C18 SPE zip tip was studied. A solution containing 500µM of [U-$^{12}C_6$]glucose was prepared. The C18 SPE zip tip was then used as described on section 4.5. To activate the stationary phase 40µL of 50% ACN: H_2O were passed through the zip tip, and then 120µL of 2% ACN:H_2O were passed to equilibrated it. Then 50µL of the 500µM [U-$^{12}C_6$]glucose solution was passed through the zip tip and harvested (0% ACN:H_2O). The zip tip was then eluted with different percentages of ACN:H_2O, 2, 10, 20, 30, 40, 50, 60, 70 and 80% respectively, being each consecutive elution volume harvested for analysis. Each sample was then evaporated at 60°C under vacuum and resuspended in 100µL of 2% ACN:H_2O. Samples were sonicated with the cup-horn at 40% for 2min with pulses of 1 sec and pauses of 1sec. After vortex and spin, samples

were diluted in order to inject only 25pmol into the MS system in the flow injection analysis (FIA) mode, where samples are analyzed by LC-MS/MS without the use of a column.

4.8. Analytical method validation

The calculi, the statistical tests, and the criteria applied were all performed with the help of a Microsoft Excel® spreadsheet created for this purpose. The specific criteria used by this Excel® spreadsheet are presented below.

4.8.1. Selectivity

Selectivity is the ability of the method to distinguish an analyte unequivocally from any other components present in the sample matrix, which might include impurities, degradents, and other matrix components. [99][113]. It is recommended to start the validation study with a test on selectivity, because if this parameter is not acceptable, major changes may have to be applied to the method [97].

The selectivity was evaluated by using six blank matrixes which were spiked with 5nmol of [U-$^{12}C_6$]glucose/[1,2,3-$^{13}C_3$]glucose, other six with 5nmol of [1,2-$^{13}C_2$]glucose/[U-$^{13}C_6$]glucose and compared with the six blank matrix without the spike (negative samples). The blank matrix negative controls were not spiked, not even with IS. To prepare the samples for analysis, the DBS were punched, the positive samples spiked, and 500µM of a 9:1 EtOH:H_2O solution were added to both positives and negatives. To the spiked samples was also added 5nmol of [U-$^{13}C_6$, U-$^{2}H_7$]glucose (IS). Samples were processed using an ultrasonic bath for 45min at room temperature and were centrifuged for 5min at 13,900×g. Supernatant was transferred to a new micro centrifuge tube, evaporated at 60°C under vacuum and resuspended in 50µL of H_2O. Samples were sonicated with a cup-horn at 40%, for 2min, with pulses of 1sec and pauses of 1sec. After vortex and spin samples were cleaned up using a C18 SPE zip tip. To activate the stationary phase, 40µL of 50%ACN:H_2O were added to the zip tip, and then 120µL of 2%ACN:H_2O for equilibration. Afterwards, 50 µL of sample passed through the C18 SPE zip tip and were harvested. The same volume of 50%ACN:H_2O was added to elute the C18 SPE zip tip and dilute the sample. Vortex and spin were performed before transferring the samples into a vial for analysis. No IS was added to the negative samples.

The criteria used for the selectivity parameter were defined by the World Anti-Doping Agency (WADA) identification criteria for qualitative assays incorporating column chromatography and mass spectrometry [114]. The criteria applied to this parameter were defined based on data from one positive (spiked sample). The relative abundance was calculated as described on

Table 4.4). The interval of RT (ΔRT) was calculated as ± 2% of the RT of the analyte or as ± 0.1min, which ever resulted in the smallest value. Alternatively, the laboratory may choose to use the interval of RT_{Ratio} (ΔRT_{Ratio}), which can be calculated as ± 1% of the RT_{Ratio} of the analyte or in the case of stable isotopic labelled IS, calculated as ± 0.1%. In order to fulfil the criteria, the relative area of the positive samples had to be within the relative abundance interval, the RT of the analyte studied in the positive samples had to be within the ΔRT, and so did the RT_{Ratio} to the ΔRT_{Ratio}. To the negative samples, the opposite criteria were applied, indeed, the relative area, RT of the analyte and RT_{Ratio} had to be outside the intervals criteria. Other criteria used, was that the S/N must be over 3 for the positive samples and under 3 for the negative samples [114].

Table 4.4| Criteria of the relative abundance applied with the different percentages of relative area [114].

Relative area	Relative abundance
> 50%	± 10% (absolute)
25% - 50%	± 20% (relative)
5% - 25%	± 5% (absolute)
< 5%	± 50% (relative)

4.8.2. Linearity

For a reliable quantification, it is necessary to chose an appropriate calibration model, therefore the relationship between the concentration of the analyte in the sample and the correspondent systems response must be evaluated.

For the linearity study, it is recommended to use six or more calibration standards. Also, the calibrants should be evenly spaced over the concentration range, which should include 0-150% or 50-150% of the concentration likely to be encountered [115]. Therefore, to assess the linearity of the method, one calibration curve with a wide range of concentrations was prepared for each analyte. Two calibration curves were prepared, one for [U-$^{12}C_6$]glucose and [1,2,3-$^{13}C_3$]glucose and another for [1,2-$^{13}C_2$]glucose and [U-$^{13}C_6$]glucose, as established in the assay of

the abundance of different glucose isotopes (Section 5.2.2), with 15 calibrators, distributed across the working range: 0.2; 0.3; 0.4; 1; 1.5; 2; 3; 5; 15; 30; 50; 100; 150 and 250µM.

The classical least squares regression was used to establish the relation between instrumental response (y) and the analyte concentration (x), which is given as the equation $y = ax + b$, where a is the slope and b is the y interception. Values over 0.99 are considered acceptable for the correlation coefficient (R) and the coefficient of determination (R^2) of the calibration curves [116]. The standard error of the regression ($S_{y/x}$) can also be used as a measure of the goodness of fit and the residuals should also be examined, in order to exclude the absolute residual values over the double of the $S_{y/x}$ [117]. The zero value should be within the confidence interval of 95% [118], and a visual inspection was performed on both the concentration vs. peak area ratio plot as for the concentration vs. residuals.

4.8.2.1. Working Range

The working range is the interval between the upper and lower concentration of analyte in the sample which can be accepted for interpolation of results from the calibration curve's equation [115]. Because of the expected differences in concentrations of the analytes between the samples, a wide concentration range was maintained for the construction of calibration curves and its evaluation. Afterwards, when quantifying the samples, according to the sample and analyte, the range of calibrants can be restricted.

4.8.2.2. Mandel test

The use of the correlation coefficient derived from the regression analysis alone is a poor test for linearity [119]. Hence, the Mandel test was used to verify whether data followed a linear or a quadratic behaviour [120][121]. Data from one calibration curve was used for this test, where it is necessary to determine the difference of variances (DS^2), between the variance of the linear correlation ($S^2_{y/x}$) and the variance of the non-linear correlation (quadratic) (S^2_{y2}). The test value (F_{cal}) is calculated with equation (6) [120][122]. The F_{cal} is then compared to the value F_{crit}, which is obtained from the Fisher-Snedecor table (N-1; N-1; α) (α=0.95). The criteria applied, to assess if the calibration function follows a linear or non-linear behaviour were:

- If $F_{cal} \leq F_{crit}$, there is no significant difference between the variances, and therefore, the calibration function follows a linear behaviour;
- If $F_{cal} > F_{crit}$, there is a significant difference between the variances, and therefore, the calibration function follows a non-linear behaviour.

$$F_{cal} = \frac{(N-2) \times S^2_{y/x} - (N-3) \times S^2_{y^2}}{S^2_{y^2}} \quad (6)$$

N – number of samples

$S^2_{y/x}$ - variance of the linear correlation

S^2_{y2} - variance of the non-linear correlation (quadratic)

4.8.2.3. Test of homoscedasticity of variances

Homoscedasticity of variances is the term used to express that random variables in a sequence or vector have the same finite variance. The linear regression is the most commonly adopted calibration model, however, variances among a large concentration range may sometimes determine the use of weighting schemes for linear regression analysis to compensate for unequal variances. An F test may be performed to confirm data homoscedasticity [123], however, in some situations experimental data may present an heterogeneous variance across the calibration range. When methods are associated with significant heteroscedasticity, data should be mathematically transformed or a weighted least squares model should be applied to see which model best compensates for this type of variance [97][99][113].

To know whether the calibration curve presents homoscedastic or heteroscedastic behaviour, the variance across a calibration range was assessed. For this test, the calibrants 5µM and 250µM were selected as the first and last calibrator, and ten replicates of each of these calibrants produced to assess variability. To 50µL of every sample was added 50µL of IS (30µM [U-$^{13}C_6$, U-$^{2}H_7$]glucose). After calculating the variance of the first and last calibrator, depending on their values, the equations (7) and (8) were applied [123][124]. The F_{cal} is then compared to the value F_{crit}, which is obtained from the Fisher-Snedecor table (N-1; N-1; α) (α=0.95). The criteria applied, to assess if the calibration function follows a homoscedastic or heteroscedastic behaviour were:

- If $F_{cal} \leq F_{crit}$, there is no significant difference between the variances, and therefore, the calibration function follows a homoscedastic behaviour;
- If $F_{cal} > F_{crit}$, there is a significant difference between the variances, and therefore, the calibration function follows a heteroscedastic behaviour.

$$F_{cal} = \frac{S_{10}^2}{S_1^2}, if\ S_{10}^2 > S_1^2 \quad (7)$$

S^2_1 – variance of the first calibrator

S^2_{10} – variance of the last calibrator

$$F_{cal} = \frac{S_1^2}{S_{10}^2}, if\ S_1^2 > S_{10}^2 \quad (8)$$

S^2_1 – variance of the first calibrator

S^2_{10} – variance of the last calibrator

4.8.2.4. Weighted least squares regression

Ordinary least squares regression models are only applicable for homoscedastic data sets. When calibration curves present significant heteroscedasticity, data should be mathematically transformed or a weighted least squares model applied [97]. Using empirical weights such as $1/x$; $1/x^2$; $1/x^{1/2}$; $1/y$; $1/y^2$; $1/y^{1/2}$, the best weighting factor (w_i) is chosen according to the percentage of relative error (%RE), and the evaluation of the R and R^2. The %RE compares the regressed concentration (C_{obs}) calculated from the regression equation obtained for each w_i, with the nominal standard concentration (C_{nom}), as represented on equation (9) [123].

$$\%RE = \frac{C_{obs} - C_{nom}}{C_{nom}} \times 100 \quad (9)$$

C_{obs} – regressed concentration

C_{nom} – nominal standard concentration

To evaluate the %RE, the plot of %RE vs. concentration was analysed. The best w_i is the one which presents a narrow horizontal band of randomly distributed %RE around the concentration axis and the least sum of %RE across the whole concentration range [123]. In addition, the modulus of the %RE should fall within 15 or 20% for the LOQ, in order for a model to be accepted [98]. To assist with the evaluation of the best calibration model, the R^2 was also evaluated for each w_i, obtained by the equation (10) [124][125].

If the best calibration model should use a weighted least squares regression, the model parameters (m and b) for each w_i, as well as their R, can be calculated. The unweighted least squares are converted into their weighted equivalents by adding the term w_i and the estimated values for the m, b and R parameters can be obtained by equations (11), (12) and (13) [123][124].

$$w_i = \frac{1/S_{yi}^2}{(\sum 1/S_{yi}^2)/N} \quad (10)$$

N – number of experimental points

S^2_{yi} - variance of the calibration points by different weighting models

$$m = \frac{\sum w_i \times \sum w_i x_i y_i - \sum w_i x_i \times \sum w_i y_i}{\sum w_i \times \sum w_i x_i^2 - (\sum w_i x_i)^2} \quad (11)$$

$$b = \frac{\sum w_i x_i^2 \times \sum w_i y_i - \sum w_i x_i \times \sum w_i x_i y_i}{\sum w_i \times \sum w_i x_i^2 - (\sum w_i x_i)^2} \quad (12)$$

$$R = \frac{\sum w_i \times \sum w_i x_i y_i - \sum w_i y_i \times \sum w_i y_i}{\sqrt{\sum w_i \times \sum w_i x_i^2 - (\sum w_i x_i)^2} \times \sqrt{\sum w_i \times \sum w_i y_i^2 - (\sum w_i y_i)^2}} \quad (13)$$

In order to evaluate the best calibration model through the weighted least squares regression, five calibration curves were prepared as described on section 4.4 on five non-consecutive days and analysed.

4.8.3. Limit of detection (LOD) and limit of quantification (LOQ)

The limit of detection (LOD) is defined as the lowest amount of analyte necessary to obtain a signal that can be distinguished from the background noise, but not necessarily be quantified as an exact value [97][126]. There are several approaches for determining the LOD. One of them is by visual evaluation. The LOD is determined in this way by analysing several blank samples with known analyte concentrations, and establishing the minimum level at which the analyte is reliably detected. Another approach is to calculate the LOD from the standard deviation of the blank. This method appears to be quite popular amongst analysts performing validation studies. In this method, LOD is expressed as a mean sample blank value plus two or three times the standard deviations of the blank samples [115][126]. However, this method appears to have a probability of reporting a false negative for the $2S_{blank}$ of 50% and for the $3S_{blank}$ of 16% [126]. Another common approach is to compare the measured signals from samples with known low concentrations of analyte with blank samples to establish a minimum concentration at which the analyte can reliably be detected with acceptable S/N of 2 or 3 [115]. Using the parameters of the calibration curve's equation it is also possible to estimate the LOD, using equation (14) [115][116][126]. This approach provides the determination of LOD with a high level of confidence [126], however, it can produce errors when linearity and homogeneity are not meet.

$$LOD = \frac{3.3 \times S_{y/x}}{m} \quad (14)$$

$S_{y/x}$ – standard deviation of the linear correlation

m – slope of the calibration curve's equation

Limit of quantification (LOQ) is defined as the lowest amount of analyte in a sample that can be quantitatively determined with suitable precision and accuracy [126]. Similarly to the LOD, LOQ can be determined by visual evaluation and through the S/N ratio, with the acceptable criteria of S/N of 10 [126]. LOQ can also be obtained by multiplying the LOD three times, or as the 50% value above the lowest calibrant concentration used in method validation [115]. Another method is to define the LOQ as the lowest concentration that can be quantified with acceptable precision and accuracy, which should be of at least 20% for the precision and ±20% for accuracy [84][98][99]. Similarly to the LOD, the LOQ can also be evaluated through equation (15) [126][116]. Nevertheless, it presents the same problem, described for the LOD, which is the need for a linear and homoscedastic calibration curve.

$$LOQ = \frac{10 \times S_{y/x}}{m} \quad (15)$$

$S_{y/x}$ – standard deviation of the linear correlation

m – slope of the calibration curve's equation

If a weighting scheme must be applied, the previous equations for the calculations of LOD and LOQ no longer apply, because the model was not truly linear. Instead, the standard deviation of the weighted correlation ($S_{(y/x)w}$) was calculated using equation (16) [117][119][124][125].

$$S_{(y/x)w} = \sqrt{\frac{\sum_i w_i (y_i - \hat{y}_i)^2}{N - 2}} \quad (16)$$

N – number of experimental points

w_i - weighting appropriate to the value of y_i

y_i – experimental response

$\hat{y}_i$ - points on the calculated regression line corresponding to the individual x-values

Data from one calibration curve was used to study the LOD and LOQ. The LOD and LOQ were determined for three different working ranges. 0.15–6µM. 0.15–50µM and 1.5–250µM. There is no particular preference on the validation guidelines for which approach to use. Nevertheless, this was considered the most reliable method to calculate the LOD and LOQ [126]. Therefore, equations (14) and (15) were used, calculating the standard deviation by equation (16).

4.8.4. Precision

Precision, is described as the closeness of repeated individual measures of analyte [127]. Precision may be considered at three levels: repeatability, intermediate precision and reproducibility. Repeatability or within-run precision expresses the precision under the same operating conditions over a short interval of time. Intermediate precision expresses within-laboratories variations, such as the influence of performing analysis in different days, with different analysts or different equipment. And finally, reproducibility expresses the precision between laboratories, however, this last level of the precision should only be studied if a method is supposed to be used in different laboratories [97].

Precision should be measured using a minimum of five determinations per concentration. With a minimum of three quality controls (QC) in the range of expected concentrations [99]. Precision values should also be representative of possible test conditions. [128]. As an acceptance criteria, the precision determined at each concentration level should not exceed 15% of the coefficient of variation (%CV), except for the LOQ which should not exceed 20% [97][99].

Each concentration was analysed in replicates on five separate days. For each day, a calibration curve with the working range of 0.15; 0.3; 0.45; 0.6; 1.2; 1.5; 2.1; 3; 6; 15; 30; 50; 100; 150 and 250µM was prepared. In addition, three replicates for five concentrations (1.25; 2.5; 20; 125 and 200µM) of QCs were prepared. Three of them were then selected to be analysed as the high, medium and low concentrations of 2 distinct working ranges. The IS (50µL of 30µM [U-$^{13}C_6$, U-$^{2}H_7$]glucose) was added to 50µL of all the samples.

After choosing the best calibration model for this project, the calibration curve's equation was used to determine the concentration within the QCs. Repeatability and

intermediate precision were determined using an ANOVA calculation (Supplementary Table 1) [129][130][131] and the calculus described on equations (17) and (18) [98].

$$\%CV\ Repeatability\ within = \frac{\sqrt{S^2_{within}}}{\bar{x}} \times 100 \quad (17)$$

S^2_{within} – variance within groups

$\bar{x}$ – average of measurement

$$\%CV\ Intermediate\ precision = \frac{\sqrt{S^2_{between} + S^2_{within}}}{\bar{x}} \times 100 \quad (18)$$

$S^2_{between}$ – variance between groups

S^2_{within} – variance within groups

$\bar{x}$ – average of measurements

4.8.5. Accuracy

Accuracy is described as the closeness of mean test results obtained by the method to the true value (concentration) of the analyte [99][127].

Accuracy should be measured using a minimum of five determinations per concentration. With a minimum of three concentrations in the range of expected concentrations [99]. As an acceptance criteria, the accuracy determined at each concentration level should be within 15% of the nominal value, except at LOQ, where it should not deviate by more than 20% [97][99].

Like the precision parameter, each concentration was analysed in replicates on five separate days. For each day, a calibration curve with the working range of 0.15; 0.3; 0.45; 0.6; 1.2; 1.5; 2.1; 3; 6; 15; 30; 50; 100; 150; and 250µM was prepared. In addition, three replicates for five concentrations (1.25; 2.5; 20; 125 and 200µM) of QCs were prepared. Three of them were then selected to be analysed as the high, medium and low concentrations according to the

distinct working ranges for the different expected concentrations. The IS (50µL of 30µM [U-$^{13}C_6$, U-$^{2}H_7$]glucose) was added to 50µL of all the samples.

After choosing the best calibration model for this project, the calibration curve's equation was used to determine the concentration within the QCs. Accuracy is expressed in %RE, being calculated by equation (19) [123]. Recovery of the QCs analysis was also calculated, as a ratio of the observed concentration and the nominal concentration, as represented by equation (20).

$$\%RE\ Accuracy = \frac{C_{obs} - C_{nom}}{C_{nom}} \times 100 \quad (19)$$

C_{obs} – regressed concentration

C_{nom} – nominal concentration

$$\%Recovery = \frac{C_{obs}}{C_{nom}} \times 100 \quad (20)$$

C_{obs} – regressed concentration

C_{nom} – nominal concentration

4.8.6. Carry-Over

Carry-over is the appearance of analyte signal in blank samples after the analysis of samples, usually occurring after the injection of samples with high analyte concentration [127]. This can influence the analysis, especially when following an injection of a highly concentrated sample. Accordingly, carry-over must be avoided by proper method development and analysis of blanks between samples.

The carry-over effect can be evaluated by injecting blanks after the samples and analysing if signal from the previously injected sample is present [99][113]. To study the carry-over effect, three replicates of the highest calibrator (250µM) and the medium (15µM) were injected, followed by the injection of three blanks.

As a criteria for this study, carry-over in the blank sample following a high concentration standard should not be greater than 20% of the LOQ and 5% for the IS [84][98][127].

4.8.7. Recovery

Recovery is the ratio of the detector response obtained from an amount of the analyte added to and extracted from the biological matrix, compared to the detector response obtained for the true concentration of a pure standard. To measure recovery, at least three concentration results of extracted samples should be compared to pure solvents, which represent 100% recovery [99][113]. However, in LC-MS/MS, the recovery study should be performed together with the matrix effect study because part of the change of the response in prepared samples in comparison to pure standards might be attributable to matrix effects, which is why the spiked samples before extraction were compared to spiked samples after extraction [97]. Usually, the selected concentrations are often the ones from the low and high, or low, mid and high QCs spiked before sample extraction. Then the blank DBS extracted samples are post-spiked with both the analytes and the IS at the same concentrations as the pre-spiked samples [84].

The recovery study was performed for every analyte, except the IS. Two DBS of 3 different animals for each of the different replicates were punched, one for the samples spiked before extraction, and another from the same animal for the samples spiked after extraction. Half of the samples were then spiked with 50µL of 500µM, 30µM and 1.2µM of spike solutions of every analyte (glucose/[1,2,3-$^{13}C_3$]glucose and [1,2-$^{13}C_2$]glucose/[U-$^{13}C_6$]glucose, assessed separately). The same volume of H_2O was added to the other samples. Then, to every sample 450µL of EtOH ware added. Samples were processed using an ultrasonic bath for 45min at room temperature and were centrifuged for 5min at 13,900×g. Supernatant was transferred to a new microcentrifuge tube, evaporated at 60°C under vacuum and resuspended in 50µL of H_2O. Samples were sonicated with a cup-horn at 40%, for 2min, with pulses of 1sec and pauses of 1sec. After vortex and spin samples were passed through a C18 SPE zip tip as described on section 4.5. Then, to the samples already spiked before extraction, 50µL of H_2O were added, while to the other samples, 50µL of the spike solutions were added to the correspondent samples. Finally, 50µL of IS solution (30µM [U-$^{13}C_6$, U-$^{2}H_7$]glucose) were added to every sample. Because the samples were diluted in order to be processed with the same volumes, 2µL of sample were analyzed, instead of 1µL.

Recovery is not a parameter considered essential for method validation, however it is interesting to evaluate if the sample treatment is effective enough. According to the FDA, recovery of the analyte does not need to be 100%, but the extent of recovery of an analyte and its IS should be consistent, precise and reproducible [99]. There are no specific criteria for this parameter, only some guidelines suggest that recovery values should be greater than 50% [97], and that both the analyte as the IS should be evaluated [132]. The calculi for the recovery was performed through the equation (21) [84][121].

$$\%Recovery = \frac{A_{Ab}/A_{ISb}}{A_{Aa}/A_{ISa}} \times 100 \quad (21)$$

A_{Aa} – peak area of the analyte after sample extraction

A_{Ab} – peak area of the analyte before sample extraction

A_{ISa} – peak area of the IS after sample extraction

A_{ISb} – peak area of the IS before sample extraction

4.8.8. Matrix Effect

When using LC-MS techniques, the evaluation of matrix effects is obligatory, since co-eluting compounds can influence the ionization of the compounds of interest, leading to suppression or enhancement of the peak abundance. One approach to study this effect is to compare the peak areas of the analyte of interest spiked to blank matrix extracts from different origins with pure standards. This should be done using at least 6 blank samples from different origins and for 3 concentrations [98]. The addition of IS should be done immediately before analysis for this study.

Post-spiked samples were prepared as described on section 4.8.7. The pure standard solutions, on the other hand, were prepared by adding 50µL of each spike solution with 100µL of H_2O and 50µL of IS (30µM [U-$^{13}C_6$, U-$^{2}H_7$]glucose), in order for the samples to be in the same volume as the post-spiked samples. As for the recovery study, 2µL of sample volume were analyzed.

Matrix effect can be expressed in terms of matrix influence factor f as denoted on equation (22). Using this equation, an f value of zero would represent no matrix effect; a

negative value would indicate ion suppression, while a positive one, ion enhancement. As a criteria for the matrix effect study, the coefficient of variation calculated from f determined from different pools of matrix should be lower than 15% [98].

$$f = \frac{A_{post} - A_{pure\ standard}}{A_{pure\ standard}} \quad (22)$$

A_{post} – peak area of the analyte obtained by spiking a blank sample after extraction

$A_{pure\ standard}$ – peak area of the analyte as a pure reference standard solution

The IS is often used in order to compensate for matrix effect, specially labelled analogues, because their co-elution with the analyte of interest, results in the same matrix influence. Nevertheless, the relative matrix-influencing factor (f_{IS}) should also be evaluated, as even a slight difference in RT can diminish this compensation effect [98]. The area of the IS will also be influenced by matrix effects and therefore the relative matrix-influencing factor (f_{IS}) was also evaluated to observe whether the IS compensates for the differences in ionization. The f_{IS} was obtained as f, but the peak areas of the compound of interest were divided by the peak areas of the applied IS [98].

4.8.9. Stability

Analyte's stability is a function of the storage conditions, chemical properties of the drug, the matrix and the samples container. The evaluation of the analyte's stability is important in the way that it reflects situations likely to be encountered during sample processing, manipulation and analysis. Five tests are usually performed to evaluate stability: freeze and thaw stability, short-term temperature stability, long-term stability, stock solution stability, and post-preparative stability [99][113]. However, the analyst should consider which experimental set up is necessary. The IS should be added to the instability samples just before analysis. Otherwise, if it is present during the instability conditions, it also degrades and thus back calculated concentrations will not reflect the actual compound degradation [98]. The recommendations, are to perform stability experiments at least at low and high concentrations [99][133].

To evaluate the freeze and thaw stability, the FDA recommends that at least three aliquots at each of the low and high concentrations should be stored at the intended storage temperature for 24 hours and afterwards thawed unassisted at room temperature. Samples should be refrozen for 12 to 24 hours under the same conditions, being this freeze and thaw cycle repeated two more times, and analysed at the third cycle [99][133]. To study the freeze and thaw stability, because of the large working range, there was the need to include a third concentration. Three concentrations were prepared, each with three replicates at high (200µM), medium (20µM) and low (1.25µM) concentrations. These solutions were then divided and both frozen. The stability samples suffered three freeze and thaw cycles, being analysed at the third cycle, while the comparative samples were defrosted on the day of the third cycle and analysed as well.

For the short-term temperature stability, three aliquots of each of the low and high concentrations should be thawed at room temperature and kept at this temperature from 4 to 24 hours [99][133]. This stability study refers to the stability of the analyte under the conditions of sample preparation (room temperature, RT and time required for sample preparation) [134]. This parameter was not evaluated in this project.

The time determined for the long-term stability evaluation should exceed the time between the date of the first sample collection and the date of the last sample analysis. It should be determined by storing at least three aliquots of each of the low and high concentrations under the same conditions as the study samples, being these aliquots analysed on three separate occasions [99][133].

The stability of stock solutions of analytes and IS should be evaluated at room temperature for at least 6 hours. If the stock solutions are refrigerated or frozen for the relevant period, this stability should be documented [99]. To study the stock solution stability, three concentrations were prepared, each with three replicates at high (200µM), medium (20µM) and low (1.25µM) concentrations from stock solutions of [U-$^{12}C_6$]glucose, [1,2-$^{13}C_2$]glucose, [1,2,3-$^{13}C_3$]glucose and [U-$^{13}C_6$]glucose that had been prepared one month before, and compared to freshly prepared solutions at the same concentrations.

The post-preparative stability refers to the stability of processed samples, including the time they spend in the autosampler before their analysis. Samples at three concentrations, each with three replicates at high (200µM), medium (20µM) and low (1.25µM) concentrations, were

freshly prepared and analysed. After their analysis they were kept in the autosampler while other analysis were performed. These samples were reanalysed at the end of the batch.

The criteria, applied for acceptance to every stability study mentioned above, except for the post-preparative stability, was that the mean of the stability samples should be within 90-110% of the mean of the control samples, and the 90% confidence interval of the stability samples should fall within an 80-120% range of the control sample results [98][133][134].

5. RESULTS

5. RESULTS

5.1. Analytical method development

This section presents the results obtained during method development and used to determine which parameters to use in the spectrometric settings throughout the project.

5.1.1. Fragmentation spectra

As a part of method development, fragmentation spectra for each analyte of interest were obtained to ascertain which transitions to monitor. A fragmentation spectrum represents the fragments that can be obtained for a certain analyte after the collision cell (q2). In order to obtain all the possible fragments an analyte can originate, a gradual increase in the collision energy is applied to the analyte and the resulting fragments for each energy values are registered. This is called a collision energy ramping. On Fig. 5.1 it is represented the collision energies resulting in higher fragment intensity of the [U-$^{12}C_6$]glucose analyte. Besides revealing which fragments are produced more frequently under the different collision energies, this result shows that the smaller fragments, such as m/z of 59.0 and 57.0 need higher collision energies to be produced, while the larger fragments, such as m/z of 119.0 and 112.9 are produced with lower collision energies.

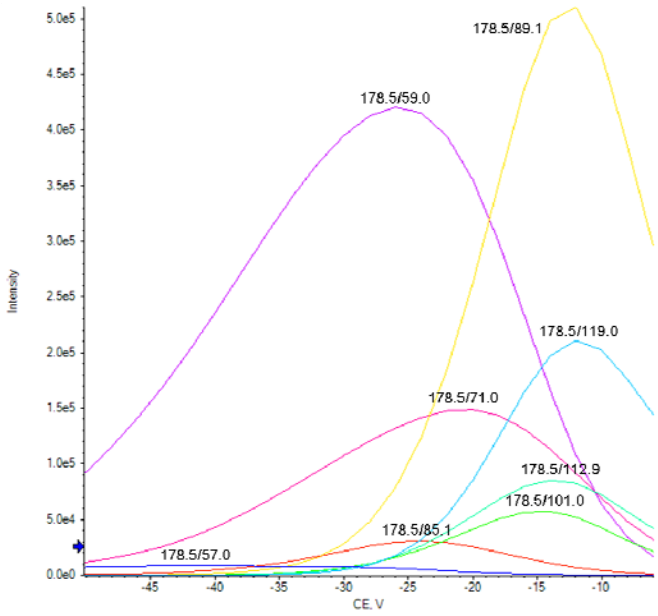

Fig. 5.1| Representation of the ideal collision energies to produce each of the 8 fragments of [U-$^{12}C_6$]glucose. Smaller fragments, need higher collision energies, while the larger fragments are produced with lower energies.

The figures presented next (Fig. 5.2 - Fig. 5.6), correspond to the fragment spectra of the analytes of interest to this project, representing the fragments obtained when applying a collision energy range of -20 to -5V. On Fig. 5.2 it is represented the mean fragmentation spectrum of [U-$^{12}C_6$]glucose. From the analysis of this spectrum, several fragments can be distinguished, being the fragment with m/z of 89 the most intense and the fragment 119 the second most intense. Less intense fragments should also be noted, such as m/z of 59, 71, 101 and 113. When applying the least amount of collision energy, in this case, -5V, that energy is not enough to fragment the analyte, so the peak with m/z of 179 corresponds to the m/z value of the entire analyte of [U-$^{12}C_6$]glucose. The most intense fragments, m/z of 89 and 119, were chosen to be monitored as [U-$^{12}C_6$]glucose fragments in all studies of this project. These two fragments, as it will be shown, have analogues in the other glucose analytes, making them interesting fragments to follow. D-glucose is always present in plasma samples, therefore it is expected to have high [U-$^{12}C_6$]glucose levels relative to the administered labelled glucose or recycling products. Thus, for quantification of this analyte there is no need to monitor other fragments.

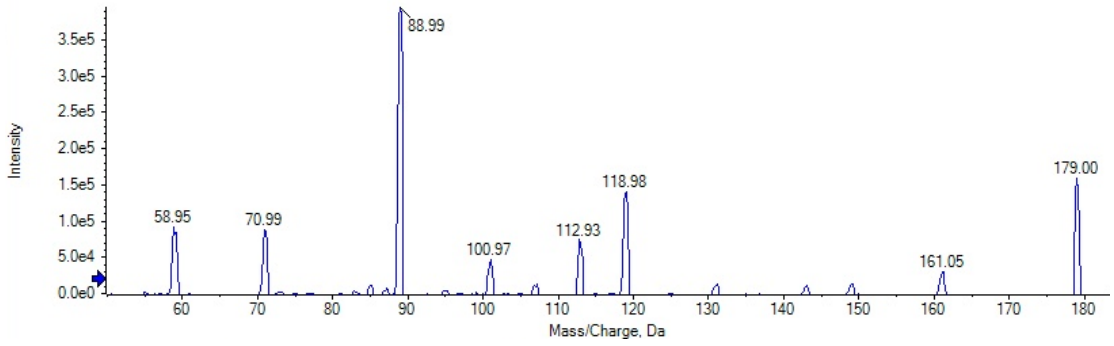

Fig. 5.2| Mean fragmentation spectrum of [U-$^{12}C_6$]glucose (M), obtained by CID. Representation of fragments obtained by ESI in negative ionization mode and varying the collision energy from -20V to -5V of direct infusion at 10µL/min of a 200µM [U-$^{12}C_6$]glucose solution.

The same analysis was performed for [1,2-$^{13}C_2$]glucose (Fig. 5.3) with two fragments with m/z of 89 and 91 being the most intense in comparison to [U-$^{12}C_6$]glucose with only m/z of 89, and hence they were chosen for monitoring in further studies. Fragment with m/z of 119 was obtained using the same CE applied to the fragments 89 and 91 (Supplementary Fig. 1), being also monitored as it is also present in the [U-$^{12}C_6$]glucose. Fragment with m/z of 59, however, was obtained with a higher CE, being the molecule fragmented on a distinct site, originating therefore distinct fragments. Fragment 59m/z was also chosen, since it requires higher CE, it is

less likely to be produced, unlike other fragments, which can usually be produced by losing a water molecule for example, being therefore a more sensitive fragment. However, it shows a low S/N, therefore it was cast out. The fragments 89m/z, 91m/z and 119m/z were all chosen to be monitored as fragments of the analyte [1,2-$^{13}C_2$]glucose. This molecule is present in smaller concentrations than [U-$^{12}C_6$]glucose, and therefore more transitions were monitored to chose the best transitions out of the three, in case one transition does not show satisfactory sensitivity.

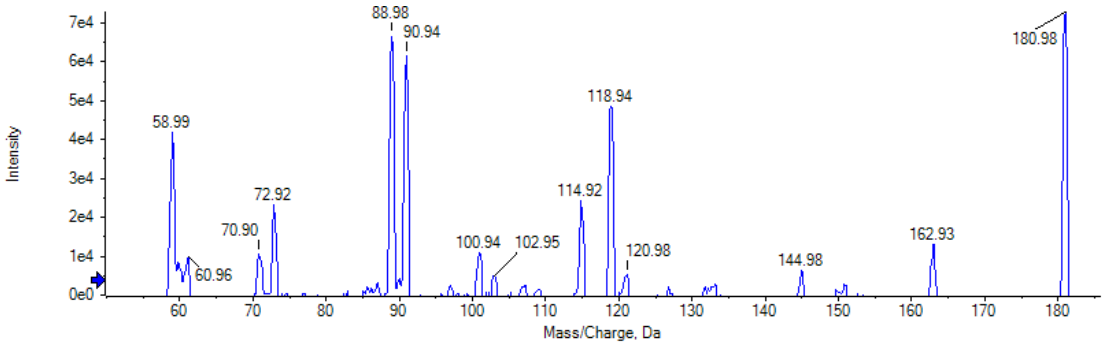

Fig. 5.3| Mean fragmentation spectrum of [1,2-$^{13}C_2$]glucose (M+2), obtained by CID. Representation of fragments obtained by ESI in negative ionization mode and varying the collision energy from -20V to -5V of direct infusion at 10µL/min of a 200µM [1,2-$^{13}C_2$]glucose solution.

Fragmentation spectra of [1,2,3-$^{13}C_3$]glucose (Fig. 5.4), presents intense peaks for fragments with m/z of 89 and 92, similar to the fragments obtained for [U-$^{12}C_6$]glucose (Fig. 5.2) and [1,2-$^{13}C_2$]glucose (Fig. 5.3), corresponding these fragments to the m/z of 89 on the [U-$^{12}C_6$]glucose fragmentation spectrum and 89 and 91 respectively on the [1,2-$^{13}C_2$]glucose fragmentation spectrum. Fragments with m/z of 89 and 92 were monitored, as well as the fragment with the m/z of 120, which also presented high peak intensities, and corresponded to analogues of the fragments already monitored for [U-$^{12}C_6$]glucose (Fig. 5.2) and [1,2-$^{13}C_2$]glucose (Fig. 5.3). Again, three fragments were chosen to be monitored for the reasons stated before.

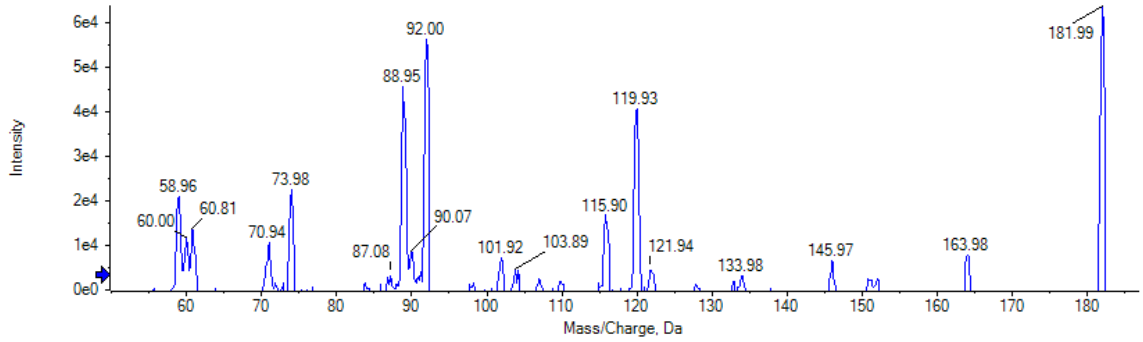

Fig. 5.4| Mean fragmentation spectrum of [1,2,3-$^{13}C_3$]glucose (M+3), obtained by CID. Representation of fragments obtained by ESI in negative ionization mode and varying the collision energy from -20V to -5V of direct infusion at 10µL/min of a 200µM [1,2,3-$^{13}C_3$]glucose solution.

Fragmentation spectra of [U-$^{13}C_6$]glucose (Fig. 5.5) had the most intense fragment with m/z of 92, but fragments 123 and 61 were also intense, and these fragments (92 and 123) are analogues of the fragments chosen for the previous analytes, these fragments were therefore chosen to be monitored. Since this analyte would only have 2 fragments, according to the previous selection criteria, the fragment with m/z of 61 was also chosen.

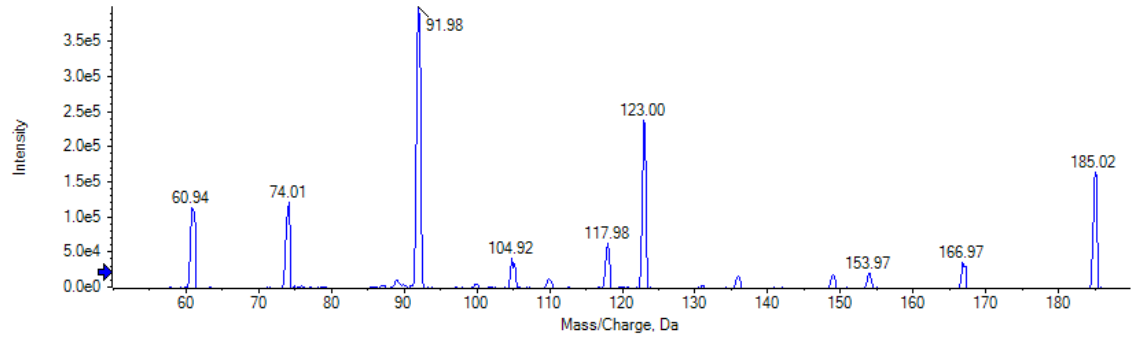

Fig. 5.5| Mean fragmentation spectrum of [U-$^{13}C_6$]glucose (M+6), obtained by CID. Representation of fragments obtained by ESI in negative ionization mode and varying the collision energy from -20V to -5V of direct infusion at 10µL/min of a 200µM [U-$^{13}C_6$]glucose solution.

The fragmentation spectra of [U-$^{13}C_6$, U-$^{2}H_7$]glucose (Fig. 5.6) shows fragment with the m/z of 128 as the most intense. Several other fragments present show enough peak intensities to be used for monitoring, but fragments with m/z of 128 and 94 were chosen. Because this analyte is added as an IS, it is expected a high intensity signal for this analyte, accordingly, as explained for [U-$^{12}C_6$]glucose, there is no need to select other transitions. Since this analyte is the IS, fragments common to every other analytes of interest were chosen in order to perform

the ratio between peak areas of the analytes of interest and the peak area of the IS, taking into account that the peak area of the analyte should be divided by the peak area of the IS with the corresponding fragment.

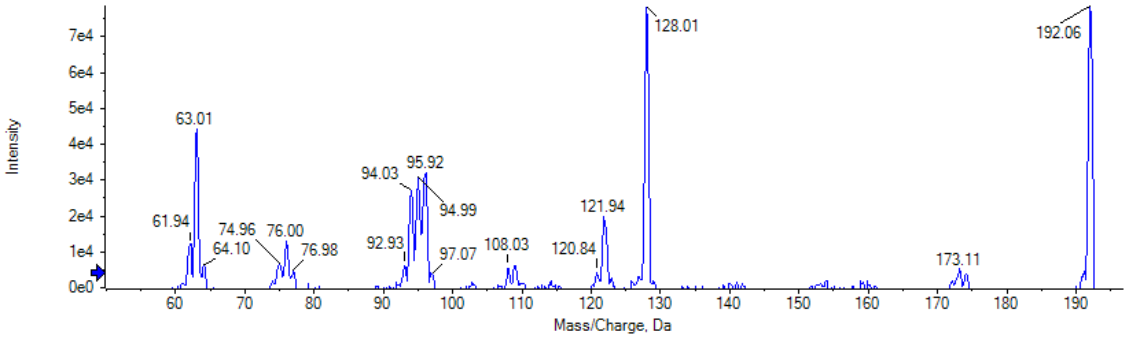

Fig. 5.6| Mean fragmentation spectrum of [U-$^{13}C_6$, U-$^{2}H_7$]glucose (M+13), obtained by CID. Representation of fragments obtained by ESI in negative ionization mode and varying the collision energy from -20V to -5V of direct infusion at 10µL/min of a 200µM [U-$^{13}C_6$, U-$^{2}H_7$]glucose solution.

5.2. Method and sample treatment optimization

5.2.1. Differentiation of fructose from glucose with the MRM method

Glucose is the most predominant hexose in human blood, however, other hexoses of identical molecular mass such as fructose, mannose and galactose may interfere with glucose concentration analysis. It is therefore important to perceive whether or not the current method for glucose is capable of separating the other hexoses. In particular, glucose, fructose and sucrose produce similar fragmentation spectra [101], because these molecules break with common fragments. While the concentration of glucose is normally approximately a hundred times that of fructose, and a thousand times that of manose, abnormal nutritional or pathological states could increase the abundance of fructose or mannose relative to glucose. The MRM method was developed for [U-$^{12}C_6$]fructose, the hexose with the highest potential for interfering with [U-$^{12}C_6$]glucose concentration analysis in our experimental settings, and compared to the method designed for [U-$^{12}C_6$]glucose. As demonstrated on Fig. 5.7, the fragments obtained for [U-$^{12}C_6$]glucose and [U-$^{12}C_6$]fructose were almost identical.

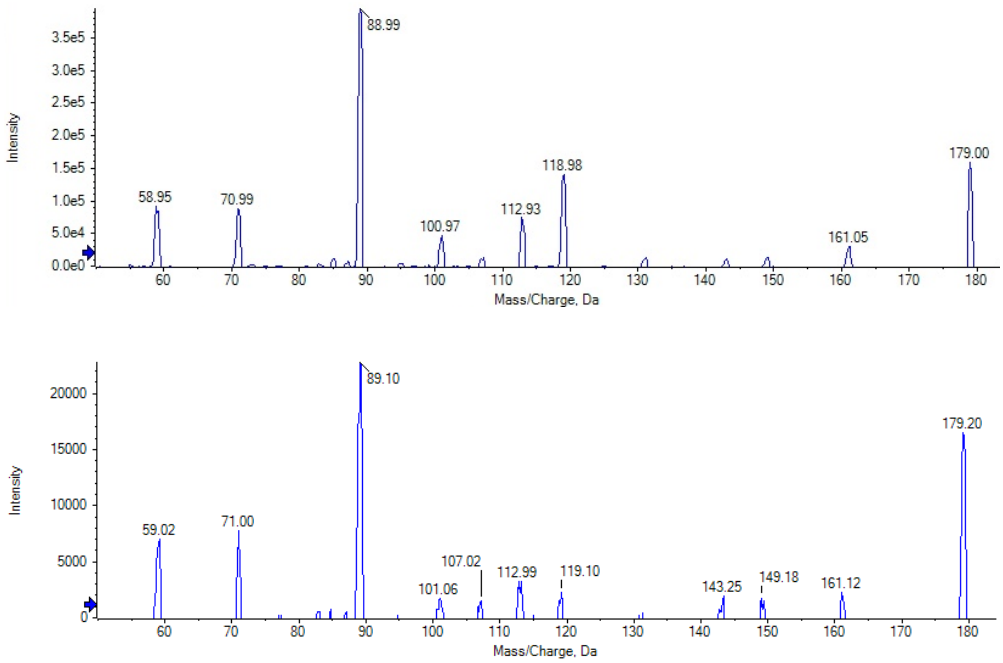

Fig. 5.7| Mean fragmentation spectra of [U-$^{12}C_6$]glucose (top) and [U-$^{12}C_6$]fructose (bottom), obtained by CID. Representation of fragments obtained by ESI in negative ionization mode and varying the collision energy from -20V to -5V. Fragments originated from [U-$^{12}C_6$]glucose and [U-$^{12}C_6$]fructose were practically the same, with minor differences in the fragmentation ratios.

In order to differentiate these two molecules from each other, their behaviour within the chromatographic column was tested. On Fig. 5.8 it is possible to see the differentiation between [U-$^{12}C_6$]fructose and [U-$^{12}C_6$]glucose using the NH_2 column because [U-$^{12}C_6$]fructose has a RT of approximately 7min, while [U-$^{12}C_6$]glucose as a RT of 8min. From these results it was determined that the method for [U-$^{12}C_6$]glucose is capable of separating [U-$^{12}C_6$]glucose from [U-$^{12}C_6$]fructose. The reason these two analytes present different signal intensities is because for this test, [U-$^{12}C_6$]fructose was freshly prepared, while [U-$^{12}C_6$]glucose was from a stored stock solution.

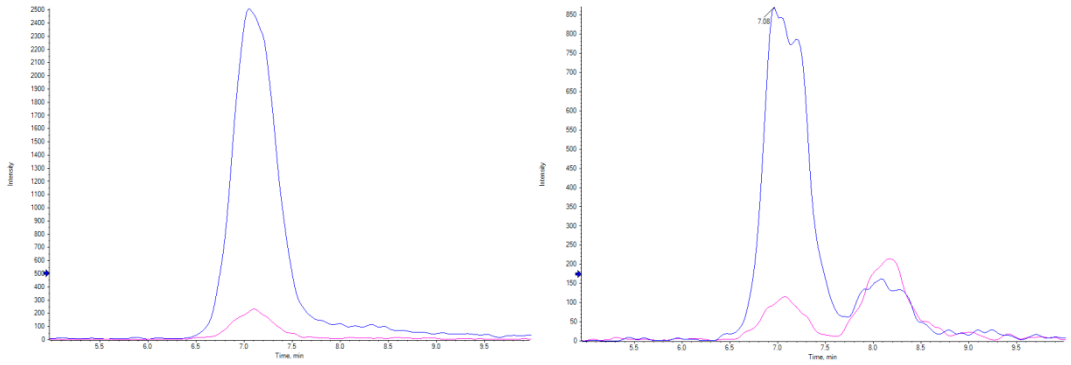

Fig. 5.8| Chromatographic spectra of [U-$^{12}C_6$]fructose (left) and a mixture of [U-$^{12}C_6$]fructose and [U-$^{12}C_6$]glucose (right). The blue line corresponds to the results for transition 179/89, while the rose line corresponds to transition 179/59. The image on the right demonstrates the separation between [U-$^{12}C_6$]fructose and [U-$^{12}C_6$]glucose through the NH_2 column, where [U-$^{12}C_6$]fructose has a RT of 7min, while [U-$^{12}C_6$]glucose has a RT of 8min. The differences between the intensity of [U-$^{12}C_6$]fructose and [U-$^{12}C_6$]glucose are due to non-equimolar solutions.

5.2.2. Test on the abundance of the different glucose isotopes

Because of the natural abundance of ^{13}C of 1.109% and the impurity of the glucose isotopes used in the stock solutions of this project, the abundance of other isotopes within each analyte was analysed to see if their presence represents a great influence in the quantification of each analyte. From the analysis of 250µM solutions of each analyte individually, it was possible to perceive the contributions of other isotopes (Fig. 5.9). The analyte with the highest isotopic abundance, other than [U-$^{12}C_6$]glucose itself, is [1,2-$^{13}C_2$]glucose (Fig. 5.9.a). Since ^{13}C has a natural abundance of 1.109% of being randomly distributed among the six glucose carbons, there is a low but finite probability of [1,2-$^{13}C_2$]glucose isotopomers being present as well (0.0109^2=0.012%). The most abundant isotopes, other than [1,2-$^{13}C_2$]glucose, are the [U-$^{12}C_6$]glucose and the [1,2,3-$^{13}C_3$]glucose (Fig. 5.9.b). In the case of [1,2,3-$^{13}C_3$]glucose, its abundance in [1,2-$^{13}C_2$]glucose is around 1%, which is in agreement with the natural abundance of ^{13}C of 1.109%. The abundance of [U-$^{12}C_6$]glucose in [1,2-$^{13}C_2$]glucose is probably due to some labelling loss or impurities. In the case of [1,2,3-$^{13}C_3$]glucose, the most abundant isotope is [1,2-$^{13}C_2$]glucose (Fig. 5.9.c), which is also due to some labelling loss, however, it's percentage is so low that it should not be considered. The analytes with the highest isotopic abundance, in the case of [U-$^{13}C_6$]glucose, are [U-$^{12}C_6$]glucose and [1,2,3-$^{13}C_3$]glucose (Fig. 5.9.d), however their percentages are so low that they should not be considered. Finally, the analysis of the isotopic abundance of other analytes in a [U-$^{13}C_6$, U-$^{2}H_7$]glucose solution shows a minor abundance of [U-$^{13}C_6$]glucose (Fig. 5.9.e), which is low enough as not to compromise the measurement of [U-$^{13}C_6$]glucose isotopomers present in the samples (see below). These results demonstrate which analytes can be analyzed together as a pure solvent solution for the construction of the

calibration curves. Therefore, calibration curves presented in this project were prepared as a mixture of [U-$^{12}C_6$]glucose (M) and [1,2,3-$^{13}C_3$]glucose (M+3) and a second calibration curve as a mixture of [1,2-$^{13}C_2$]glucose (M+2) and [U-$^{13}C_6$]glucose (M+6). While the IS has a small percentage of [U-$^{13}C_6$]glucose, since a constant amount is added to every sample and every calibrant, its contribution to observed [U-$^{13}C_6$]glucose is systematic and can therefore be subtracted if necessary (i.e. if the overall [U-$^{13}C_6$]glucose abundance is very low).

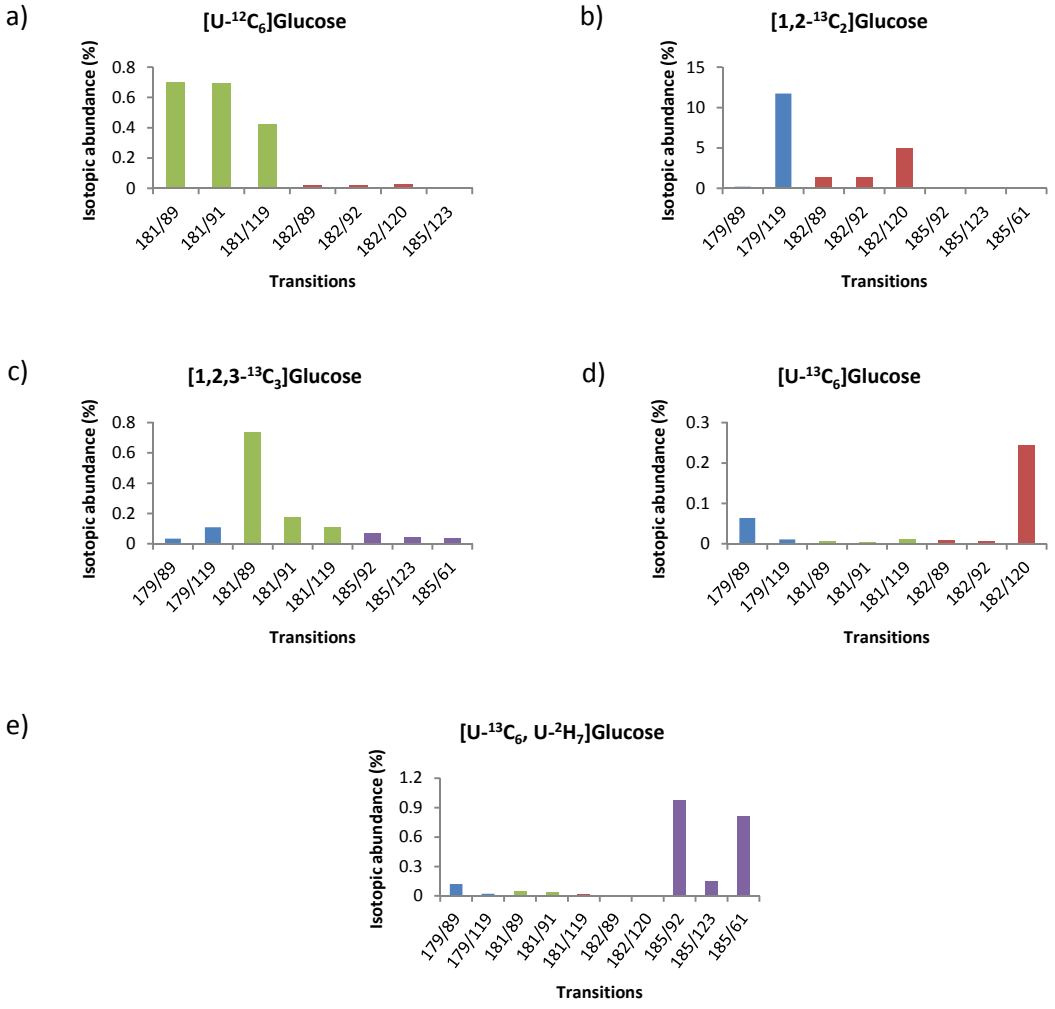

Fig. 5.9| Abundance of other analytes for each transition from the analysis of 250µM of each individual analyte, represented by their transitions. a) Representation of the abundance of other analytes of glucose. The most evident isotope present is the [1,2-$^{13}C_2$]glucose. b) Representation of the abundance of other analytes of [1,2-$^{13}C_2$]glucose. It is evident a high percentage of [1,2,3-$^{13}C_3$]glucose, but also a strong presence of [U-$^{12}C_6$]glucose. c) Representation of the abundance of other analytes of [1,2,3-$^{13}C_3$]glucose. The most evident isotope present is the [1,2-$^{13}C_2$]glucose. d) Representation of the abundance of other analytes of [U-$^{13}C_6$]glucose. Even though the results show some abundance of [U-$^{12}C_6$]glucose and [1,2,3-$^{13}C_3$]glucose, in fact, their percentages are so low that they will be disregarded. e) Representation of the abundance of other analytes of [U-$^{13}C_6$, U-$^{2}H_7$]glucose. Even though the results show some abundance of [U-$^{13}C_6$]glucose, in fact, they can be disregarded.

The isotopic abundance of the glucose analytes used on this project was also studied in 6 control DBS mice samples (B10.Q strain), being the mean of the percentages of each isotopic analyte obtained from these samples calculated (Fig. 5.10). The [1,2-$^{13}C_2$]glucose is the most abundant glucose isotope within this samples, that is studied on this project. Because of the influence of the natural isotopic abundance, a correction of this abundance is necessary for the ATGL$^{-/-}$ and wild-type samples analysis. Results from biological samples are in agreement with the results of the natural isotopic abundance from the pure standard solutions of [U-$^{12}C_6$]glucose, therefore, correction of the natural isotopic abundance will be calculated from the data of the calibration curves (equation (1)). Because these mice received an infusion and will produce [1,2-$^{13}C_2$]glucose, this analyte may form by natural isotopic abundance [1,2,3-$^{13}C_3$]glucose, therefore, the analogous correction will be performed (equation (2)).

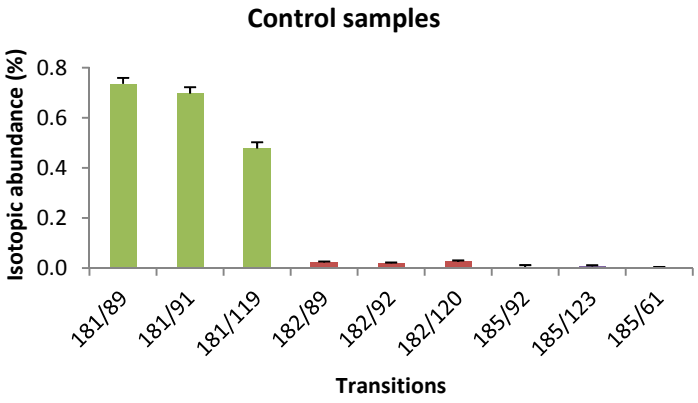

Fig. 5.10| Percentages of the isotopic abundance and the 95% confidence interval of glucose analytes found in 6 different control DBS mice samples. These mice did not receive any labelling, therefore theoretically they would only have [U-$^{12}C_6$]glucose, however, the natural abundance of ^{13}C originates naturally other glucose isotopes studied in this project. The [1,2-$^{13}C_2$]glucose is the isotopic analyte with the greatest abundance, that was obtained by the MRM method developed for the project.

5.2.3. Evaluation of the influence of C18 SPE clean-up in glucose analysis

The C18 SPE step in the sample preparation protocol is intended to be a cleaning step before the analysis by the LC-MS/MS system. Biological matrixes may interfere in the ionization of the sample, especially in LC-MS/MS analysis using ESI. To reduce matrix effect, a proper cleaning step before analysis should be added, which is the reason the C18 SPE step is performed at the end of sample preparation. With this evaluation it is intended to ascertain the

best ACN percentage for elution, after the sample has passed through the C18 SPE zip tip. C18 SPE is a reversed phase chromatography, and since C18 retains mostly hydrophobic compounds, and glucose is hydrophilic, it is expected that glucose will go through the stationary phase and everything else that is hydrophobic, such as lipids, will be retained in the stationary phase.

The results demonstrate that glucose has a very weak interaction with the C18 SPE zip tip, being mostly harvested without any elution step (Fig. 5.11), since glucose is hydrophilic and C18 is an hydrophobic stationary phase. Also it is not relevant the amount of ACN:H_2O that is used for elution (Fig. 5.11). Because of the amount of impurities which can be eluted with a higher concentration of ACN:H_2O and because of the differences in the chromatographic run between samples and calibrants, which are prepared in water, the elution of the C18 SPE zip tips, was performed with a 2% ACN:H_2O solution, which means that the sample will be only in 1% of ACN. This concentration of ACN is not enough to elute hydrophobic compounds, but still removes some residual analytes that might have been left behind.

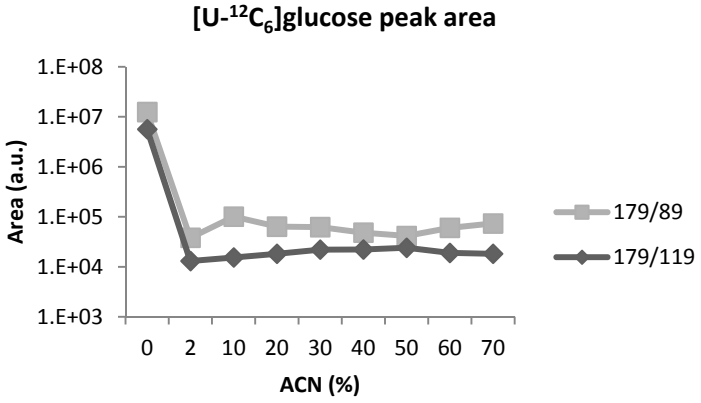

Fig. 5.11| Peak area intensity of the samples harvested at different ACN concentrations in H_2O from the C18 SPE zip tip. Most glucose elutes from the C18 SPE zip tip without adding any ACN.

5.3. Analytical method validation

Data presented in this section was analysed by the Excel® spreadsheet created for the analysis of analytical method validation, applying the criteria mentioned on section 4.2. Because of the amount of results data for each validation parameter, only the summary results or examples are presented.

5.3.1. Selectivity

Six blank sample matrixes spiked with 100µL of 5µM solutions of [U-$^{12}C_6$]glucose/[1,2,3-$^{13}C_3$]glucose and [U-$^{13}C_6$, U-$^{2}H_7$]glucose (IS), and the other six with 5µM solutions of [1,2-$^{13}C_2$]glucose/[U-$^{13}C_6$]glucose and [U-$^{13}C_6$, U-$^{2}H_7$]glucose (IS), were compared with blank matrix negative controls using the WADA criteria (Table 5.1) [114]. In terms of the analysis of the performance of the chromatographic separation, the WADA guidelines state that RT of the analyte (R_A) or a RT_{Ratio} may be used to assess this parameter. For this project, the RT of the analyte was the chosen criteria, since using the RT_{Ratio} would not allow the validation of this parameter, because some values did not fulfil the described criteria. This is probably due to the difference between the structures of the glucose analytes with the [U-$^{13}C_6$, U-$^{2}H_7$]glucose. The fact that this IS is a deuterated analogue might justify slight differences in RT from the other analytes which are only ^{13}C labelled. The positive samples all fulfilled the respective criteria, while negative samples did not. However, these results were already expected, since the negative samples were not absolute negatives, as they were blood of mice that did not receive any labelling, therefore would have present the [U-$^{12}C_6$]glucose analyte, as well as some of their isotope analogues due to the natural isotopic abundance. This is the reason why the results for the [U-$^{13}C_6$, U-$^{2}H_7$]glucose (IS) all fulfil the criteria, because the mice samples would not naturally have this analyte present. It is also possible to see an increase in the negative sample values that fulfil their criteria with an increase in the labelling of the glucose analytes (Supplementary Table 3 - Supplementary Table 7). According to the WADA criteria, if these criteria are met, the developed method is selective for the targeted analytes.

Table 5.1| Example of the application of the acceptance criteria for the identification of [U-$^{12}C_6$]glucose. ND=non-detectable.

	Transition	Relative abundance		S/N	ΔRT	
Criteria	179/89	90.000	110.000	3	7.771	7.971
	179/119	49.480	69.480		7.763	7.963
	Transition	**Absolute area**	**Relative area**	**S/N**	**RT_A**	**RT_{IS}**
Positive#1	179/89	21530842.947	100.000	26997.093	7.871	7.868
	179/119	12806600.755	59.480	28255.335	7.863	7.868
	Transition	**Absolute area**	**Relative area**	**S/N**	**RT_A**	**RT_{IS}**
Negative#1	179/89	13248818.008	100.000	16178.830	7.941	ND
	179/119	7639020.528	57.658	17656.685	7.948	ND

5.3.2. Linearity

Every transition of the method was analysed with the classical linear regression statistics and residuals study (Table 5.2). In terms of the criteria applied to the classical linear regression, all transitions fulfilled such criteria, with every R^2 value above 0.99 and a confidence interval containing zero. However, the residuals study revealed that even though visually, most transitions present a randomly distribution around the x axis, there were some absolute values of residuals that did not fulfil the criteria of being less than the double of $S_{y/x}$ (Supplementary Fig. 2 and

Supplementary Fig. **3**). In fact, these residuals that did not fulfilled the criteria, belonged to the highest calibrants of the transitions of labelled glucoses. This is probably due to poor signal detection for the lowest calibrants because once some of those were eliminated, all the remaining residuals fulfilled the criteria or to variability between the different concentrations. The transitions of [U-$^{12}C_6$]glucose were the only ones which fulfilled all the acceptance criteria within a large range of concentrations. However, upon the visual evaluation of the distribution of residuals within the x axis, these transitions were the ones that presented most variability, because given the larger $S_{y/x}$ for these transitions, the residuals were able to fulfil the acceptance criteria. Upon elimination of the residuals that presented values above the double of the $S_{y/x}$ the calibrants range becomes restricted (Table 5.2).

Table 5.2| Results obtained from the study of the classical linear regression for each of the transitions studied.

Analyte	Transition	Calibrants range (pmol/µL)	Equation	R^2	$S_{y/x}$	95% Confidence interval	
						Lower limit	Upper limit
[U-$^{12}C_6$]glucose	179/89	0.15-250	y = 0.267x + 0.116	0.99901	0.651	-0.328	0.559
	179/119	0.15-250	y = 0.144x + 0.077	0.99918	0.321	-0.142	0.296
[1,2-$^{13}C_2$]glucose	181/89	0.4-250	y = 0.165x – 0.050	0.99973	0.226	-0.225	0.125
	181/91	3-250	y = 0.158x + 0.030	0.99993	0.123	-0.114	0.175
	181/119	1.5-250	y = 0.107x + 0.020	0.99989	0.097	-0.070	0.109
[1,2,3-$^{13}C_3$]glucose	182/89	2-250	y = 0.149x – 0.192	0.99879	0.472	-0.676	0.292
	182/92	1-250	y = 0.150x – 0.086	0.99965	0.238	-0.285	0.113
	182/120	1.5-250	y = 0.102x – 0.125	0.99865	0.330	-0.429	0.179
[U-$^{13}C_6$]glucose	185/92	3-250	y = 0.388x + 0.051	0.99971	0.626	-0.688	0.790
	185/123	2-250	y = 0.156x – 0.052	0.99993	0.123	-0.178	0.074
	185/61	1-250	y = 0.308x – 0.007	0.99997	0.154	-0.136	0.123

5.3.2.1. Mandel test

The Mandel test was used to confirm the linearity of the calibration curves [119]. Some calibrants were eliminated in order to get a perception of the curves behaviour at the concentrations of interest according to the analyte in question. On Table 5.3, the range of concentrations used on the study of each transition after the minimum points have been eliminated is also presented.

Every value of F_{cal} was less than the value of F_{crit}, which means that there is no significant difference between the variances, and therefore, the calibration function follows a linear behaviour using that calibrants range. From these results, it can also be observed that for [U-$^{12}C_6$]glucose would probably be preferable to use transition 179/89 over 179/119 since it presents less variability over a large range of concentrations, and [U-$^{12}C_6$]glucose concentrations are expected to be near the highly concentrated calibrants. For [1,2-$^{13}C_2$]glucose, it would be advisable not to use transition 181/89 since it does not present a linear behaviour over a wide range of concentrations, nevertheless, this analyte is expected to be in low concentrations in this project samples, therefore, considering the working range, it may still be used for quantification. As for [1,2,3-$^{13}C_3$]glucose and [U-$^{13}C_6$]glucose, the less variable transitions over a large range of concentrations were the 182/92 and 185/123 and 185/92 respectively, but the others may still be used in the quantification.

Table 5.3| Results obtained from the Mandel test for each of the transitions studied.

Analyte	Transition	Calibrants range (pmol/µL)	F_{cal}	F_{crit} (N-1; N-1; 0.95)
[U-$^{12}C_6$]glucose	179/89	0.15-250	$1.152X10^{-3}$	2.463
	179/119	0.15-150	1.132	2.550
[1,2-$^{13}C_2$]glucose	181/89	0.15-5	$5.312X10^{-1}$	3.179
	181/91	0.15-250	$6.569X10^{-2}$	2.550
	181/119	0.15-250	1.372	2.550
[1,2,3-$^{13}C_3$]glucose	182/89	0.15-100	1.787	2.788
	182/92	0.15-150	$9.164X10^{-1}$	2.660
	182/120	0.15-100	$8.139X10^{-1}$	2.788
[U-$^{13}C_6$]glucose	185/92	0.15-250	1.644	2.550
	185/123	0.15-250	$6.462X10^{-1}$	2.550
	185/61	0.15-150	$4.102X10^{-1}$	2.660

5.3.2.2. Homoscedasticity test

When using a large calibration range, it should not be expected for that range to have equal variances [133][123]. Using an F test and a low and high calibrant it was possible to confirm that data was indeed heteroscedastic for every transition of every analyte, since the values of F_{cal} were all greater than the values of F_{crit}, indicating a significant difference between the variances (Table 5.4). When the calibrants range is somewhat larger, it might be expected that the variance of each data point to be different. Larger concentrations, tend to present larger deviations, which will influence (weight) the regression line more than smaller deviations associated with smaller concentrations [123]. In the case of this project, this is verified, with the highest calibrant presenting greater deviations than the smaller concentrations, as demonstrated through the example of the plot of the residuals vs. concentration for the transition 179/89 of [U-$^{12}C_6$]glucose (Fig. 5.12).

The linearity of the ESI response is often lost, specially at high concentrations, probably due to a limited amount of excess charge available on ESI droplets or saturation of the ESI droplets with analyte at their surfaces, inhibiting ejection of ions trapped inside the droplets [102].

Table 5.4| Summary of the results obtained from the Homoscedasticity test for each of the transitions studied.

Analyte	Transition	Homoscedasticity test (F_{cal})	F_{crit} (N-1; N-1; 0.95)
[U-$^{12}C_6$]glucose	179/89	916.445	2.978
	179/119	4549.736	
[1,2-$^{13}C_2$]glucose	181/89	591.267	
	181/91	560.743	
	181/119	1488.274	
[1,2,3-$^{13}C_3$]glucose	182/89	600.842	
	182/92	529.280	
	182/120	1461.851	
[U-$^{13}C_6$]glucose	185/92	517.309	
	185/123	423.961	
	185/61	1102.104	

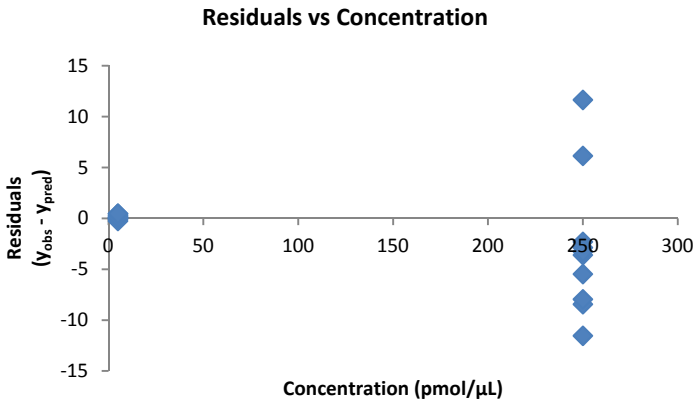

Fig. 5.12| Plot of the residuals vs. concentration used in the homoscedasticity study of the [U-$^{12}C_6$]glucose 179/89 transition. Ten replicates of the lowest and highest calibrant were analyzed to evaluate their variance. The highest calibrant presents significant variance when compared to the lowest calibrant.

5.3.2.3. Weighted least squares regression

Since heteroscedasticity was proven through the Homoscedasticity test (Section 0.), the choice of an appropriate calibration model is recommended [133][124]. Only when data is homoscedastic, the ordinary least squares regression models may be applied [97]. Because of the influence of higher concentrations being different than the influence of smaller concentrations, it becomes necessary to use a weighted least squares regression to compensate these deviations. In this project, empirical weights 1/x; $1/x^2$; $1/x^{1/2}$; 1/y; $1/y^2$; $1/y^{1/2}$ were studied, for the best calibration fit, through the evaluation of the %RE and R^2.

Some of the lowest concentration calibrants could not be properly detected. Whether it is the lack of enough analyte in the solution, a poorly prepared solution, the degradation of the analyte, or a bad sample injection, several reasons can explain why some calibrants are not detected, but most of the times one can only speculate. In the study of the calibration curves prepared in five different days, some calibrants were not detected. In the cases where, signal could not be detected, calculations for the study of the weighted least squares regression preceded without those values, analysing each concentration with the remaining data. Only data of one day for each transitions and each calibrant were affected, remaining the data for the other 4 days and other calibrants. The calibrant 0.15µM was the one which most frequently was poorly detected, which is understandable since it is the lowest calibrant of the calibration curve. The only transition that has their data set complete is the 185/92, however, for all the others, only one or two values of each concentration for the weighted least squares regression evaluation for a specific transition were affected.

On Table 5.5, it is represented the data of the %RE for transition 179/89 of [U-$^{12}C_6$]glucose. First of all, these results show that for every model, most errors occur in the lower concentrations. But most importantly, these results show which is the best fitting model for the calibration curves. By analysing the sum of the %RE, is possible to verify that the models with the lowest errors are the model 2 (1/x) and the model 4 ($1/x^2$), which are the most used factor to compensate for heteroscedasticity [97]. The second criteria that was used for the choice of the best calibration model, was that R^2 should be greater than 0.99. Comparing the mean R^2 values between the five days, of the two pre-selected models, the model 4 ($1/x^2$) does not fulfil this criteria, hence, the model 2 (1/x) is considered the best model to express the calibration curves behaviour.

Table 5.5| Relative errors (%RE) calculated for ordinary and weighted least squares regression for every empirical factor, relative to transition 179/89 of [U-$^{12}C_6$]glucose.

Concentration (pmol/µL)	Model 1 $\frac{1}{x^0}$	Model 2 $\frac{1}{x}$	Model 3 $\frac{1}{y}$	Model 4 $\frac{1}{x^2}$	Model 5 $\frac{1}{y^2}$	Model 6 $\frac{1}{\sqrt{x}}$	Model 7 $\frac{1}{\sqrt{y}}$
0.15	849.868	204.893	368.650	52.224	284.000	364.251	454.540
0.3	699.147	218.290	325.216	167.428	285.667	329.917	380.921
0.45	339.958	145.335	70.817	224.954	107.861	121.758	86.471
0.6	202.392	114.319	81.856	144.766	90.346	96.178	86.063
1.2	122.107	34.210	50.833	40.444	48.759	28.524	41.442
1.5	126.352	95.264	72.683	95.256	71.730	80.914	66.464
2.1	60.112	46.184	32.290	28.821	27.352	30.453	23.685
3	47.129	22.478	28.696	34.803	28.352	21.121	25.575
6	46.320	37.309	34.637	38.588	46.272	37.708	35.543
15	15.071	19.952	17.838	26.400	11.449	19.346	18.117
30	28.458	29.648	28.489	16.353	15.132	30.214	29.513
50	11.140	10.743	11.533	39.575	21.014	11.530	12.070
100	27.780	26.357	26.965	68.162	46.032	27.171	27.576
150	19.136	18.414	18.193	44.360	21.637	18.919	18.712
250	4.306	4.182	4.723	49.878	26.200	4.562	4.813
$\sum \lvert \%RE \rvert$	2599.275	1027.577	1173.419	1072.012	1131.804	1222.566	1311.504
$\overline{R^2}$	0.99818	0.99703	0.99757	0.92185	0.98033	0.99814	0.99817

The results regarding the transitions of other analytes were similar to the ones presented for the transition 179/89 of [U-$^{12}C_6$]glucose, as verified by the results on Table 5.6. Even though, sometimes, model 4 ($1/x^2$) might present a lower value for the sum of the %RE, the

R^2 almost never fulfilled the criteria, which is why it was determined by these data that the transitions of all the analytes should use the 1/x fitting model. Even using smaller working ranges, this model was considered the best. From these results, it can also be observed which transitions present the lowest %RE. In the case of [U-$^{12}C_6$]glucose, it would be the transition 179/89, for [1,2-$^{13}C_2$]glucose it would be 181/91, for [1,2,3-$^{13}C_3$]glucose it would be 182/92, and for [U-$^{13}C_6$]glucose it is the transition 185/92.

Table 5.6| Results obtained from the weighted least squares regression evaluation. This table includes the sum of %RE and the mean of R^2 calculated for ordinary and weighted least squares regression for every empirical factor, relative to every transition of the studied analytes.

Analyte	Transition		Model 1 $\frac{1}{x^0}$	Model 2 $\frac{1}{x}$	Model 3 $\frac{1}{y}$	Model 4 $\frac{1}{x^2}$	Model 5 $\frac{1}{y^2}$	Model 6 $\frac{1}{\sqrt{x}}$	Model 7 $\frac{1}{\sqrt{y}}$
[U-$^{12}C_6$]glucose	179/89	$\sum \lvert\%RE\rvert$	2599.3	1027.6	1173.4	1072.0	1131.8	1222.6	1311.5
		$\overline{R^2}$	0.99818	0.99703	0.99757	0.92185	0.98033	0.99814	0.99817
	179/119	$\sum \lvert\%RE\rvert$	9523.8	1190.1	1221.3	1322.4	1256.6	1577.9	1580.9
		$\overline{R^2}$	0.99569	0.99459	0.99523	0.89505	0.96936	0.99579	0.99588
[1,2-$^{13}C_2$]glucose	181/89	$\sum \lvert\%RE\rvert$	7264.7	884.6	998.0	784.5	1206.8	1707.5	1632.3
		$\overline{R^2}$	0.99805	0.99556	0.99567	0.96180	0.91470	0.99734	0.99742
	181/91	$\sum \lvert\%RE\rvert$	6833.1	849.8	953.8	781.7	1078.9	1579.9	1604.3
		$\overline{R^2}$	0.99841	0.99666	0.99684	0.95986	0.94023	0.99791	0.99799
	181/119	$\sum \lvert\%RE\rvert$	5105.8	875.5	996.5	791.6	1337.9	1197.0	1180.8
		$\overline{R^2}$	0.99789	0.99663	0.99645	0.95538	0.89520	0.99770	0.99774
[1,2,3-$^{13}C_3$]glucose	182/89	$\sum \lvert\%RE\rvert$	3334.4	829.4	963.7	811.1	1249.1	1093.4	1133.0
		$\overline{R^2}$	0.99874	0.99778	0.99758	0.95011	0.92192	0.99866	0.99864
	182/92	$\sum \lvert\%RE\rvert$	2110.3	726.0	853.9	699.6	1041.9	812.4	869.9
		$\overline{R^2}$	0.99854	0.99794	0.99785	0.95687	0.94288	0.99860	0.99860
	182/120	$\sum \lvert\%RE\rvert$	4399.3	979.4	1090.6	873.3	1558.5	1366.6	1405.8
		$\overline{R^2}$	0.99881	0.99706	0.99653	0.95848	0.88167	0.99846	0.99842
[U-$^{13}C_6$]glucose	185/92	$\sum \lvert\%RE\rvert$	6223.6	717.1	838.7	661.2	975.7	1381.4	1354.4
		$\overline{R^2}$	0.99858	0.99666	0.99697	0.96830	0.94791	0.99806	0.99817
	185/123	$\sum \lvert\%RE\rvert$	6501.1	1388.3	1609.3	1732.0	1859.9	1743.2	1799.4
		$\overline{R^2}$	0.99816	0.99539	0.99585	0.87133	0.90404	0.99758	0.99766
	185/61	$\sum \lvert\%RE\rvert$	5846.0	782.3	904.7	701.7	996.9	1266.1	1239.2
		$\overline{R^2}$	0.99820	0.99673	0.99676	0.96630	0.94459	0.99788	0.99790

5.3.3. Limit of detection (LOD) and limit of quantification (LOQ)

The LOD and LOQ were determined for three different working ranges, 0.15–6 µM, 0.15–50µM and 1.5–250µM, by the equations (14) and (15). Three different working ranges were chosen, on one hand because of the expected different sample concentrations, and on the other hand to evaluate the change of LOD and LOQ as the working range varies. From the results obtained with the weighted least squares regression (section 5.3.2.3), it was determined that the best calibration model was 1/x for all transitions. Therefore, the calculi of the standard deviation had to be recalculated using the equation (16).

A summary of the results obtained through the LOD and LOQ calculations is presented on Table 5.7. The results demonstrate that the LOD and LOQ decrease when using working ranges with smaller concentrations. In terms of the evaluation of the LODs and LOQs for each transition, different transitions may be preferable for different working ranges. In the case of [U-$^{12}C_6$]glucose, it seems that transition 179/89 is always preferable, since it presents the lowest values for LOD and LOQ. For [1,2-$^{13}C_2$]glucose, the transition 181/91 is also suitable for all working ranges. However, when analysing the results for [1,2,3-$^{13}C_3$]glucose, the transition 182/89 seems preferable for working ranges with lower concentrations, while transition 182/120 is preferable for higher concentrated working ranges. In the case of [U-$^{13}C_6$]glucose, the preferable transitions for the working ranges of 0.15-6µM and 0.15-50µM, is 185/61, while transition 185/92 is preferable for the higher concentration working ranges. Actually, the fact that a certain transition has the lowest LOD and LOQ values, does not mean, it is the best transition for quantification, these values are only a suggestion. In fact, LOD should be used as information of the performance to the analyst and not as a cut-off, meaning that just because the limit exists, it does not indicate that values obtained under that limit should not be considered [135].

Both LOD and LOQ can be affected by the chromatography. Hence, in the event that the method is altered in the future, efforts to sharper the peaks should be taken, because, sharper peaks will result in higher S/N, and will consequently lower the LOD and LOQ [116].

Table 5.7| Results obtained for the calculi of LOD and LOQ with the 1/x weighted regression model for each of the transitions studied.

Analyte	Transition	LOD			LOQ		
		0.15-6 pmol/µL	0.15-50 pmol/µL	1.5-250 pmol/µL	0.15-6 pmol/µL	0.15-50 pmol/µL	1.5-250 pmol/µL
[U-$^{12}C_6$]glucose	179/89	0.134	0.192	0.478	0.405	0.581	1.450
	179/119	0.213	0.330	2.986	0.644	0.999	9.048
[1,2-$^{13}C_2$]glucose	181/89	0.240	0.343	2.253	0.726	1.040	6.827
	181/91	0.208	0.326	1.421	0.631	0.989	4.307
	181/119	0.209	0.372	2.453	0.633	1.128	7.435
[1,2,3-$^{13}C_3$]glucose	182/89	0.152	0.401	1.280	0.460	1.214	3.880
	182/92	0.191	0.350	1.119	0.578	1.060	3.392
	182/120	0.255	0.270	0.729	0.773	0.818	2.209
[U-$^{13}C_6$]glucose	185/92	0.186	0.213	1.280	0.564	0.645	3.879
	185/123	0.259	0.458	3.351	0.784	1.388	10.153
	185/61	0.131	0.206	2.395	0.396	0.624	7.257

5.3.4. Precision

Precision can be divided into repeatability, intermediate precision and reproducibility. In the context of this validation, only repeatability and the intermediate precision were studied, because reproducibility only has to be studied if the method is going to be used by other laboratories.

The data used in this study was the same as for the weighted least squares regression, which means that, the study of the same transitions was affected by the poor signal detection of a few samples (Section 5.3.2.3). Calculations of the calibration curve's equation were preformed even without one or two calibrants for the precision as well. To study the precision of [U-$^{12}C_6$]glucose, QCs samples with concentrations of 200µM, 20µM and 2.5µM were used as the high, medium and low concentration, respectively. However, for the [1,2-$^{13}C_2$]glucose, [1,2,3-$^{13}C_3$]glucose and [U-$^{13}C_6$]glucose was used an even smaller concentration, the 1.25µM, because based on the preliminary results it is expected for these analytes to be quantified in lower concentrations, compared to [U-$^{12}C_6$]glucose. In cases where the signal of a replicate was not detected, the mean results were obtained by the mean value of the remaining replicates.

On Table 5.8 are represented the %CV regarding repeatability and intermediate precision, as well as the mean nominal and observed concentrations. The %CV values that did not follow the stipulated criteria, which determines that precision calculated at each

concentration level should not exceed 15% of the %CV except for the LOQ, where it should not exceed those values by more than 20%, were highlighted. From the results on Table 5.8, it is possible to distinguish which transitions were calculated with highest precision, which are the ones that fulfil the above mentioned criteria. The typical assumption is that there is no change in precision with analyte level or that the standard deviation is proportional to the analyte level, but often precision varies with analyte concentration [128]. This is once again verified by the results presented on Table 5.8, where it is possible to observe a tendency for the lowest concentrations to be more imprecise.

In the case of [U-$^{12}C_6$]glucose, it can be seen that none of the transitions fully fulfilled their criteria, nevertheless, concentrations on the order of 2.5µM are not expected to be encountered on the animal samples. Comparing the two [U-$^{12}C_6$]glucose transitions, transition 179/89 is therefore more likely to be used for quantification, since it is only imprecise at very low concentrations, rather than transition 179/119, which at even medium concentrations does not entirely fulfil the criteria for precision. In the case of the other analytes, [1,2-$^{13}C_2$]glucose, [1,2,3-$^{13}C_3$]glucose, [U-$^{13}C_6$]glucose, it is more critical that the transitions fulfil their criteria at lower concentrations. However, none of the transitions fulfilled the criteria for the lower concentrations, even though a weighted calibration model was used to calculate the concentrations. This is justified by the use of a wide range of concentrations in the construction of the calibration curves. On section 4.8.3, it was discussed the differences in the LOD and LOQ according to the different concentration ranges, which is the case. The imprecision observed for the lower concentrations is critical for the [1,2,3-$^{13}C_3$]glucose, where the lowest concentrations are expected. For the biological samples, calibrations curves for [1,2-$^{13}C_2$]glucose, [1,2,3-$^{13}C_3$]glucose and [U-$^{13}C_6$]glucose will have a working range near to the lower concentrations.

Because one replicate of the lowest concentration (1.25µM) for the transitions of the analytes [1,2-$^{13}C_2$]glucose, [1,2,3-$^{13}C_3$]glucose and [U-$^{13}C_6$]glucose was not properly detected, the precision parameter was not validated for this concentration, however, results are presented to give an idea of the precision of the method for low concentrations.

Table 5.8| Results obtained from the precision study. Repeatability and intermediate precision were studied for 3 different concentrations, each with 3 replicates. Values that do not fulfil the criteria are highlighted.

Analyte	Transition	Nominal concentration (pmol/µL)	Mean observed concentration (pmol/µL)	Repeatability (%CV)	Intermediate precision (%CV)
[U-$^{12}C_6$]glucose	179/89	2.5	2.0	13.1	29.3
		20	19.3	10.6	9.8
		200	205.5	8.4	7.4
	179/119	2.5	2.3	10.4	24.7
		20	20.3	15.2	14.5
		200	212.1	11.0	13.4
[1,2-$^{13}C_2$]glucose	181/89	1.25	1.1	25.9	33.1
		20	19.8	8.3	8.9
		125	130.0	7.5	9.0
	181/91	1.25	1.1	32.9	34.6
		20	19.7	8.1	7.3
		125	130.5	10.5	14.7
	181/119	1.25	1.1	32.5	37.3
		20	17.6	8.1	11.3
		125	122.7	11.1	11.4
[1,2,3-$^{13}C_3$]glucose	182/89	1.25	1.1	37.6	45.2
		20	19.4	10.2	9.1
		125	122.6	8.4	8.6
	182/92	1.25	1.1	36.1	37.7
		20	19.7	9.5	8.9
		125	125.1	10.9	9.9
	182/120	1.25	1.3	39.2	35.0
		20	19.7	8.2	10.0
		125	122.9	7.4	8.9
[U-$^{13}C_6$]glucose	185/92	1.25	1.2	27.7	31.0
		20	20.3	9.4	8.4
		125	130.8	7.9	11.4
	185/123	1.25	0.8	32.7	58.1
		20	18.2	9.7	10.9
		125	124.2	9.1	10.3
	185/61	1.25	1.2	28.8	29.1
		20	19.7	8.0	7.2
		125	127.1	6.5	8.8

5.3.5. Accuracy

The closeness of mean test results obtained by the method to the true concentration of the analyte is the accuracy of the method [99]. Alongside the accuracy study, it was also calculated the recovery of each analyte, which in this case is the detector response compared to the nominal response. Since calibration curves throughout this project were made in pure solvent solutions, it is important not only to evaluate the recovery obtained by the study within biological matrixes, but also in pure standard solutions.

Data used for the accuracy study, was the same used for precision, therefore, injection errors, and the respective corrections referred on section 5.3.4, where the same.

On Table 5.9 it is represented the %RE for the determination of the method's accuracy, the recovery percentage, as well as the mean nominal and observed concentrations for each QC. The %RE values that did not follow the stipulated criteria were highlighted; these include the mean values which are not within 15% of the actual value, except at LOQ, where the mean values should not deviate by more than 20%. Similarly to the precision study, it is also possible to analyse through Table 5.9 which are the most accurate transitions. These results show that the lowest concentration QCs were usually the most inaccurate, which is also revealed by the lower values of recovery in this concentrations when compared to the others within the same transition.

There was only one transition which did not fulfilled the above mentioned criteria, the 185/123 of the [U-$^{13}C_6$]glucose analyte. Therefore, it is not advisable to use this transition for quantification.

Similar to the precision parameter, because of the poor detection of one replicate of the lowest concentration (1.25µM) for the transitions of the analytes [1,2-$^{13}C_2$]glucose, [1,2,3-$^{13}C_3$]glucose and [U-$^{13}C_6$]glucose, the accuracy parameter was not validated for this concentration, however, results are presented to give an idea of the accuracy of the method for low concentrations.

Table 5.9| Results obtained from the accuracy study. Accuracy and recovery of standard solutions were studied for 3 different concentrations, each with 3 replicates. Values that do not fulfil the criteria are highlighted.

Analyte	Transition	Nominal concentration (pmol/µL)	Mean observed concentration (pmol/µL)	Accuracy (%RE)	Recovery (%)
[U-$^{12}C_6$]glucose	179/89	2.5	2.0	-18.4	81.6
		20	19.3	-3.5	96.5
		200	205.5	2.8	102.8
	179/119	2.5	2.3	-9.3	90.7
		20	20.3	1.7	101.7
		200	212.1	6.0	106.0
[1,2-$^{13}C_2$]glucose	181/89	1.25	1.1	-9.6	90.4
		20	19.8	-0.9	99.1
		125	130.0	4.0	104.0
	181/91	1.25	1.1	-15.5	84.5
		20	19.7	-1.3	98.7
		125	130.5	4.4	104.4
	181/119	1.25	1.1	-9.7	90.3
		20	17.6	-11.8	88.2
		125	122.7	-1.9	98.1
[1,2,3-$^{13}C_3$]glucose	182/89	1.25	1.1	-10.5	89.5
		20	19.4	-2.8	97.2
		125	122.6	-1.9	98.1
	182/92	1.25	1.1	-8.2	91.8
		20	19.7	-1.6	98.4
		125	125.1	0.04	100.0
	182/120	1.25	1.3	1.0	101.0
		20	19.7	-1.3	98.7
		125	122.9	-1.7	98.3
[U-$^{13}C_6$]glucose	185/92	1.25	1.2	-4.5	95.5
		20	20.3	1.3	101.3
		125	130.8	4.6	104.6
	185/123	1.25	0.8	-35.7	64.3
		20	18.2	-8.9	91.1
		125	124.2	-0.7	99.3
	185/61	1.25	1.2	-1.5	98.5
		20	19.7	-1.7	98.3
		125	127.1	1.7	101.7

5.3.6. Carry-Over

When carry-over is verified, it can influence analysis, particularly if after a highly concentrated sample the system is not effectively cleaned by the developed method, resulting in some signal from the previous analysis added to the signal of the following sample. To test if the analytes used in this project were suffering carry-over through several runs, three replicates of the highest calibrator (250µM) and the medium (15µM) were injected, followed by the injection of three blanks.

Data used in the carry-over analysis is absolute peak areas instead of peak area ratios. On Fig. 5.13 it is represented the chromatograms obtained for the medium (15µM) and high (250µM) concentrations and the respective blanks for the 179/89 transition of [U-$^{12}C_6$]glucose. This is an example of the visual evaluation preformed for the carry-over study.

On Table 5.10 it is represented the mean results obtained for the replicate's absolute peak area, and the mean absolute peak areas of the blank injection that followed. It should be noted that these results, which represent some signal detection in the blanks, do not mean that for every replicate a signal was detected, but instead these results are the mean results in which no signal detection is translated into a zero. For each transition it was calculated the LOQ from three replicates to apply the criteria mentioned on section 4.8.6, which states that carry-over in a blank sample following a high concentration standard should not be greater than 20% of the LOQ and 5% for the IS [84][98][127]. The values that did not fulfil these criteria were highlighted. Overall, results show that there was no carry-over observed for most of the transitions. Only transitions 179/119, 185/123 and 185/61 presented some signal in the blank samples, but from these transitions only transition 185/123 did not fulfilled the criteria, hence it is not advisable to use this transition for quantification. In this particular case, the fact that this transition was proven to be imprecise and inaccurate, might justify the aberrant values for the carry-over study. For analytes [1,2-$^{13}C_2$]glucose and [1,2,3-$^{13}C_3$]glucose, none of the transitions presented carry-over, but for [U-$^{12}C_6$]glucose, transition 179/89 should be chosen for quantification over 179/119, which might present some carry-over nevertheless. As for [U-$^{13}C_6$]glucose, only transition 185/92 does not seem to present any carry-over.

To prevent the carry-over effect, the chromatographic method was developed, in order to have 2 blank programs between each sample injection. In each blank program, 19µL of H_2O are injected to clean the system, and elute any remaining analytes from the column. The first blank program has 4min and is preformed in the positive mode, with the purpose of degrading any clusters that might form in the emitter. The following 8min blank program is preformed in the negative mode with an increasing gradient of ACN to equilibrate the column before the next injection. Also, the samples' program has 15min, while the analytes have a RT of 8min, therefore it is expected to observe most of the analytes at 8min and not at the end of the 15min. Furthermore, other concerns were applied, such as the analysis of calibration samples from low concentration to high [98] and the injection of two blank samples using the samples running program between different calibration curves.

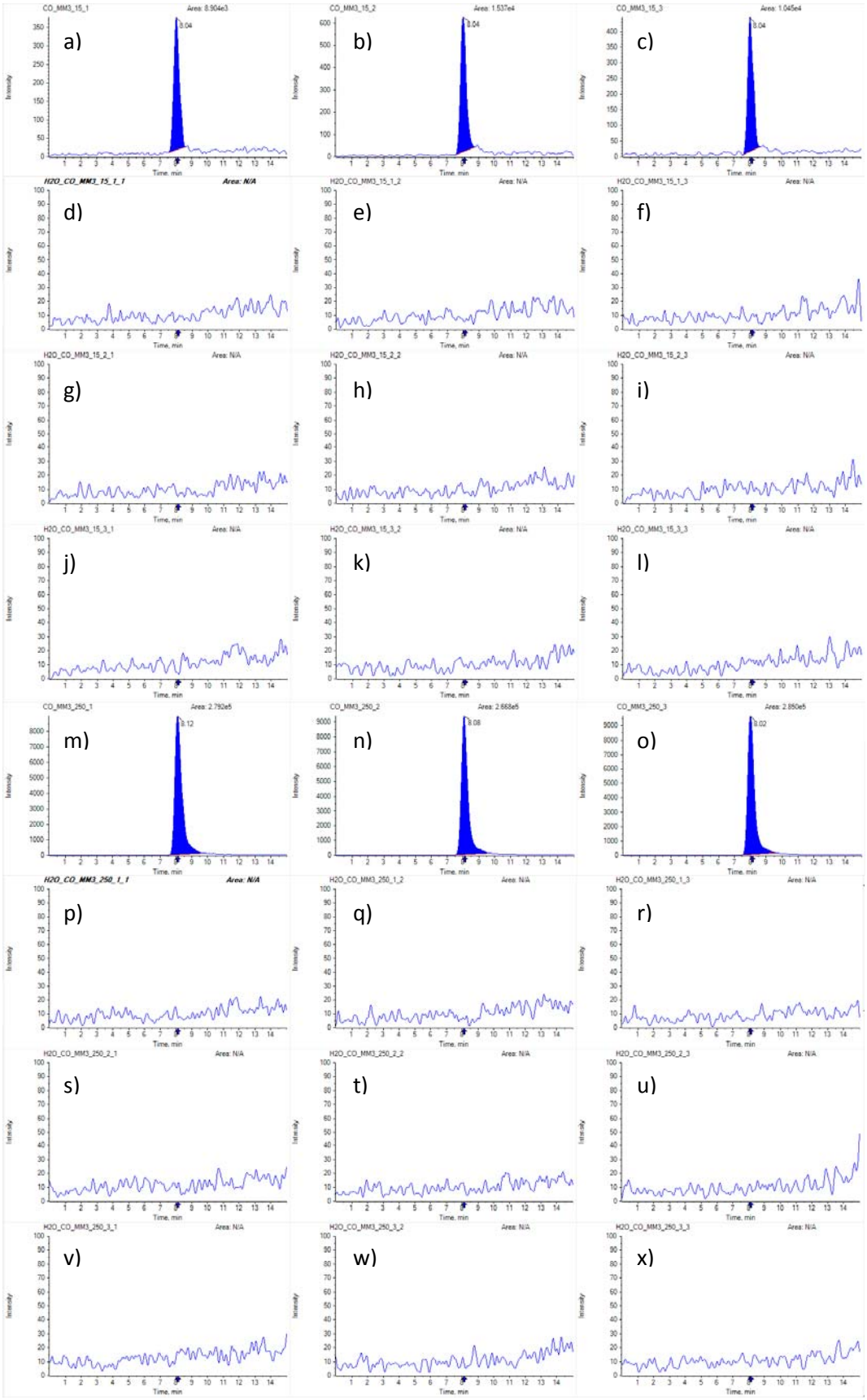

Fig. 5.13| Representation of the chromatograms of the 15µM replicates and respective blank injections (above) and of the 250µM replicates and respective blank injections (below), relative to transition 179/89 of [U-$^{12}C_6$]glucose. a-c) 15µM replicates; d-f) Blanks of replicate a; g-i) Blanks of replicate b; j-l) Blanks of replicate c; m-o) 250µM replicates; p-r) Blanks of replicate m; s-u) Blanks of replicate n; v-x) Blanks of replicate o.

Table 5.10| Results obtained from the carry-over study. Values that do not fulfil the criteria are highlighted. ND=non-detectable.

Analyte	Transition	Nominal concentration (pmol/µL)	Mean replicate's absolute peak area	Mean blank #1 absolute peak area	Mean blank #2 absolute peak area	Mean blank #3 absolute peak area
[U-$^{12}C_6$]glucose	179/89	15	6943.7	ND	ND	ND
		250	166197.2	ND	ND	ND
	179/119	15	8458.8	ND	51.4	42.6
		250	176537.8	120.8	52.3	ND
[1,2-$^{13}C_2$]glucose	181/89	15	5308.2	ND	ND	ND
		250	118657.9	ND	ND	ND
	181/91	15	9367.1	ND	ND	ND
		250	119296.7	ND	ND	ND
	181/119	15	2879.0	ND	ND	ND
		250	54906.0	ND	ND	ND
[1,2,3-$^{13}C_3$]glucose	182/89	15	3596.7	ND	ND	ND
		250	85143.5	ND	ND	ND
	182/92	15	4260.6	ND	ND	ND
		250	94073.1	ND	ND	ND
	182/120	15	1785.8	ND	ND	ND
		250	41796.0	ND	ND	ND
[U-$^{13}C_6$]glucose	185/92	15	10860.6	ND	ND	ND
		250	231375.9	ND	ND	ND
	185/123	15	2908.5	89.1	58.6	ND
		250	56981.2	79.2	136.4	34.0
	185/61	15	8340.5	ND	83.9	128.1
		250	167089.9	ND	ND	42.7

5.3.7. Recovery

Even though recovery may not be considered essential as a validation parameter for some guidelines, in this project it was studied the recovery of analytes using the sample treatment as described on section 4.5. As recommended for LC-MS/MS analysis, the recovery study was performed together with the matrix effect experiments [97].

Recovery was calculated for 3 concentrations, 0.6µM, 15µM and 250µM, corresponding respectively to the low, medium and high concentrations, with 3 replicates each (Table 5.11). Recovery was calculated as a percentage by the ratio of the mean relative area of samples spiked before extraction and the mean relative area of samples spiked after extraction. For these

results only the signal of one sample spiked before extraction of the low concentration sample regarding transition 185/123 was not detected, therefore the mean value presented for this transition at low concentrations was calculated using only the two other values.

These results all fulfilled the criteria, which was that the recovery percentage should be above 50% [97]. Even though all transitions fulfilled the criteria, some differences in recovery values can be noticed. The lowest values of recovery in the high concentration samples are probably due to the step of transference of supernatant. In this step, there is always some volume that is not transferred and that might contain analytes. Also, this study was performed using 1.5mL microcentrifuge tubes, with a funnel shape. It was observed that, when using 2mL microcentrifuge tubes with round shape, more volume is harvested, this would represent higher values of recovery. Therefore, it would be interesting to study this difference in the future.

For this project it is not critical that the recovery percentages are not 100%. First of all, the IS is added in the first step of analyte extraction from the filter paper, therefore any losses of analyte that might occur, will occur for both the analyte and the IS, correcting those losses. It would be preferable to add the IS at the moment of sampling, however, for this project this was not possible. Also, because the aim is to calculate enrichments, it is not as important the amount of analyte present in the sample, but the ratios between the analytes in the sample.

Table 5.11| Results obtained from the recovery study.

Analyte	Transition	Low concentration recovery (%)	Medium concentration recovery (%)	HIgh concentration recovery (%)
[U-$^{12}C_6$]glucose	179/89	96.4	94.9	78.0
	179/119	95.0	97.4	82.6
[1,2-$^{13}C_2$]glucose	181/89	78.7	84.1	67.4
	181/91	91.8	86.9	70.1
	181/119	78.5	81.0	69.4
[1,2,3-$^{13}C_3$]glucose	182/89	71.1	84.2	73.3
	182/92	69.4	78.3	68.6
	182/120	79.4	92.8	69.7
[U-$^{13}C_6$]glucose	185/92	87.2	72.3	69.1
	185/123	93.5	70.5	72.5
	185/61	102.9	76.0	70.4

5.3.8. Matrix Effect

Some matrix components might interfere with analyte detection, and one of the reasons is ionization suppression or enhancement. The mechanism of analyte signal suppression/enhancement is not clear, but one hypothesis is that matrix components, such as non-volatile or less volatile solutes, cause a change in the spray droplet solution properties [136], another is that molecules with higher mass will suppress the signal of smaller molecules [137], and finally that more polar analytes are more susceptible to suppression [138]. Particularly in LC-MS techniques with ESI it is mandatory to evaluate matrix effects [98].

The matrix effect was studied on samples spiked after extraction at three concentrations (0.6µM, 15µM and 250µM), with 3 replicates each (same samples used for the recovery study) and the spike solutions as the pure solvent solutions (Table 5.12). The f value was then calculated using equation (22). As mentioned on the recovery results (section 5.3.7), the signal of the low concentration sample, spiked before extraction, regarding transition 185/123 was not detected, therefore the mean value presented for this transition was calculated using only the two other values as well.

Using equation (22) to assess matrix effect, an f value equal to zero would represent no matrix effect; a negative value would indicate ion suppression and a positive one, ion enhancement [98]. The results on Table 5.12, indicate that according to the concentrations studied, they vary in a way that it is not possible to state that an analyte suffers ions suppression or ion enhancement. For most analytes, studied in this project, f value was close to zero indicating low matrix effect. Only [U-$^{12}C_6$]glucose and [1,2-$^{13}C_2$]glucose were an exception, with high values of matrix effect, especially for the low concentrations. Because [U-$^{12}C_6$]glucose is an endogenous compound, and as demonstrated on section 5.2.2, there is still some abundance of [1,2-$^{13}C_2$]glucose, when performing the calculation of the f value, the spiked solution will not be at the same concentration as the pure solvent solution, resulting in incorrect f values for the matrix effect. This is also the reason why the lower concentrations seem to be the most affected, because there is a significant difference in concentrations. Another approach should be used in order to study the matrix effect for these two analytes.

Even though f values were not high, several %CV did not fulfil the criteria of being below 15%. These values were highlighted on Table 5.12. The results, indicate that the matrix effect varies greatly among samples, which is why it is recommended to add an IS, so that those

differences among samples can be compensated, because it is expected that the matrix effect observed for the analyte, will be similar to the matrix effect observed for the IS.

Table 5.12| Results obtained from the matrix effect study regarding the f value. f value and %CV were calculated for each transition at 3 different concentrations. Values that do not fulfil the criteria are highlighted.

Analyte	Transition		Low concentration	Medium concentration	High concentration
[U-$^{12}C_6$]glucose	179/89	f	288.244	16.426	0.738
		%CV	25.576	12.932	20.031
	179/119	f	258.916	13.722	0.655
		%CV	25.076	15.742	14.372
[1,2-$^{13}C_2$]glucose	181/89	f	9.020	-0.04	-0.119
		%CV	16.865	305.173	158.916
	181/91	f	6.010	-0.051	-0.135
		%CV	30.247	99.558	150.007
	181/119	f	4.487	0.137	-0.089
		%CV	22.325	49.769	192.667
[1,2,3-$^{13}C_3$]glucose	182/89	f	-0.298	-0.116	-0.130
		%CV	64.374	68.812	12.558
	182/92	f	-0.092	-0.101	-0.153
		%CV	207.062	25.049	2.330
	182/120	f	0.132	-0.003	-0.118
		%CV	150.701	1451.330	20.318
[U-$^{13}C_6$]glucose	185/92	f	-0.153	-0.165	-0.145
		%CV	78.271	34.633	114.627
	185/123	f	0.180	-0.142	-0.178
		%CV	18.646	98.812	98.478
	185/61	f	0.135	-0.182	-0.145
		%CV	97.623	48.563	107.962

It is believed that labelled analogues minimize matrix effects as they co-elute with the compound of interest, and thus are influenced in the same way by the matrix. However, f_{IS} should always be evaluated as even a slight difference in RT can diminish this compensation effect. In the results obtained on selectivity (section 5.3.1), a slight difference in RT was in fact observed, hence the f_{IS} was calculated to ensure the IS was compensating for the matrix effect. Not always the analyte/IS response compensates entirely for the matrix effect (Table 5.13), as demonstrated by the highlighted values of %CV, which did not fulfil the criteria. It should be noted however, that just as the f matrix effect factor data from [U-$^{12}C_6$]glucose and [1,2-

$^{13}C_2$]glucose were not considered, the respective relative f_{IS} matrix effect factor were not considered as well. The fact that the sample treatment protocol had to be adapted to perform this study, may affect the results, because with the dilution of samples, matrix effect is decreased, but with the injection of more sample volume, the matrix effect is increased. However, the protocol was performed this way in order to add the same volumes of spike solution and IS solution, injecting the same number of moles. Also, Wang et al. have shown that a deuterium labelled IS was not able to entirely compensate for the observed matrix effects [139]. Usually, a uniformly ^{13}C labelled analogue would be preferable, since deuterium and hydrogen have greater differences in their physical properties than ^{12}C and ^{13}C [102], but because [U-$^{13}C_6$]glucose will be studied in this project, the alternative was to use its deuterated analogue. Since a smaller volume of sample is usually injected, the matrix effect study should be repeated, using a different protocol.

Table 5.13| Results obtained from the matrix effect study regarding the f_{IS} value. Values that do not fulfil the criteria are highlighted.

Analyte	Transition		Low concentration	Medium concentration	High concentration
[U-$^{12}C_6$]glucose	179/89	f_{IS}	511.892	18.361	1.111
		%CV	33.118	20.369	42.541
	179/119	f_{IS}	459.634	15.368	1.006
		%CV	32.446	22.633	39.232
[1,2-$^{13}C_2$]glucose	181/89	f_{IS}	10.834	0.137	-0.010
		%CV	9.202	96.118	1321.774
	181/91	f_{IS}	7.541	0.134	-0.034
		%CV	45.689	107.296	306.092
	181/119	f_{IS}	5.716	0.356	0.025
		%CV	42.145	44.725	400.677
[1,2,3-$^{13}C_3$]glucose	182/89	f_{IS}	0.253	-0.028	0.053
		%CV	192.262	183.619	346.039
	182/92	f_{IS}	0.600	-0.007	0.025
		%CV	69.481	1246.830	710.552
	182/120	f_{IS}	0.968	0.104	0.066
		%CV	25.152	136.290	269.019
[U-$^{13}C_6$]glucose	185/92	f_{IS}	0.001	-0.002	-0.038
		%CV	6933.742	7359.397	291.391
	185/123	f_{IS}	0.379	0.0119	-0.077
		%CV	97.732	563.784	148.530
	185/61	f_{IS}	0.346	-0.026	-0.034
		%CV	40.481	464.135	345.172

Several reasons have been proposed to explain matrix effects. For example, that endogenous compounds can outcompete analytes for the limited charge on the droplet surfaces. With an increase in viscosity and surface tension of the droplets caused by interfering compounds, reducing solvent evaporation and the ability of the analyte to reach the gas phase can occur. Non-volatile materials, can in turn, decrease the efficiency of droplet formation through coprecipitation of the analyte or by preventing droplets from reaching their critical radius required for gas phase ions to be emitted. Analyte ions can also be neutralized in the gas phase via deprotonation reactions with high gas phase alkaline substances, leading to suppression of their response signal [102].

Matrix effects can be reduced, for example by using proper sample clean-up, which was the reason to add the C18 clean-up step after sample extraction. Also, injecting smaller volumes or diluting the samples can help decrease the matrix effect, which is already done, because only 1µL of sample is injected, and before injection samples are diluted by 50% with the IS solution. Another approach is to use an IS to compensate for the alteration in signal [102]. Indeed for this study, the IS was used, however, the fact that 2µL of sample were injected instead of 1µL might have influenced the results. Matrix effect cannot be totally avoided, but the most important, is that when applying an analytical method, the matrix effects observed are independent of the origin of the matrix. Meaning that different pools of matrix will not affect the observed matrix effects differently [98].

5.3.9. Stability

Several studies of stability can be performed. It is important that during these studies, sample handling and storage conditions mimic the actual conditions, being studied with the same storage vessels, same storage temperature and time, and same matrix [98][134]. In this project only the freeze and thaw, the stock solution, and post-preparative stability were studied, and the criteria applied for the freeze and thaw and the stock solution stability were the same.

The freeze and thaw study was performed in three concentrations (1.25µM, 20µM and 250µM), with three replicates each. Samples were prepared, divided in aliquots and both frozen. One of the aliquots was then subjected to three freeze and thaw cycles prior to analysis (Supplementary Table 8). For the high concentration samples, only the transition of [U-$^{13}C_6$]glucose 185/123 failed to meet the criteria of the confidence interval limits, but as observed in the other validation parameters, these transitions is associated with variability. For the

medium concentration samples, none of the [U-$^{12}C_6$]glucose transitions fulfilled the confidence interval criteria, for [1,2-$^{13}C_2$]glucose, only transition 181/89 fulfilled the criteria, for [1,2,3-$^{13}C_3$]glucose, none of the transitions fulfilled the criteria, and for [U-$^{13}C_6$]glucose, only transition 185/123 fulfilled the criteria. Regarding the lowest concentration, for [U-$^{12}C_6$]glucose, transition 179/119 fulfilled the criteria, for [1,2-$^{13}C_2$]glucose none of the transitions fulfilled the criteria, for [1,2,3-$^{13}C_3$]glucose only transition 182/89 fulfilled the criteria and for [U-$^{13}C_6$]glucose none of the transitions fulfilled the criteria. From these results, it is recommended that no freeze and thaw cycles should be performed on the samples, since they introduce significant variability to the ^{13}C-isotopomer measurements.

The study of the stability of stock solutions was also performed on the same three concentrations as studied for the freeze and thaw stability study, with three replicates each. For these test, solutions prepared from one stock solution were compared to solutions prepared from a one month older stock solution (Supplementary Table 9). For the high and medium concentrations, the only results that fulfilled the criteria were the values for the [U-$^{12}C_6$]glucose transitions. However, for the low concentrations, those transitions no longer fulfilled the criteria. The other analytes, most did not fulfilled the criteria, which can be due to increase in variability as referred for the freeze and thaw stability study, or to increased instability by the labelled compounds, or to solvent variations, since the stability samples were higher than the respective controls. The calibration curve used in this study should also be taken into consideration, because control samples were produced from the same stock solution that originated the calibration curve, while the stability solutions were not, leading to misinterpretation of concentration values. Taking these results into consideration, it is not advisable to use stock solutions that are more than one month old.

The post-preparative stability was studied for the same concentrations as the other stability studies. Samples were left in the autosampler after their analysis, and after the analysis of several other samples, these were reanalyzed. From the visual inspection of the absolute peak areas, it is evident a decrease in signal intensity for all analytes (Fig. 5.14), which is due not only to analyte degradation but system loss of sensitivity at the end of several analysis. When ratios were evaluated, apparently the intensities were maintained (Fig. 5.15), even though when acceptance criteria were applied, some transitions did not fulfil their acceptance criteria (Supplementary Table 10). These variations can be due to solvent evaporation after the rubber seal has been punctured in the first analysis, which would lead to sample concentration. Also, because the autosampler during the entire project was not being refrigerated, samples are more

likely to degrade under these conditions. Because this is a solution that has already been prepared, and therefore already contains IS, it is expected that the IS will compensate for any alterations. It was not evident a decrease or increase in sample concentration values, they presented however some variability amongst each other that resulted in not being able to fulfil the acceptance criteria. However, by the visual inspection of the data it is clear that the IS compensates for the systems loss of sensitivity or alterations in sample concentrations (Fig. 5.15).

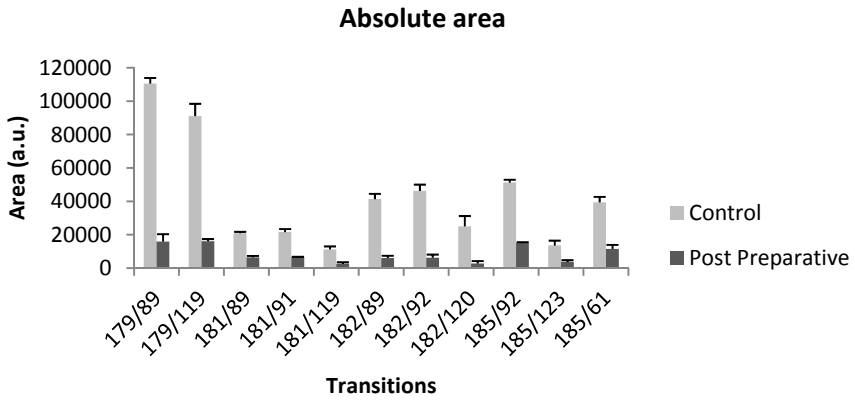

Fig. 5.14| Mean peak areas and 95% confidence intervals of the control and post-preparative 20µM samples for the study of all transitions. After injecting 3 concentrations, each with 3 replicates, samples are kept in the autosampler until they are reinjected at the end of the batch. Some degradation and loss of sensitivity from the instrument of analysis decrease the area intensity over the time.

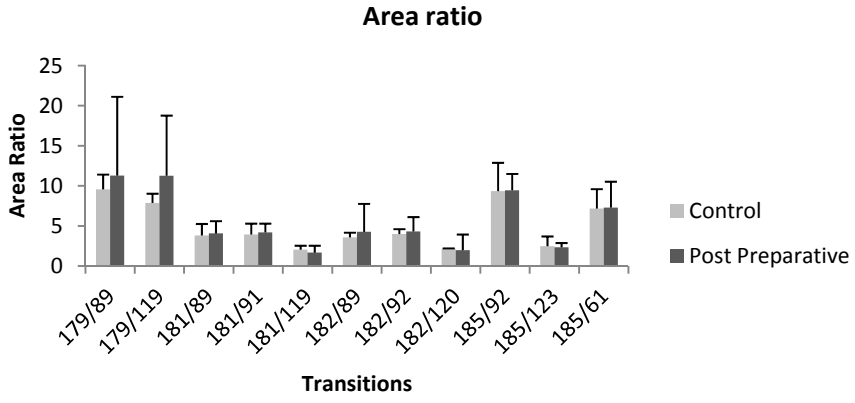

Fig. 5.15| Mean peak area ratios and 95% confidence intervals of the control and post-preparative 20µM samples for the study of all transitions. After injecting 3 concentrations, each with 3 replicates, samples are kept in the autosampler until they are reinjected at the end of the batch. The IS compensates for degradation and loss of the instrument's sensitivity.

The results for the three stability parameters studied were not clear in terms of stability of the glucose analytes. However, it is advisable that in the future solutions should be freshly prepared and the autosampler should be properly refrigerated. Relatively to the stability parameters, that were not studied, it is recommended that they will be studied in the future.

5.4. Biological samples

For the analysis and quantification of the biological samples, calibration curves were prepared in triplicate as described on section 4.4. Due to the results obtained from the method validation, the weighted least squares regression model 1/x was applied to the calibration curves, the working range for different analytes was restricted and the LOD and LOQ were taken into consideration. In addition, only the results regarding transition 179/89 for [U-$^{12}C_6$]glucose, 181/91 for [1,2-$^{13}C_2$]glucose, 182/92 for [1,2,3-$^{13}C_3$]glucose and 185/92 for [U-$^{13}C_6$]glucose will be presented and analysed. In terms of the working ranges used in samples quantification, it was determined that for [U-$^{12}C_6$]glucose the working range would be from 1.2µM to 250µM, which would represent a LOD of approximately 0.4µM and a LOQ of 1.4µM. For [1,2-$^{13}C_2$]glucose, the working range was narrowed to 1.2µM to 50µM. Because the concentration values for this analyte were low, the working range was reduced to obtain lower LOD and LOQ, which would be of 0.3µM and 1µM respectively. In the case of [1,2,3-$^{13}C_3$]glucose, even smaller concentrations needed to be quantified, therefore its working range was narrowed to a calibration curve from 0.15µM to 15µM with a LOD of approximately 0.15µM and a LOQ of approximately 0.5µM. Because [U-$^{13}C_6$]glucose was the analyte given in the infusion it is expected to be in high concentrations, therefore the working range chosen was of 1.2µM to 250µM, which yields a LOD of approximately 1.2µM and a LOQ of 3.8µM. The values for LOD and LOQ for each transition were taken into consideration, with the samples being quantified above these limits. The samples that could not be interpolated from the calibration curves were not quantified. Furthermore, due to the natural isotopic abundance, the values of the concentration of [1,2-$^{13}C_2$]glucose and [1,2,3-$^{13}C_3$]glucose were subtracted by their natural isotopic abundance calculated from the calibration curves as explained on section 4.6. The samples concentration values will not be presented because this concentration concerns the concentration within the DBS punch and not within the animal. Instead, the enrichment values for each animal were calculated and analysed.

Table 5.14| Transitions and respective calibrants range, equation and R^2 for the quantification of each analyte.

Analyte	Transition	Calibrants range (pmol/µL)	Equation	R^2
[U-$^{12}C_6$]glucose	179/89	1.2 - 250	y = 0.490x – 0.133	0.99908
[1,2-$^{13}C_2$]glucose	181/91	0.6 – 50	y = 0.244x + 0.024	0.99919
[1,2,3-$^{13}C_3$]glucose	182/92	0.15 – 15	y = 0.225x – 0.006	0.99828
[U-$^{13}C_6$]glucose	185/92	1.2 - 250	y = 0.608x - 0.103	0.99842

DBS samples were separated into wild-types and knock-outs, and furthermore into the 3 sampling times: 105, 110, and 115min. Using the enrichment values, a Grubbs test was performed to detect outliers within groups. This test resulted in the exclusion of two knock-out samples from the 3 sampling times. These two mice had unrealistically high values for [U-$^{13}C_6$]glucose, which might indicate an artefact arising from incomplete mixing of infused [U-$^{13}C_6$]glucose with endogenous [U-$^{12}C_6$]glucose in these animals. After eliminating the values that could not be quantified and the outliers, for the sampling time of 105min after start of infusion, 5 knock-outs and 11 wild-types were analysed For the sampling times 110 and 115min, evaluations were performed on 6 knock-outs and 13 wild-types. The data presented next represents mean results with a confidence interval of 95%. The isotopic abundance of [1,2-$^{13}C_2$]glucose, [1,2,3-$^{13}C_3$]glucose and [U-$^{13}C_6$]glucose were verified for 0min, and were neglected.

The reason why sampling was performed at minutes 105, 110 and 115min is to indicate if plasma glucose levels were at isotopic steady-state, as seen by a constant level of glucose isotopomer enrichments over the 105-115min interval. The results (Fig. 5.16, Fig. 5.17 and Fig. 5.18) show that enrichments of [1,2-$^{13}C_2$]glucose, [1,2,3-$^{13}C_3$]glucose and [U-$^{13}C_6$]glucose were constant over this period, indicating attainment of isotopic steady-state.

The mean enrichment values of [1,2-$^{13}C_2$]glucose, [1,2,3-$^{13}C_3$]glucose and [U-$^{13}C_6$]glucose for the ATGL$^{-/-}$ mice were higher than the respective values for the wild-types, even though this was contrary of what was expected (Fig. 5.16 - Fig. 5.18). The difference between ATGL$^{-/-}$ and WT for [1,2,3-$^{13}C_3$]glucose enrichment however, was not statically significant (105min, P=0.200; 110min, P=0.364; 115min, P=0.615), but there is a tendency for the enrichment of this analyte to be higher in ATGL$^{-/-}$. Higher enrichment in [U-$^{13}C_6$]glucose indicates that this tracer was not diluted by the EGP as much as for the wild-types. Moreover, less recycling through the Cori cycle was expected for ATGL$^{-/-}$ mice, however higher enrichment values at least for [1,2-$^{13}C_2$]glucose in the ATGL$^{-/-}$ mice contradict this hypothesis.

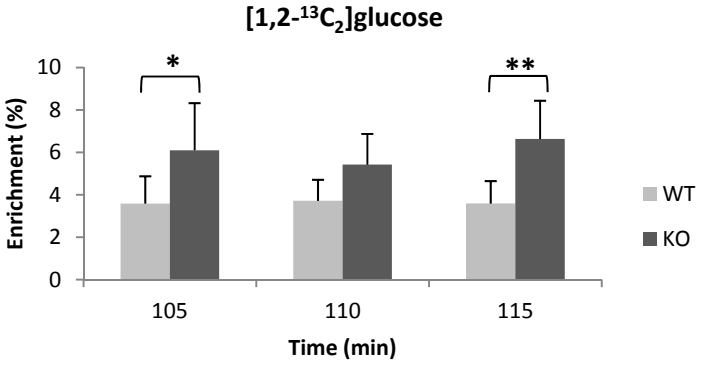

Fig. 5.16| Mean enrichment and 95% confidence intervals of wild-types and ATGL$^{-/-}$ at 105, 110 and 115 minutes sampling for the [1,2-$^{13}C_2$]glucose analyte. ATGL$^{-/-}$ presented higher enrichment of the isotope [1,2-$^{13}C_2$]glucose than the wild-types. *P<0.05, **P<0.01, KO vs. WT at the same time point; ATGL$^{-/-}$, n=5; WT, n=11.

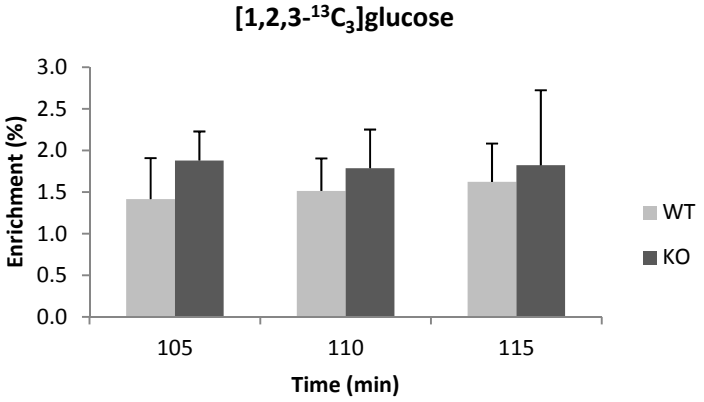

Fig. 5.17| Mean enrichment and 95% confidence intervals of wild-types and ATGL$^{-/-}$ at 105, 110 and 115 minutes sampling for the [1,2,3-$^{13}C_3$]glucose analyte. ATGL$^{-/-}$ presented higher enrichment of the isotope [1,2,3-$^{13}C_3$]glucose than the wild-types. Results not statistical different. ATGL$^{-/-}$, n=6; WT, n=13.

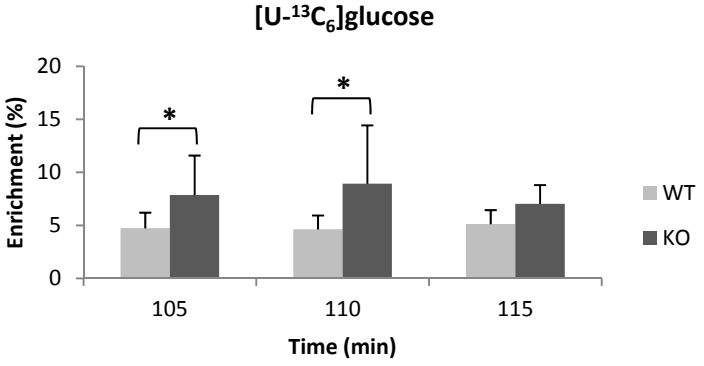

Fig. 5.18| Mean enrichment and 95% confidence intervals of wild-types and ATGL$^{-/-}$ at 105, 110 and 115 minutes sampling for the [U-$^{13}C_6$]glucose analyte. ATGL$^{-/-}$ presented higher enrichment of the isotope [U-$^{13}C_6$]glucose than the wild-types. *P<0.05, KO vs. WT at the same time point; ATGL$^{-/-}$, n=6; WT, n=13.

An important feature to mention from the analysis of the enrichments of both wild-types and ATGL$^{-/-}$ mice is the proportion of the enrichments of [1,2-$^{13}C_2$]glucose and [1,2,3-$^{13}C_3$]glucose. [1,2-$^{13}C_2$]glucose is generated due to some labelling loss from entering other metabolic cycles, and [1,2,3-$^{13}C_3$]glucose is generated by direct entry of glucose into the Cori cycle. The results illustrate that the enrichment of [1,2-$^{13}C_2$]glucose is in fact higher than the enrichment of [1,2,3-$^{13}C_3$]glucose (Fig. 5.19), showing that it is more likely that glucose is used as an intermediate for other metabolic cycles, than to be recycled immediately.

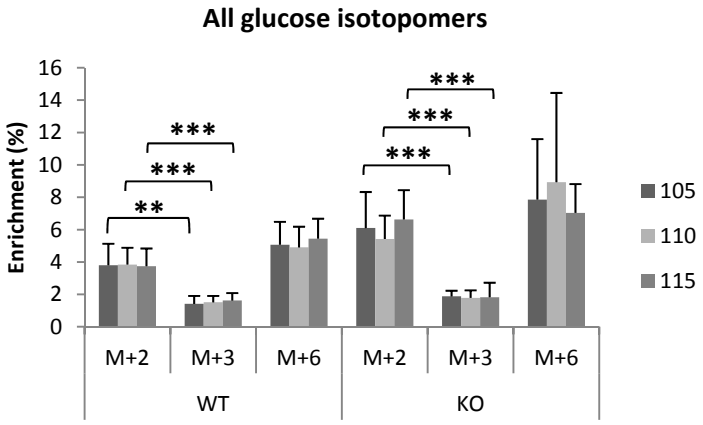

Fig. 5.19| Mean enrichment and 95% confidence intervals of wild-types and ATGL$^{-/-}$ at 105, 110 and 115 minutes sampling for all analytes. **P<0.01, ***P<0.001 M+2 vs. M+3 at the same time point. For time point 105min, ATGL$^{-/-}$, n=5; WT, n=11; 110min, ATGL$^{-/-}$, n=6; WT, n=13; and 115min, ATGL$^{-/-}$, n=6; WT, n=13.

As demonstrated by the high [U-$^{13}C_6$]glucose enrichment in the ATGL$^{-/-}$ mice (Fig. 5.18), EGP in these animals is less than EGP in wild-type animals. Even though, these values are not statistically significant (105min, P=0.252; 110min, P=0.089; 115min, P=0.335), there is a propensity for gluconeogenesis in ATGL$^{-/-}$. The mean values for the three steady state conditions were calculated for enrichment of the infusion [U-$^{13}C_6$]glucose, as well as the Ra and EGP (Table 5.15). Results for KO5, WT5 and WT10 were calculated by the mean values of 110 and 115min, since the values for time 105 had been eliminated previously. From this values, it is also possible to see that EGP tends to present smaller values for the ATGL$^{-/-}$, even though results were once again not statistically significant.

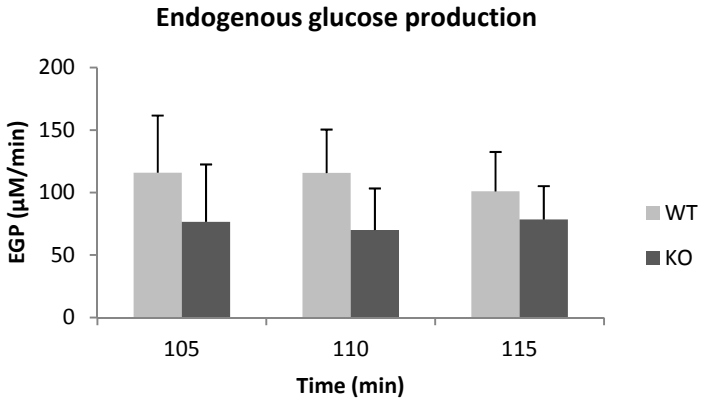

Fig. 5.20| Mean endogenous glucose production and 95% confidence intervals of wild-types and ATGL$^{-/-}$ at 105, 110 and 115 minutes sampling. No statistical significant difference was observed, although there is a tendency for a decrease EGP in ATGL$^{-/-}$; For time point 105min, ATGL$^{-/-}$, n=5; WT, n=11; 110min, ATGL$^{-/-}$, n=6; WT, n=13, 115min, ATGL$^{-/-}$, n=6; WT, n=13.

Table 5.15| Results for the mean steady-state values for each animal concerning the enrichment of the infusion, Ra and EGP. No statistical difference was observed between ATGL$^{-/-}$ (KO) and WT.

Sample	[U-$^{13}C_6$]glucose enrichment (%)	Ra (µM/min)	EGP (µM/min)
WT1	6.078	84.851	79.643
WT2	7.379	72.316	66.928
WT3	7.160	55.939	51.894
WT4	6.287	68.248	63.923
WT5	4.660	86.493	82.461
WT6	4.496	93.598	89.275
WT7	8.930	43.834	39.891
WT8	3.280	145.364	141.127
WT9	4.044	160.912	155.547
WT10	4.076	139.651	134.286
WT11	2.546	218.834	213.228
WT12	3.316	167.120	161.589
WT13	4.086	163.168	156.447
Mean±SD	5.103±1.898	115.402±53.384	110.480±52.824
KO1	13.353	46.094	40.413
KO2	9.486	41.858	37.927
KO3	6.533	86.000	80.395
KO4	5.806	105.568	99.380
KO5	5.787	97.667	91.959
KO6	5.993	112.164	105.407
Mean±SD	7.827±3.052	81.559±30.418	75.913±29.669

To assess the amount of glucose that was being recycled through the Cori cycle, it was considered the ratio of the enrichment of both [1,2-$^{13}C_2$]glucose and [1,2,3-$^{13}C_3$]glucose by the enrichment of [U-$^{13}C_6$]glucose (Fig. 5.21). From these results it is confirmed that there are no differences in the recycling of glucose between wild-types and ATGL$^{-/-}$ mice.

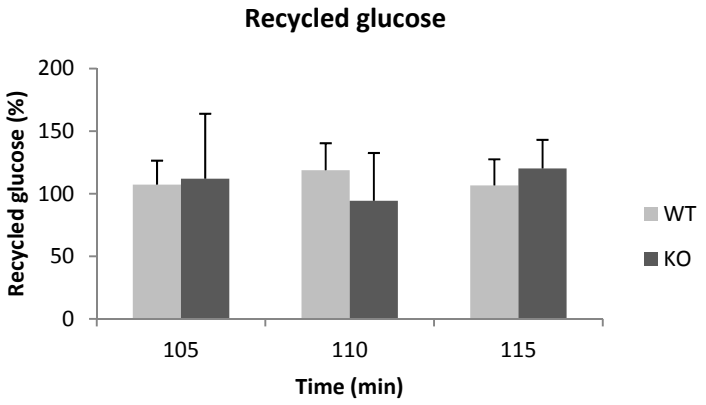

Fig. 5.21| Mean percentage of recycled glucose and 95% confidence intervals of wild-types and ATG$^{-/-}$ at 105, 110 and 115 minutes sampling. No statistical significant difference was observed for the Cori cycle recycling between ATGL$^{-/-}$ and wild-types. For time point 105min, ATGL$^{-/-}$, n=5; WT, n=11; 110min, ATGL$^{-/-}$, n=6; WT, n=13; and 115min, ATGL$^{-/-}$, n=6; WT, n=13.

6. DISCUSSION

6. DISCUSSION

Diabetes mellitus describes a metabolic disorder of multiple aetiology characterized by chronic hyperglycaemia with disturbances of carbohydrate, fat and protein metabolism resulting from defects in insulin secretion, insulin action, or both [140].

Some mechanisms have been proposed for the development of insulin resistance. In particular, TAG have been associated with suppression of oxidative and non-oxidative glucose disposal and increased hepatic glucose output. Although FFAs may induce insulin secretion and play a critical role in maintaining the insulin secretory response to glucose after a prolonged fast, a prolonged exposure to elevated concentrations of FFAs, impairs the insulin secretory response to glucose [10]. Particularly, knock-out mice for ATGL, an enzyme involved in the hydrolysis of TAG, presented surprisingly high insulin sensitivity and glucose tolerance [50][54][141]. This fact makes $ATGL^{-/-}$ mice a unique model to better understanding the relationship between intracellular TAG metabolism and insulin resistance.

The aim of this project was to study these $ATGL^{-/-}$ mice in terms of their metabolic pathways. Given that circulating FFAs are reduced in $ATGL^{-/-}$ mice, the hypothesis for this project was that in the fasting state, they are restricted in utilizing FAs to obtain energy, and are therefore more dependent on glucose oxidation. If glucose oxidation is increased in $AGTL^{-/-}$, a higher proportion of glycolytic flux would be oxidized by the Krebs cycle, resulting in less lactate availability for Cori cycling and a smaller contribution of the Cori cycle to EGP. To study this hypothesis, [U-$^{13}C_6$]glucose was infused and its enrichment measured to quantify EGP rates and the fraction of glucose carbons that were recycled via Cori cycling were evaluated by analysis of daughter glucose M+2 and M+3 isotopomers – whose formation is assumed to be solely via the Cori cycle. The animal model used in this project were mice, which are expected to have higher rates of carbohydrate metabolism, and therefore a more pronounced isotope dilution. However, collecting sufficient material from these animals for ^{13}C NMR analysis would require their sacrifice and the pooling of several blood samples. In addition, $ATGL^{-/-}$ have typically lower baseline plasma glucose levels, therefore further restricting the available amount of glucose for analysis. Therefore, for this project, DBS were used for the sampling of the animal, allowing the harvesting of 3 different time points, and an increase stability of the analytes. Samples were then analysed by LC-MS/MS, which by its great sensitivity, allow the use of a small (≈10µL) sample volume within the DBS.

Method development and validation are important stages of any project regarding LC-MS/MS. With the development of the method, chromatographic and spectrometric settings were perfected for the study of the glucose analytes. Thus, method validation was performed in order to attest the selectivity, accuracy and precision of the developed method. To assist with the calculation and application of the acceptance criteria for the method validation, an Excel® spreadsheet was created, with the purpose of developing a practical and user-friendly tool for performing the tests and calculations implicated for every parameter, as described throughout this thesis. The fact that glucose is an endogenous molecule, limited the proper validation of some of the parameters, such as selectivity and matrix effect, because the control samples used in those tests were not truly negative samples for those analytes. The alternative in those cases would be to use a surrogate matrix, but a surrogate may not always behave exactly as the real matrix and the method of surrogate matrix is still developing to become as accurate as possible [142]. The choice of the proper IS is also of great importance. The IS should be as similar as possible to the molecules of interest, in order to behave exactly the same, degrade at the same rate, elute from the column in the same way, and suffer the same losses and changes during transportation, or sample processing. Usually, uniformly labelled analogues are recommended, but because [U-$^{13}C_6$]glucose was used in the infusion, the deuterated analogue [U-$^{13}C_6$, U-$^{2}H_7$]glucose was preferred. Throughout the validation of the method, some limitations to this IS were encountered, due to a slight change in the RT of this analyte, nonetheless, for this analysis this was still the best alternative. Even thought RT_{Ratio} criteria could not be used for the selectivity of the method, the alternative, the RT alone of each analyte, proved to fulfil the acceptance criteria, despite the limitations of studying endogenous analytes. And as for the matrix effect, the f influence factor had values near to zero for [1,2,3-$^{13}C_3$]glucose and [U-$^{13}C_6$]glucose, which represents low matrix effect. These analytes should behave the same as [U-$^{12}C_6$]glucose and [1,2-$^{13}C_2$]glucose, which did not have the same results due to the fact that they are endogenous molecules, and could not be compared to their pure solvent solutions. [1,2,3-$^{13}C_3$]glucose and [U-$^{13}C_6$]glucose, on the other hand, may be present, even at a very small percentage, in negative samples due to the ^{13}C natural isotopic abundance, which is why they could not entirely fulfil the selectivity and matrix effect acceptance criteria. In terms of the calibration curves, it was determined that the best calibration model was the weighted linear regression model 1/x (Table 5.6) and the best transitions for the quantification of the biological samples were 179/89 for [U-$^{12}C_6$]glucose, 181/91 for [1,2-$^{13}C_2$]glucose, 182/92 for [1,2,3-$^{13}C_3$]glucose and 185/92 for [U-$^{13}C_6$]glucose. To determine the working range, a preliminary analysis had been done on a few samples and from those results it was determined the range of

0.15µM to 250µM. However, after analysing the biological samples, some results had to be excluded to not calculate concentrations by data extrapolation. In the future, validation parameters of stability and matrix effect should be studied in different conditions, including the IS. Even though recovery studies were preformed with the same samples as the matrix effect, they were compared with the pre-spiked samples from the exact same mice, and therefore could be analysed, however, the studies of the recovery for the IS should also be repeated. Also, the evaluation of analytes stability in both samples and pure solutions should be analysed, especially by evaluating the stability of glucose within the DBS.

The animal model used in this project, was placed under fasting conditions, 6 hours prior to sample harvesting, therefore by the time of sampling, these animals no longer had glycogen stores for glucose production, and therefore, contribution to gluconeogenesis was only coming from EGP, which is why EGP can be quantified by the dilution of the [U-$^{13}C_6$]glucose tracer. The results demonstrate that ATGL$^{-/-}$ mice presented a tendency to have less EGP (Fig. 5.20) and the same recycling rate (Fig. 5.21) in comparison to the wild-types. In the absence of ATGL, the release of FAs from TAG is blocked, which theoretically would lead to massive TAG accumulation, decreased FA oxidation and consequently increase glucose utilization for energy production. In the literature it was confirmed that ATGL$^{-/-}$ mice have an enhanced glucose metabolism, which was demonstrated by Huijsman et al., through the increase respiratory exchange ratio in the fasting state and reduced muscle and liver glycogen stores [52]. Indeed, the [U-$^{12}C_6$]glucose concentration within the samples of ATGL$^{-/-}$ mice was smaller than the wild-types.

The fact that EGP was decreased in comparison to wild-type mice, indicates that the ATGL$^{-/-}$ mice should be dependent on the constant intake of glucose for survival. This is confirmed by the fact that their non-stimulated glucose uptake was enhanced [50]. During fasting, however, since ATGL$^{-/-}$ mice are unable of mobilizing the stored fat, the result would be a reduced energy expenditure and decline in body temperature, with consequent premature death when animals are stressed by cold exposure or food deprivation [50]. But even though ATGL$^{-/-}$ mice are not capable of hydrolysing TAG, they present increased levels of DAG [54]. ATGL$^{-/-}$ have decreased intracellular lipolysis [41], but peripheral lipolysis is not affected by deletion of ATGL because it uses other mechanisms for the hydrolysis of TAGs [18], and therefore, some FFAs can be produced. Also, the broad specificity of HSL, may induce TAG hydrolysis as well [18][35][37][38]. Because the levels of FFAs in ATGL$^{-/-}$ are lower when compared to wild-type animals [41], possibly those FFAs will not be incorporated into TAGs, but

will be used for energy production. Therefore, during fasting conditions, after oxidizing glucose, they resort to FAs.

Changes in FFAs produce acute changes in gluconeogenesis and reciprocal changes in glycolysis [143]. The mechanism by which FFAs regulate gluconeogenesis has not been investigated at the present time, but it has been proposed that FFAs promote gluconeogenesis by increasing the production of ATP and NADH, and by increasing pyruvate carboxylase activity via acetyl-CoA, which is generated during FFA oxidation [143]. In the case of the $ATGL^{-/-}$ mice, it was demonstrated that EGP has a tendency to be decreased, which is likely related to lower levels of plasma FFAs. Because peripheral lipolysis is restricted, coupling of peripheral TAG lipolysis to muscle FFA oxidation is probably much tighter and the normal lipolytic "overshoot" that generates excess circulating FFAs is likely to be greatly reduced. Consequently, the liver will have less available FFAs such that gluconeogenesis and EGP are restricted. The recycling of glucose by the Cori cycle was maintained in $ATGL^{-/-}$ mice, indicating that as for wild-type mice, plasma lactate was the main gluconeogenic precursor and essentially no glucose was oxidized by skeletal muscle during the fasted state.

Overall, the results on the comparison between $ATGL^{-/-}$ mice and wild-type mice indicate that $ATGL^{-/-}$ mice prioritize the maintenance of glucose levels under fasting conditions. When confronted with these conditions, while they are limited in the generation of FAs, it is sufficient to meet basal muscle energy demand so there is no requirement for glucose to be oxidized. However, the limited availability of surplus FAs to the liver means that gluconeogenesis is restricted, as demonstrated by the tendency for lower EGP rates. The Cori cycle contribution to gluconeogenesis were maintained in $ATGL^{-/-}$ mice and is consistent with EGP being limited by a lack of energy sources to fuel gluconeogenesis rather than by a shortage of lactate precursors. The limitation in EGP in part explains their lower plasma insulin levels of $ATGL^{-/-}$ mice compared to wild-types under these conditions [55].

As it is proposed that the reduced glucose production is due to the low FA availability to induce gluconeogenesis, I also conjecture that the production of ketone bodies will also be reduced. Therefore, in future studies the levels of ketone bodies should also be evaluated. Moreover, the mice utilized in this study were at a basal, non-feeding and non-exercising state, consequently it would also be interesting to evaluate the metabolism of these animals under different conditions.

7. CONCLUSION

7. CONCLUSION

The objective of the project was to contribute to the elucidation of the metabolic mechanisms used by $ATGL^{-/-}$ mice, since these mice are potential targets for investigation of T2DM. $ATGL^{-/-}$ mice are not capable of hydrolysing TAGs due to deletion of ATGL, an enzyme responsible for intracellular lipolysis, however, they are insulin sensitive and glucose tolerant [41], the opposite characteristics of T2DM. The study was performed by infusing [U-$^{13}C_6$]glucose and determining the EGP and differences in Cori cycling by analysing the enrichments of [1,2-$^{13}C_2$]glucose, [1,2,3-$^{13}C_3$]glucose and [U-$^{13}C_6$]glucose.

Using the practical sampling technique of DBS and the sensitivity of the LC-MS/MS it was possible to analyse whole blood samples for [U-$^{12}C_6$]glucose, [1,2-$^{13}C_2$]glucose, [1,2,3-$^{13}C_3$]glucose and [U-$^{13}C_6$]glucose. The method for the analysis of these analytes was developed and validated. To assist with method validation, an Excel® spreadsheet was created to perform the necessary calculations for the tests of each validation parameter, providing a practical tool that can be used by others who wish to validate an analytical method for LC-MS/MS. Given that glucose is an endogenous molecule, some validation parameters, do not fulfil the acceptance criteria, because most validation guidelines refer to drugs and other exogenous molecules. Nevertheless, taking these facts into consideration, the study of the parameters has ascertain that the developed method for the glucose analytes is reliable, and also which parameters should be further studied for improvement of the method, such as the choice of IS and the matrix effect.

Regarding the metabolism of $ATGL^{-/-}$ mice in comparison to wild-types, it was hypothesized that the lack of FFAs in these mice would lead to the oxidation of high amounts of glucose, which would, in turn, increase gluconeogenesis. However, $ATGL^{-/-}$ presented less EGP and the same Cori cycling recycling. Although glucose recycling was not changed, the low amount of FFAs in these mice will probably limit the rate of gluconeogenesis, which resulted in lower EGP.

In summary, the results present in this study contribute to a better understanding of the metabolism of $ATGL^{-/-}$ mice, but also to the validation of the results. After development and validation, the LC-MS/MS method for these glucose isotopomers can be used in future studies using those analytes. Also, the Excel® spreadsheet can be used to assist the analytical validation of other developed methods. And the results regarding the metabolism of $ATGL^{-/-}$ may contribute to future strategies in the treatment and prevention of T2DM.

SUPPLEMENTARY DATA

Supplementary Table 1| Calculation for a single-factor ANOVA, used in the repeatability and intermediate precision study.

Variation	Sum of Squares	α	Mean Square
Between groups (Factor)	$SS_F = J\sum(\overline{x_i}-\overline{x_t})^2$	$I-1$	$MS_F = SS_F/(I-1)$
Within groups (Residual)	$SS_R = \sum\sum(x_{ij}-\overline{x_i})^2$	$I(J-1)$	$MS_R = SS_R/(I(J-1))$
Total	$SS_T = \sum\sum(x_{ij}-\overline{x_t})^2$	$IJ-1$	

$$\overline{x_i} = \frac{1}{J}\sum_{j=1}^{J} x_{ij} \quad (23)$$

$$\overline{x_t} = \frac{1}{IJ}\sum_{i=1}^{I}\sum_{j=1}^{J} x_{ij} \quad (24)$$

I – number of analytical sequences in which the sample is tested

J – number of replicates preformed for every analytical sequence

x_{ij} - individual result of a sample analysed on the j replicate and the i sequence

$\overline{x_i}$ - average of j replicates obtained in the i sequence, obtained by equation (23)

$\overline{x_t}$ – average of the average results in I diferent sequences, obtained by the equation (24)

Supplementary Table 2| Calculation of variances and coefficients of variation (%) used in the repeatability and intermediate precision study.

Variance	Expression
Between groups	$S^2_{between} = \frac{(MS_{between} - MS_{within})}{J}$
Within groups	$S^2_{within} = MS_{within}$

$MS_{between}$ – mean square within groups

MS_{within} – mean square between groups

J – number of replicates performed at every analytical sequence

Supplementary Table 3| Application of the acceptance criteria for the identification of [U-$^{12}C_6$]glucose. Values that do not fulfil the criteria are highlighted. ND=non-detectable.

	Transition	Relative abundance		S/N	ΔRT	
Criteria	179/89	90.000	110.000	3	7.771	7.971
	179/119	49.480	69.480		7.763	7.963
	Transition	**Absolute area**	**Relative area**	**S/N**	**RT_A**	**RT_{IS}**
Positive#1	179/89	21530842.947	100.000	26997.093	7.871	7.868
	179/119	12806600.755	59.480	28255.335	7.863	7.868
Positive#2	179/89	15000123.163	100.000	18317.467	7.855	7.847
	179/119	8390242.412	55.934	17715.987	7.854	7.847
Positive#3	179/89	12299002.524	100.000	17771.754	7.901	7.876
	179/119	7604692.366	61.832	19094.142	7.888	7.876
Positive#4	179/89	15581020.055	100.000	17535.740	7.918	7.892
	179/119	9353376.679	60.031	20767.890	7.915	7.892
Positive#5	179/89	15112038.103	100.000	17311.521	7.950	7.937
	179/119	9309691.056	61.604	19680.582	7.948	7.937
Positive#6	179/89	14558350.927	100.000	16956.934	7.954	7.926
	179/119	9096103.960	62.480	17088.674	7.950	7.926
	Transition	**Absolute area**	**Relative area**	**S/N**	**RT_A**	**RT_{IS}**
Negative#1	179/89	13248818.008	100.000	16178.830	7.941	ND
	179/119	7639020.528	57.658	17656.685	7.948	ND
Negative#2	179/89	10063526.660	100.000	11857.091	7.929	ND
	179/119	5483705.166	54.491	13406.451	7.932	ND
Negative#3	179/89	10029609.313	100.000	11102.987	7.936	ND
	179/119	5769372.089	57.523	13136.843	7.932	ND
Negative#4	179/89	10248058.241	100.000	11678.789	7.943	ND
	179/119	6163013.029	60.138	14912.188	7.948	ND
Negative#5	179/89	9710836.667	100.000	12146.889	7.971	ND
	179/119	5659127.024	58.276	12323.965	7.969	ND
Negative#6	179/89	8097730.714	100.000	10597.160	7.968	ND
	179/119	4687630.353	57.888	11757.295	7.960	ND

Supplementary Table 4| Application of the acceptance criteria for the identification of [1,2-$^{13}C_2$]glucose. Values that do not fulfil the criteria are highlighted. ND=non-detectable.

	Transition	Relative abundance		S/N	ΔRT	
Criteria	181/89	90.000	110.000		7.861	8.061
	181/91	88.387	108.387	3	7.861	8.061
	181/119	41.634	61.634		7.858	8.058
	Transition	**Absolute area**	**Relative area**	**S/N**	**RT_A**	**RT_{IS}**
Positive#1	181/89	297794.712	100.000	946.309	7.961	7.953
	181/91	292990.986	98.387	981.126	7.961	7.953
	181/119	153763.822	51.634	487.111	7.958	7.953
Positive#2	181/89	271122.230	100.000	914.389	7.958	7.951
	181/91	260639.464	96.134	882.305	7.957	7.951
	181/119	140876.098	51.960	473.033	7.958	7.951
Positive#3	181/89	284349.605	100.000	912.407	7.961	7.938
	181/91	260258.848	91.528	852.949	7.946	7.938
	181/119	150441.148	52.907	491.861	7.935	7.938
Positive#4	181/89	267868.628	100.000	863.423	7.970	7.960
	181/91	259196.229	96.762	882.353	7.963	7.960
	181/119	145896.448	54.466	472.320	7.968	7.960
Positive#5	181/89	272104.946	100.000	909.886	7.937	7.929
	181/91	250180.152	91.943	827.572	7.931	7.929
	181/119	142465.364	52.357	483.117	7.928	7.929
Positive#6	181/89	274196.646	100.000	909.297	7.914	7.909
	181/91	259078.950	94.487	879.080	7.916	7.909
	181/119	144397.243	52.662	464.565	7.915	7.909
	Transition	**Absolute area**	**Relative area**	**S/N**	**RT_A**	**RT_{IS}**
Negative#1	181/89	101319.859	100.000	290.292	7.948	ND
	181/91	98074.906	96.797	289.631	7.941	ND
	181/119	34765.455	34.313	101.751	7.921	ND
Negative#2	181/89	70938.991	100.000	211.167	7.919	ND
	181/91	69548.888	98.040	201.717	7.931	ND
	181/119	25188.457	35.507	73.005	7.913	ND
Negative#3	181/89	75185.456	100.000	223.775	7.940	ND
	181/91	67152.650	89.316	206.175	7.926	ND
	181/119	27350.682	36.378	72.630	7.923	ND
Negative#4	181/89	76047.501	100.000	209.664	7.948	ND
	181/91	71380.847	93.864	205.758	7.935	ND
	181/119	28668.443	37.698	76.738	7.943	ND
Negative#5	181/89	71709.336	100.000	202.078	7.960	ND
	181/91	68164.302	95.056	192.737	7.965	ND
	181/119	28208.042	39.337	72.767	7.967	ND
Negative#6	181/89	57661.432	100.000	149.192	7.965	ND
	181/91	55193.077	95.719	148.899	7.961	ND
	181/119	24108.961	41.811	59.721	7.946	ND

Supplementary Table 5| Application of the acceptance criteria for the identification of [1,2,3-$^{13}C_3$]glucose. Values that do not fulfil the criteria are highlighted. ND=non-detectable.

	Transition	Relative abundance		S/N	ΔRT	
Criteria	182/89	83.539	103.539		7.759	7.959
	182/92	90.000	110.000	3	7.759	7.959
	182/120	57.224	77.224		7.759	7.959
	Transition	**Absolute area**	**Relative area**	**S/N**	**RT_A**	**RT_{IS}**
Positive#1	182/89	153335.212	93.539	473.184	7.859	7.868
	182/92	163926.486	100.000	484.381	7.859	7.868
	182/120	110198.043	67.224	336.986	7.859	7.868
Positive#2	182/89	138574.076	96.225	450.935	7.837	7.847
	182/92	144010.200	100.000	450.879	7.841	7.847
	182/120	92288.717	64.085	279.580	7.841	7.847
Positive#3	182/89	138355.173	99.770	439.509	7.884	7.876
	182/92	138673.591	100.000	445.920	7.892	7.876
	182/120	95787.369	69.074	312.925	7.892	7.876
Positive#4	182/89	140696.162	100.000	437.735	7.904	7.892
	182/92	137967.558	98.061	450.017	7.906	7.892
	182/120	88608.680	62.979	275.310	7.906	7.892
Positive#5	182/89	139262.194	98.101	447.674	7.936	7.937
	182/92	141958.427	100.000	438.269	7.937	7.937
	182/120	96980.954	68.316	307.106	7.937	7.937
Positive#6	182/89	146594.705	96.742	451.907	7.944	7.926
	182/92	151532.246	100.000	475.733	7.944	7.926
	182/120	96922.993	63.962	303.987	7.944	7.926
	Transition	**Absolute area**	**Relative area**	**S/N**	**RT_A**	**RT_{IS}**
Negative#1	182/89	3581.702	100.000	9.249	7.944	ND
	182/92	3003.415	83.854	11.275	7.927	ND
	182/120	1732.362	48.367	5.655	7.939	ND
Negative#2	182/89	1795.782	100.000	6.271	7.953	ND
	182/92	1754.901	97.724	6.633	7.889	ND
	182/120	1452.421	80.880	5.327	7.938	ND
Negative#3	182/89	2273.879	100.000	6.365	7.972	ND
	182/92	1906.373	83.838	7.426	7.888	ND
	182/120	1871.082	82.286	7.963	7.896	ND
Negative#4	182/89	2122.615	100.000	6.861	7.975	ND
	182/92	2078.738	97.933	6.411	7.942	ND
	182/120	1769.697	83.373	5.909	7.908	ND
Negative#5	182/89	2231.239	100.000	5.301	7.973	ND
	182/92	1981.106	88.789	7.609	7.897	ND
	182/120	1286.547	57.661	4.477	7.932	ND
Negative#6	182/89	2103.650	100.000	5.828	7.989	ND
	182/92	1773.609	84.311	5.332	7.933	ND
	182/120	900.896	42.825	3.091	7.896	ND

Supplementary Table 6| Application of the acceptance criteria for the identification of [U-$^{13}C_6$]glucose. Values that do not fulfil the criteria are highlighted. ND=non-detectable.

	Transition	Relative abundance		S/N	ΔRT	
Criteria	185/92	90.000	110.000		7.849	8.049
	182/123	31.869	47.804	3	7.852	8.052
	182/161	67.605	87.605		7.845	8.045
	Transition	**Absolute area**	**Relative area**	**S/N**	**RT_A**	**RT_{IS}**
Positive#1	185/92	374852.060	100.000	1211.637	7.949	7.953
	182/123	149327.184	39.836	475.386	7.952	7.953
	182/161	290904.892	77.605	932.473	7.945	7.953
Positive#2	185/92	340924.147	100.000	1166.858	7.952	7.951
	182/123	132988.744	39.008	437.252	7.938	7.951
	182/161	287088.119	84.209	905.758	7.945	7.951
Positive#3	185/92	411438.232	100.000	1341.346	7.934	7.938
	182/123	158328.526	38.482	535.964	7.926	7.938
	182/161	323141.675	78.540	1035.013	7.940	7.938
Positive#4	185/92	370503.801	100.000	1237.420	7.961	7.960
	182/123	137356.111	37.073	460.996	7.954	7.960
	182/161	295895.788	79.863	996.686	7.952	7.960
Positive#5	185/92	367509.245	100.000	1203.587	7.926	7.929
	182/123	146205.319	39.783	478.894	7.926	7.929
	182/161	297555.167	80.965	987.370	7.926	7.929
Positive#6	185/92	372866.231	100.000	1237.977	7.899	7.909
	182/123	146228.973	39.218	493.764	7.905	7.909
	182/161	308512.741	82.741	1067.996	7.903	7.909
	Transition	**Absolute area**	**Relative area**	**S/N**	**RT_A**	**RT_{IS}**
Negative#1	185/92	168.578	34.274	1.426	8.381	ND
	182/123	491.852	100.000	2.958	8.010	ND
	182/161	387.560	78.796	2.080	8.258	ND
Negative#2	185/92	ND	ND	ND	ND	ND
	182/123	450.631	89.922	3.924	8.085	ND
	182/161	501.134	100.000	3.253	8.034	ND
Negative#3	185/92	ND	ND	ND	ND	ND
	182/123	757.087	100.000	5.546	7.846	ND
	182/161	190.207	25.124	1.479	7.851	ND
Negative#4	185/92	762.896	100.000	6.371	7.670	ND
	182/123	122.372	16.040	1.525	8.112	ND
	182/161	238.785	31.300	1.973	8.259	ND
Negative#5	185/92	150.616	27.821	1.276	7.999	ND
	182/123	541.369	100.000	4.212	8.165	ND
	182/161	271.412	50.134	1.493	8.057	ND
Negative#6	185/92	ND	ND	ND	ND	ND
	182/123	173.387	100.000	1.889	1.889	ND
	182/161	ND	ND	ND	ND	ND

Supplementary Table 7| Application of the acceptance criteria for the identification of [U-$^{13}C_6$, U-$^{2}H_7$]glucose. Values that do not fulfil the criteria are highlighted. NA=non-applicable; ND=non-detectable.

Criteria	**Transition**	**Relative abundance**		**S/N**	**ΔRT**	
	192/94	24.748	37.122	3	7.768	7.968
	192/128	90.000	110.000		7.759	7.959
	Transition	**Absolute area**	**Relative area**	**S/N**	**RT_A**	**RT_{IS}**
Positive#1	192/94	75217.264	30.935	206.868	7.868	NA
	192/128	243146.868	100.000	717.690	7.859	NA
Positive#2	192/94	65114.220	29.799	167.580	7.847	NA
	192/128	218512.293	100.000	659.528	7.836	NA
Positive#3	192/94	62541.246	28.537	176.250	7.876	NA
	192/128	219156.152	100.000	659.835	7.883	NA
Positive#4	192/94	62305.132	29.281	167.838	7.892	NA
	192/128	212784.000	100.000	628.296	7.903	NA
Positive#5	192/94	62751.512	30.546	192.860	7.937	NA
	192/128	205435.930	100.000	611.159	7.940	NA
Positive#6	192/94	68516.360	29.631	187.899	7.926	NA
	192/128	231231.502	100.000	708.819	7.933	NA
	Transition	**Absolute area**	**Relative area**	**S/N**	**RT_A**	**RT_{IS}**
Negative#1	192/94	ND	ND	ND	ND	ND
	192/128	ND	ND	ND	ND	ND
Negative#2	192/94	ND	ND	ND	ND	ND
	192/128	ND	ND	ND	ND	ND
Negative#3	192/94	ND	ND	ND	ND	ND
	192/128	ND	ND	ND	ND	ND
Negative#4	192/94	ND	ND	ND	ND	ND
	192/128	ND	ND	ND	ND	ND
Negative#5	192/94	ND	ND	ND	ND	ND
	192/128	ND	ND	ND	ND	ND
Negative#6	192/94	ND	ND	ND	ND	ND
	192/128	ND	ND	ND	ND	ND

Supplementary Table 8. Results obtained from the freeze and thaw stability study. Values that do not fulfil the criteria are highlighted.

Analyte	Transition	Nominal concentration (pmol/µL)	Mean concentration of control sample (pmol/µL)	Mean concentration of stability sample (pmol/µL)	90% confidence interval of stability sample	
					Lower limit	Upper limit
[U-$^{12}C_6$]glucose	179/89	1.25	1.15	1.27	1.16	1.38
		20	19.2	20.7	18.2	23.2
		200	215.8	214.6	210.1	219.2
	179/119	1.25	1.06	1.08	0.97	1.20
		20	18.8	20.2	17.1	23.3
		200	207.6	201.2	198.3	204.3
[1,2-$^{13}C_2$]glucose	181/89	1.25	1.74	1.83	1.50	2.16
		20	28.7	29.7	25.7	33.7
		200	325.8	314.3	264.7	363.9
	181/91	1.25	1.86	1.65	1.31	1.99
		20	27.8	30.2	26.7	33.7
		200	321.6	330.8	282.2	379.4
	181/119	1.25	2.05	1.39	1.32	1.47
		20	28.7	29.3	26.5	32.1
		200	327.2	334.0	275.8	392.2
[1,2,3-$^{13}C_3$]glucose	182/89	1.25	1.27	1.27	1.03	1.51
		20	23.9	26.1	23.5	28.7
		200	279.0	271.7	265.8	277.7
	182/92	1.25	1.36	1.51	1.30	1.73
		20	24.5	26.7	22.7	30.6
		200	284.0	274.0	271.6	276.5
	182/120	1.25	1.63	1.33	1.17	1.48
		20	26.9	28.4	25.6	31.1
		200	302.0	295.6	286.4	304.7
[U-$^{13}C_6$]glucose	185/92	1.25	1.48	1.31	1.13	1.49
		20	23.8	25.8	22.6	29.1
		200	265.1	268.7	230.0	307.3
	185/123	1.25	1.62	1.51	1.06	1.97
		20	22.9	23.9	20.5	27.3
		200	258.2	273.9	236.9	310.8
	185/61	1.25	1.57	1.38	1.08	1.69
		20	23.1	25.8	22.7	28.9
		200	255.0	263.5	221.5	305.5

Supplementary Table 9. Results obtained from the stock solution stability study. Values that do not fulfil the criteria are highlighted.

Analyte	Transition	Nominal concentration (pmol/µL)	Mean concentration of control sample (pmol/µL)	Mean concentration of stability sample (pmol/µL)	90% confidence interval of stability sample	
					Lower limit	Upper limit
[U-$^{12}C_6$]glucose	179/89	1.25	1.34	0.66	0.57	0.75
		20	19.7	19.3	18.8	19.7
		200	211.2	211.3	204.2	218.3
	179/119	1.25	1.41	0.08	0.02	0.14
		20	20.1	19.3	18.3	20.3
		200	197.0	203.1	199.6	206.6
[1,2-$^{13}C_2$]glucose	181/89	1.25	1.21	2.56	2.31	2.82
		20	19.6	28.7	28.0	29.5
		200	201.6	325.8	296.3	355.3
	181/91	1.25	1.15	2.35	2.33	2.37
		20	19.5	27.3	25.4	29.2
		200	199.6	321.6	293.5	349.6
	181/119	1.25	1.45	2.41	2.24	2.57
		20	18.7	28.9	27.5	30.4
		200	199.5	327.9	300.2	355.5
[1,2,3-$^{13}C_3$]glucose	182/89	1.25	1.42	0.80	0.65	0.94
		20	19.4	24.8	24.3	25.4
		200	207.3	273.2	262.9	283.5
	182/92	1.25	1.25	0.96	0.60	1.33
		20	20.5	25.0	23.8	26.1
		200	204.4	278.0	266.6	289.3
	182/120	1.25	1.28	1.23	1.20	1.26
		20	21.6	27.7	26.7	28.7
		200	220.5	295.6	284.7	306.4
[U-$^{13}C_6$]glucose	185/92	1.25	1.25	1.93	1.82	2.04
		20	20.0	23.9	21.8	25.9
		200	199.4	265.1	243.9	286.3
	185/123	1.25	1.50	2.45	2.35	2.54
		20	19.5	22.9	20.9	24.9
		200	202.5	258.2	233.7	282.6
	185/61	1.25	1.37	2.35	2.03	2.67
		20	18.8	23.1	20.3	25.8
		200	198.5	255.0	239.7	270.4

Supplementary Table 10. Results obtained from the post-preparative stability study. Values that do not fulfil the criteria are highlighted. ND=non-detectable.

Analyte	Transition	Nominal concentration (pmol/µL)	Mean concentration of control sample (pmol/µL)	Mean concentration of stability sample (pmol/µL)	90% confidence interval of stability sample	
					Lower limit	Upper limit
[U-$^{12}C_6$]glucose	179/89	1.25	1.34	1.51	1.26	1.75
		20	24.2	20.4	18.9	21.9
		200	195.7	213.9	192.0	235.9
	179/119	1.25	1.41	1.72	1.15	2.28
		20	28.7	19.8	18.6	20.9
		200	220.1	202.3	177.8	226.8
[1,2-$^{13}C_2$]glucose	181/89	1.25	1.21	1.20	1.02	1.37
		20	20.8	19.9	17.2	22.6
		200	214.9	196.3	175.3	217.4
	181/91	1.25	0.97	1.26	1.15	1.38
		20	20.5	19.4	17.0	21.9
		200	217.9	196.4	177.3	215.5
	181/119	1.25	1.45	ND	ND	ND
		20	15.7	19.2	17.5	20.9
		200	199.2	201.0	184.3	217.7
[1,2,3-$^{13}C_3$]glucose	182/89	1.25	1.4	1.45	1.01	1.88
		20	23.7	19.7	18.5	21.0
		200	195.8	209.9	185.4	234.4
	182/92	1.25	1.25	0.85	0.58	1.12
		20	22.0	20.2	19.0	21.4
		200	203.6	206.5	181.4	231.7
	182/120	1.25	1.28	ND	ND	ND
		20	19.5	21.0	20.8	21.2
		200	180.7	224.8	200.2	249.4
[U-$^{13}C_6$]glucose	185/92	1.25	1.13	1.53	1.34	1.72
		20	20.0	20.0	17.2	22.8
		200	218.5	196.5	178.1	214.8
	185/123	1.25	1.52	ND	ND	ND
		20	17.8	19.3	15.9	22.7
		200	203.2	199.8	182.6	216.9
	185/61	1.25	1.37	1.560	0.96	2.16
		20	20.2	20.2	17.7	22.6
		200	206.5	193.7	174.6	212.9

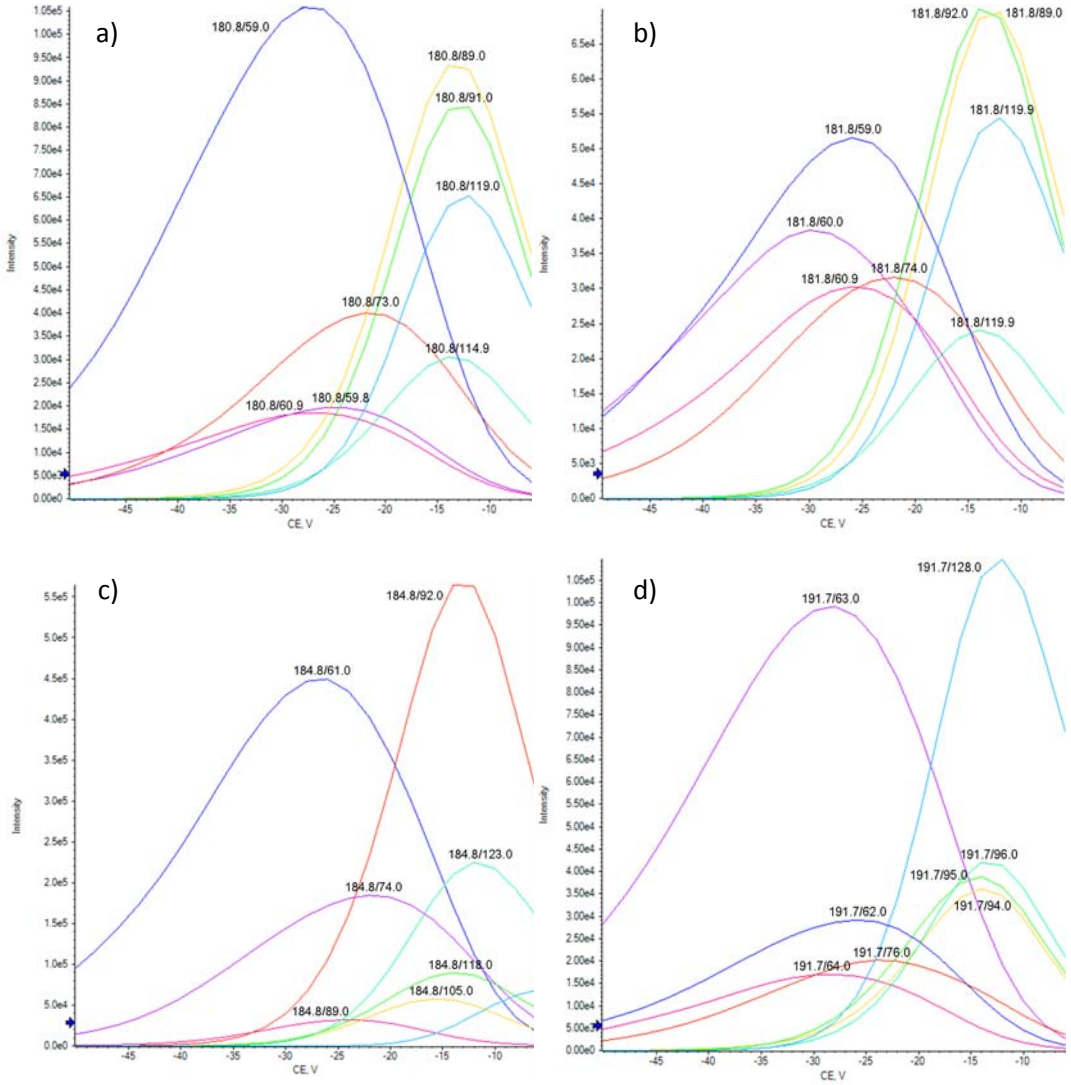

Supplementary Fig. 1| Representation of the collision energies used to produce each of the fragments of a) [1,2-$^{13}C_2$]glucose; b) [1,2,3-$^{13}C_3$]glucose; c) [U-$^{13}C_6$]glucose; d) [U-^{13}C, U-^{2}H]glucose. Smaller fragments, need higher collision energies, while the larger fragments are produced with lower energies

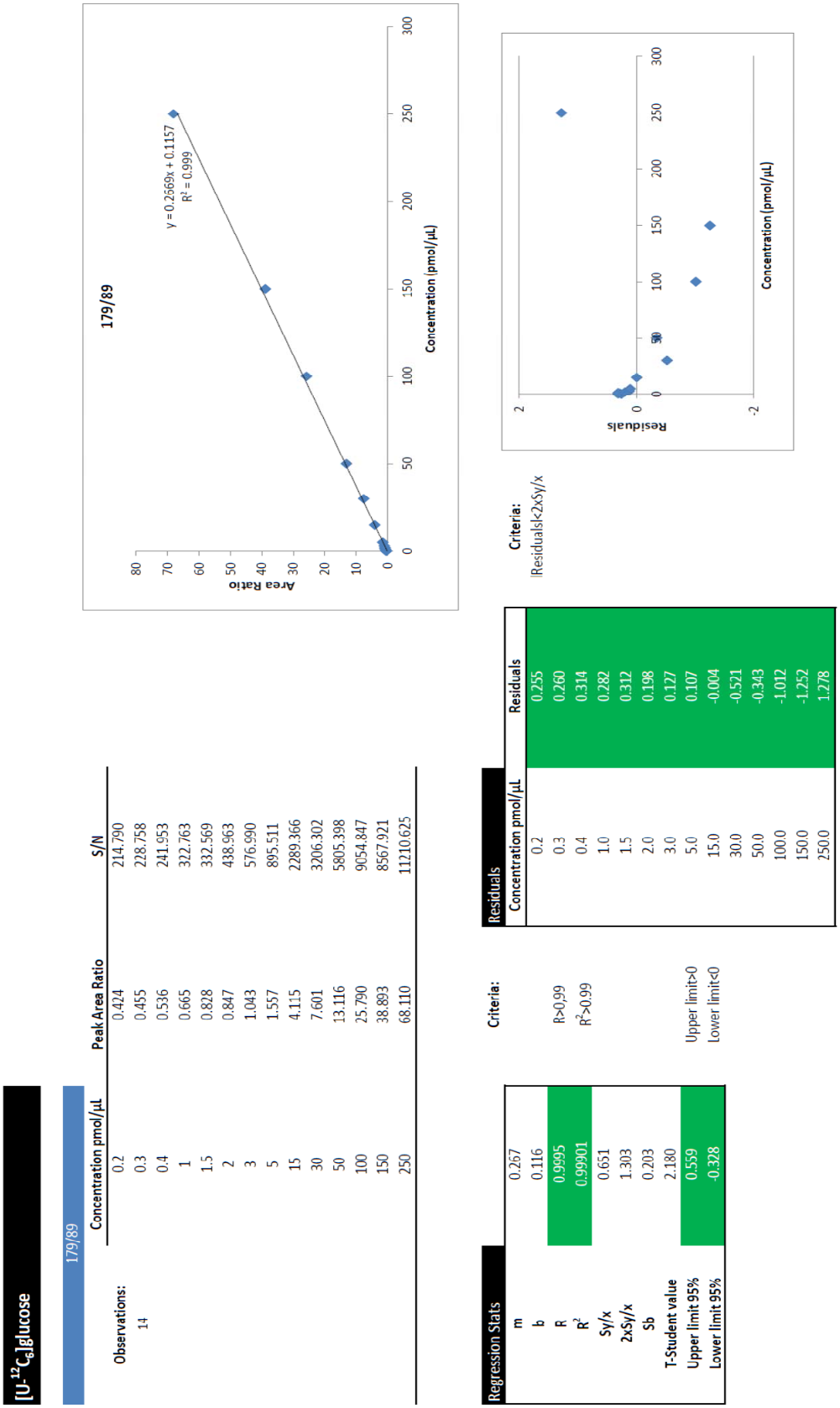

Supplementary Fig. 2| Example of the linearity analysis for the transition 179/89 of [U-$^{12}C_6$]glucose. Data evaluation was performed by an Excel® spreadsheet created to perform the necessary calculations for the statistical tests and apply the acceptance criteria (if the value fulfils the criteria cell are represented in green, and if not, they are represented in red). All validation parameters were evaluated through this spreadsheet.

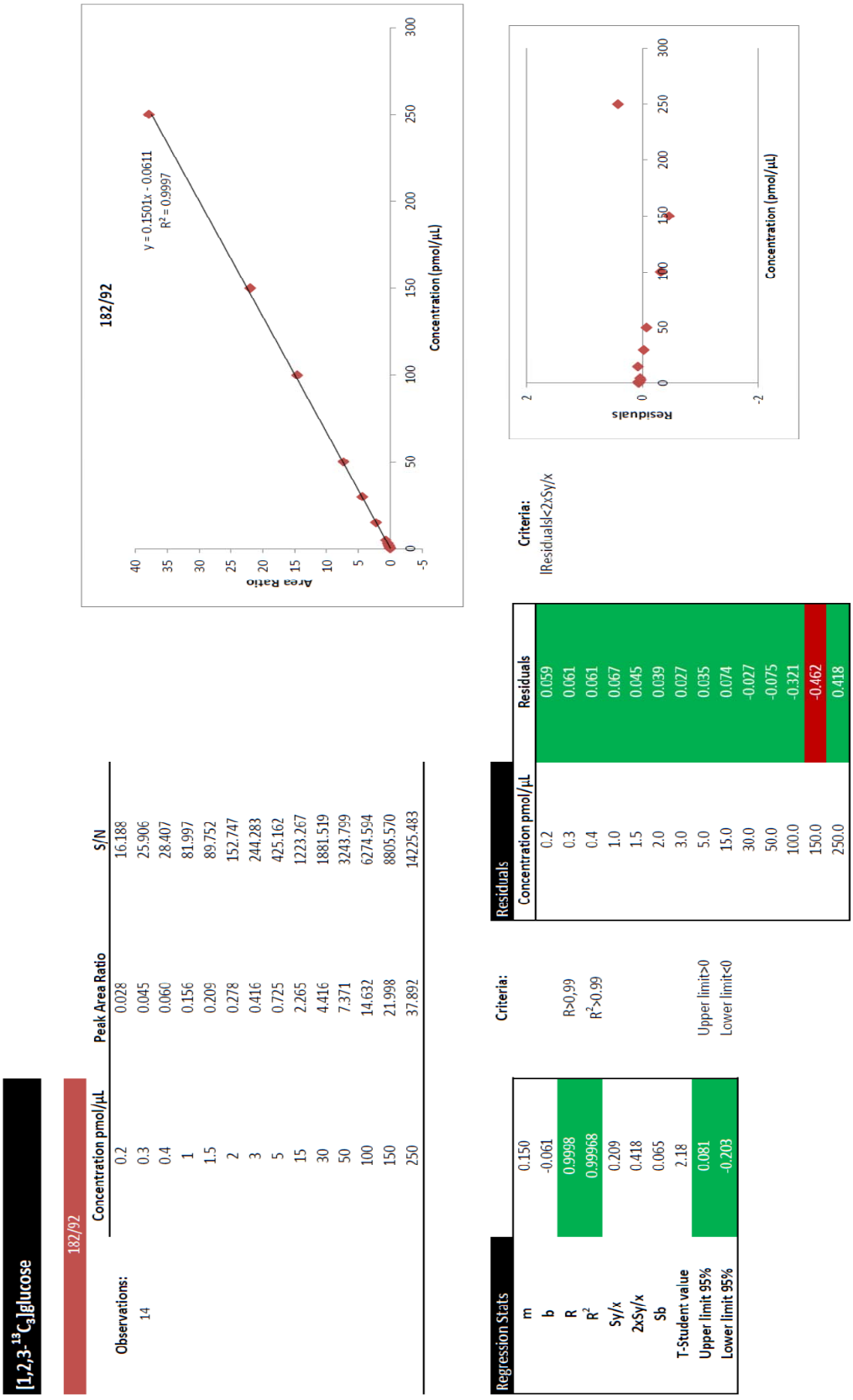

Supplementary Fig. 3| Example of the linearity analysis for the transition 182/92 of [1,2,3-$^{13}C_3$]glucose. Data evaluation was performed by an Excel® spreadsheet created to perform the necessary calculations for the statistical tests and apply the acceptance criteria (if the value fulfils the criteria cell are represented in green, and if not, they are represented in red). All validation parameters were evaluated through this spreadsheet.

REFERENCES

[1] H. King, R. E. Aubert, and W. H. Herman, “Global burden of diabetes, 1995-2025 - Prevalence, numerical estimates, and projections,” *Diabetes Care*, vol. 21, no. 9, pp. 1414–1431, 1998.

[2] A. H. Mokdad, B. A. Bowman, E. S. Ford, F. Vinicor, J. S. Marks, and J. P. Koplan, “The continuing epidemics of obesity and diabetes in the United States,” *Journal of the American Medical Association*, vol. 286, no. 10, pp. 1195–1200, Sep. 2001.

[3] G. A. Colditz, W. C. Willett, A. Rotnitzky, and J. E. Manson, “Weight gain as a risk factor for clinical diabetes mellitus in women,” *Annals of Internal Medicine*, vol. 122, no. 7, pp. 481–486, 1995.

[4] J. M. Chan, E. B. Rimm, G. A. Colditz, M. J. Stampfer, and W. C. Willett, “Obesity, fat distribution, and weight gain as risk factors for clinical diabetes in men,” *Diabetes Care*, vol. 17, no. 9, pp. 961–969, 1994.

[5] American Diabetes Association, “Diagnosis and classification of diabetes,” *Diabetes Care*, vol. 35, no. Supplement 1, pp. S64–S71, 2012.

[6] G. Boden and G. I. Shulman, “Free fatty acids in obesity and type 2 diabetes: defining their role in the development of insulin resistance and beta-cell dysfunction,” *European Journal of Clinical Investigation*, vol. 32 Suppl 3, pp. 14–23, Jun. 2002.

[7] V. T. Samuel, K. F. Petersen, and G. I. Shulman, “Lipid-induced insulin resistance: unravelling the mechanism,” *Lancet*, vol. 375, pp. 2267–2277, Jun. 2010.

[8] G. R. Steinberg, “Inflammation in obesity is the common link between defects in fatty acid metabolism and insulin resistance,” *Cell Cycle*, vol. 6, no. 8, pp. 888–894, Apr. 2007.

[9] B. B. Kahn, “Type 2 diabetes: when insulin secretion fails to compensate for insulin resistance,” *Cell*, vol. 92, no. 5, p. 593, 1998.

[10] M. K. Cavaghan, D. A. Ehrmann, and K. S. Polonsky, “Interactions between insulin resistance and insulin secretion in the development of glucose intolerance,” *The Journal of Clinical Investigation*, vol. 106, no. 3, pp. 329–333, 2000.

[11] M. Roden and E. Bernroider, “Hepatic glucose metabolism in humans - its role in health and disease,” *Best Practice & Research Clinical Endocrinology & Metabolism*, vol. 17, no. 3, pp. 365–383, Sep. 2003.

[12] P. J. Klover and R. a Mooney, “Hepatocytes: critical for glucose homeostasis,” *The International Journal of Biochemistry & Cell Biology*, vol. 36, no. 5, pp. 753–758, May 2004.

[13] D. L. . Nelson and M. M. Cox, *Lehninger Principles of Biochemistry 4th edition*, vol. 70, no. 8. 1993, p. A223.

[14] M. R. Buchakjian and S. Kornbluth, “The engine driving the ship: metabolic steering of cell proliferation and death,” *Nature reviews. Molecular cell biology*, vol. 11, pp. 715–727, Oct. 2010.

[15] C. Bogardus, S. Lillioja, D. M. Mott, C. Hollenbeck, and G. Reaven, “Relationship between degree of obesity and in vivo insulin action in man,” *American Journal of Physiology-Endocrinology And Metabolism*, vol. 248, no. 3, pp. E286–E291, 1985.

[16] C. Cori and G. Cori, “Glycogen formation in the liver from d-and l-lactic acid,” *Journal of Biological Chemistry*, vol. 81, pp. 389–403, 1929.

[17] K. F. Petersen and G. I. Shulman, “New insights into the pathogenesis of insulin resistance in humans using magnetic resonance spectroscopy,” *Obesity*, vol. 14 Suppl 1, pp. S34–S40, Feb. 2006.

[18] R. Zechner, R. Zimmermann, T. O. Eichmann, S. D. Kohlwein, G. Haemmerle, A. Lass, and F. Madeo, "Fat signals - Lipases and lipolysis in lipid metabolism and signaling," *Cell Metabolism*, vol. 15, no. 3, pp. 279–91, Mar. 2012.

[19] A. Garg, "Lipodystrophies," *The American Journal of Medicine*, vol. 108, no. 2, pp. 143–152, 2000.

[20] G. I. Shulman, "Cellular mechanisms of insulin resistance," *Journal of Clinical Investigation*, vol. 106, no. 2, pp. 171–176, 2000.

[21] S. G. Dubois, L. K. Heilbronn, S. R. Smith, J. B. Albu, D. E. Kelley, and E. Ravussin, "Decreased expression of adipogenic genes in obese subjects with type 2 diabetes," *Obesity*, vol. 14, pp. 1543–1552, Sep. 2006.

[22] E. Danforth, "Failure of adipocyte differentiation causes type II diabetes mellitus?," *Nature Genetics*, vol. 26, no. 1, p. 13, Sep. 2000.

[23] B. M. T. Burgering and P. J. Coffer, "Protein kinase B (c-Akt) in phosphatidylinositol-3-OH kinase signal transduction," *Nature*, vol. 376, pp. 599–602, 1995.

[24] M. Björnholm, Y. Kawano, M. Lehtihet, and J. R. Zierath, "Insulin receptor substrate-1 phosphorylation and phosphatidylinositol 3-kinase activity in skeletal muscle from NIDDM subjects after in vivo insulin stimulation," *Diabetes*, vol. 46, pp. 524–527, 1997.

[25] L. J. Goodyear, F. Giorgino, L. A. Sherman, J. Carey, R. J. Smith, and G. L. Dohm, "Insulin receptor phosphorylation, insulin receptor substrate-1 phosphorylation, and phosphatidylinositol 3-kinase activity are decreased in intact skeletal muscle strips from obese subjects," *Journal of Clinical Investigation*, vol. 95, no. 5, p. 2195, 1995.

[26] G. F. Lewis, A. Carpentier, K. Adeli, and A. Giacca, "Disordered fat storage and mobilization in the pathogenesis of insulin resistance and type 2 diabetes," *Endocrine Reviews*, vol. 23, no. 2, pp. 201–229, 2002.

[27] R. L. Dobbins, L. S. Szczepaniak, J. Myhill, Y. Tamura, H. Uchino, A. Giacca, and J. D. McGarry, "The composition of dietary fat directly influences glucose-stimulated insulin secretion in rats," *Diabetes*, vol. 51, pp. 1825–1833, 2002.

[28] S. A. Summers, "Ceramides in insulin resistance and lipotoxicity," *Progress in Lipid Research*, vol. 45, no. 1, p. 42, 2006.

[29] B. H. Goodpaster, J. He, S. Watkins, and D. E. Kelley, "Skeletal muscle lipid content and insulin resistance: evidence for a paradox in endurance-trained athletes," *Journal of Clinical Endocrinology & Metabolism*, vol. 86, no. 12, pp. 5755–5761, 2001.

[30] C. Thamer, J. Machann, O. Bachmann, M. Haap, D. Dahl, B. Wietek, O. Tschritter, A. Niess, K. Brechtel, and A. Fritsche, "Intramyocellular lipids: anthropometric determinants and relationships with maximal aerobic capacity and insulin sensitivity," *Journal of Clinical Endocrinology & Metabolism*, vol. 88, no. 4, pp. 1785–1791, 2003.

[31] M. A. Tarnopolsky, C. D. Rennie, H. A. Robertshaw, S. N. Fedak-Tarnopolsky, M. C. Devries, and M. J. Hamadeh, "Influence of endurance exercise training and sex on intramyocellular lipid and mitochondrial ultrastructure, substrate use, and mitochondrial enzyme activity," *American Journal of Physiology-Regulatory, Integrative and Comparative Physiology*, vol. 292, no. 3, pp. R1271–R1278, 2007.

[32] M. Vaughan, J. E. Berger, and D. Steinberg, "Hormone-sensitive lipase and monoglyceride lipase activities in adipose tissue," *The Journal of Biological Chemistry*, vol. 239, no. 2, pp. 401–409, Feb. 1964.

[33] G. Haemmerle, R. Zimmermann, J. G. Strauss, D. Kratky, M. Riederer, G. Knipping, and R. Zechner, "Hormone-sensitive lipase deficiency in mice changes the plasma lipid profile by affecting the tissue-specific expression pattern of lipoprotein lipase in adipose tissue and muscle," *The Journal of Biological Chemistry*, vol. 277, no. 15, pp. 12946–12952, Apr. 2002.

[34] J. Osuga, S. Ishibashi, T. Oka, H. Yagyu, R. Tozawa, A. Fujimoto, F. Shionoiri, N. Yahagi, F. B. Kraemer, O. Tsutsumi, and N. Yamada, "Targeted disruption of hormone-sensitive lipase results in male sterility and adipocyte hypertrophy, but not in obesity," *Proceedings of the National Academy of Sciences of the United States of America*, vol. 97, no. 2, pp. 787–792, Jan. 2000.

[35] R. Zimmermann, J. G. Strauss, G. Haemmerle, G. Schoiswohl, R. Birner-Gruenberger, M. Riederer, A. Lass, G. Neuberger, F. Eisenhaber, A. Hermetter, and R. Zechner, "Fat mobilization in adipose tissue is promoted by adipose triglyceride lipase," *Science*, vol. 306, pp. 1383–1386, Nov. 2004.

[36] K. Harada, W.-J. Shen, S. Patel, V. Natu, J. Wang, J. Osuga, S. Ishibashi, and F. B. Kraemer, "Resistance to high-fat diet-induced obesity and altered expression of adipose-specific genes in HSL-deficient mice," *American Journal of Physiology, Endocrinology and Metabolism*, vol. 285, pp. E1182–E1195, Dec. 2003.

[37] J. a Villena, S. Roy, E. Sarkadi-Nagy, K.-H. Kim, and H. S. Sul, "Desnutrin, an adipocyte gene encoding a novel patatin domain-containing protein, is induced by fasting and glucocorticoids: ectopic expression of desnutrin increases triglyceride hydrolysis," *The Journal of Biological Chemistry*, vol. 279, no. 45, pp. 47066–47075, Nov. 2004.

[38] C. M. Jenkins, D. J. Mancuso, W. Yan, H. F. Sims, B. Gibson, and R. W. Gross, "Identification, cloning, expression, and purification of three novel human calcium-independent phospholipase A2 family members possessing triacylglycerol lipase and acylglycerol transacylase activities," *The Journal of Biological Chemistry*, vol. 279, no. 47, pp. 48968–48975, Nov. 2004.

[39] L. Notari, V. Baladron, J. D. Aroca-Aguilar, N. Balko, R. Heredia, C. Meyer, P. M. Notario, S. Saravanamuthu, M.-L. Nueda, F. Sanchez-Sanchez, J. Escribano, J. Laborda, and S. P. Becerra, "Identification of a lipase-linked cell membrane receptor for pigment epithelium-derived factor," *The Journal of Biological Chemistry*, vol. 281, no. 49, pp. 38022–38037, Dec. 2006.

[40] R. S. Ahima and M. a Lazar, "Adipokines and the peripheral and neural control of energy balance," *Molecular Endocrinology*, vol. 22, no. 5, pp. 1023–1031, May 2008.

[41] R. Zechner, P. C. Kienesberger, G. Haemmerle, R. Zimmermann, and A. Lass, "Adipose triglyceride lipase and the lipolytic catabolism of cellular fat stores," *Journal of Lipid Research*, vol. 50, no. 1, pp. 3–21, Jan. 2009.

[42] C. Chung, J. a Doll, A. K. Gattu, C. Shugrue, M. Cornwell, P. Fitchev, and S. E. Crawford, "Anti-angiogenic pigment epithelium-derived factor regulates hepatocyte triglyceride content through adipose triglyceride lipase (ATGL)," *Journal of Hepatology*, vol. 48, pp. 471–478, Mar. 2008.

[43] M. L. Borg, Z. B. Andrews, E. J. Duh, R. Zechner, P. J. Meikle, and M. J. Watt, "Pigment epithelium-derived factor regulates lipid metabolism via adipose triglyceride lipase," *Diabetes*, vol. 60, pp. 1458–66, May 2011.

[44] M. J. Watt and G. R. Steinberg, "Regulation and function of triacylglycerol lipases in cellular metabolism," *The Biochemical Journal*, vol. 414, no. 3, pp. 313–325, Sep. 2008.

[45] C. Vigouroux, M. Caron-Debarle, C. Le Dour, J. Magré, and J. Capeau, "Molecular mechanisms of human lipodystrophies: From adipocyte lipid droplet to oxidative stress and lipotoxicity," *The Iternational Journal of Biochemistry & Cell Biology*, vol. 43, pp. 862–876, Jun. 2011.

[46] M. Schweiger, R. Schreiber, G. Haemmerle, A. Lass, C. Fledelius, P. Jacobsen, H. Tornqvist, R. Zechner, and R. Zimmermann, "Adipose triglyceride lipase and hormone-sensitive lipase are the major enzymes in adipose tissue triacylglycerol catabolism," *The Journal of Biological Chemistry*, vol. 281, no. 52, pp. 40236–40241, Dec. 2006.

[47] E. E. Kershaw, J. K. Hamm, L. A. W. Verhagen, O. Peroni, M. Katic, and J. S. Flier, "Adipose triglyceride lipase: function, regulation by insulin, and comparison with adiponutrin," *Diabetes*, vol. 55, pp. 148–157, Sep. 2006.

[48] J. Cohen, J. Horton, and H. Hobbs, "Human fatty liver disease: old questions and new insights," *Science*, vol. 332, no. 6037, pp. 1519–1523, 2011.

[49] D. E. Kelley, B. H. Goodpaster, and L. Storlien, “Muscle triglyceride and insulin resistance,” *Annual Review of Nutrition*, vol. 22, pp. 325–46, Jan. 2002.

[50] G. Haemmerle, A. Lass, and R. Zimmermann, “Defective lipolysis and altered energy metabolism in mice lacking adipose triglyceride lipase,” *Science*, vol. 312, pp. 734–737, 2006.

[51] J. W. Wu, S. P. Wang, F. Alvarez, S. Casavant, N. Gauthier, L. Abed, K. G. Soni, G. Yang, and M. G. A., “Deficiency of liver adipose triglyceride lipase in mice causes progressive hepatic steatosis,” *Hepatology*, vol. 54, pp. 122–132, 2011.

[52] E. Huijsman, C. van de Par, C. Economou, C. van der Poel, G. S. Lynch, G. Schoiswohl, G. Haemmerle, R. Zechner, and M. J. Watt, “Adipose triacylglycerol lipase deletion alters whole body energy metabolism and impairs exercise performance in mice,” *American Journal of Physiology, Endocrinology and Metabolism*, vol. 297, no. 2, pp. E505–E513, Aug. 2009.

[53] G. Schoiswohl, M. Schweiger, R. Schreiber, G. Gorkiewicz, K. Preiss-Landl, U. Taschler, K. a Zierler, F. P. W. Radner, T. O. Eichmann, P. C. Kienesberger, S. Eder, A. Lass, G. Haemmerle, T. J. Alsted, B. Kiens, G. Hoefler, R. Zechner, and R. Zimmermann, “Adipose triglyceride lipase plays a key role in the supply of the working muscle with fatty acids,” *Journal of Lipid Research*, vol. 51, no. 3, pp. 490–499, Mar. 2010.

[54] P. C. Kienesberger, D. Lee, T. Pulinilkunnil, D. S. Brenner, L. Cai, C. Magnes, H. C. Koefeler, I. E. Streith, G. N. Rechberger, G. Haemmerle, J. S. Flier, R. Zechner, Y.-B. Kim, and E. E. Kershaw, “Adipose triglyceride lipase deficiency causes tissue-specific changes in insulin signaling,” *The Journal of Biological Chemistry*, vol. 284, no. 44, pp. 30218–30229, Oct. 2009.

[55] M.-L. Peyot, C. Guay, M. G. Latour, J. Lamontagne, R. Lussier, M. Pineda, N. B. Ruderman, G. Haemmerle, R. Zechner, E. Joly, S. R. M. Madiraju, V. Poitout, and M. Prentki, “Adipose triglyceride lipase is implicated in fuel- and non-fuel-stimulated insulin secretion,” *The Journal of Biological Chemistry*, vol. 284, no. 25, pp. 16848–16859, Jun. 2009.

[56] S. Crowe, L. E. Wu, C. Economou, S. M. Turpin, M. Matzaris, K. L. Hoehn, A. L. Hevener, D. E. James, E. J. Duh, and M. J. Watt, “Pigment epithelium-derived factor contributes to insulin resistance in obesity,” *Cell Metabolism*, vol. 10, pp. 40–47, Jul. 2009.

[57] K. Hirano, Y. Ikeda, N. Zaima, Y. Sakata, and G. Matsumiya, “Triglyceride deposit cardiomyovasculopathy,” *New England Journal of Medicine*, vol. 359, no. 22, pp. 2396–2398, 2008.

[58] F. Campagna, L. Nanni, F. Quagliarini, E. Pennisi, C. Michailidis, F. Pierelli, C. Bruno, C. Casali, S. DiMauro, and M. Arca, “Novel mutations in the adipose triglyceride lipase gene causing neutral lipid storage disease with myopathy,” *Biochemical and Biophysical Research Communications*, vol. 377, no. 3, pp. 843–846, 2008.

[59] J. Fischer, C. Lefevre, E. Morava, J.-M. Mussini, P. Laforet, A. Negre-Salvayre, M. Lathrop, and R. Salvayre, “The gene encoding adipose triglyceride lipase (PNPLA2) is mutated in neutral lipid storage disease with myopathy,” *Nature Genetics*, vol. 39, no. 1, pp. 28–30, 2006.

[60] M. Kato, N. Higuchi, and M. Enjoji, “Reduced hepatic expression of adipose tissue triglyceride lipase and CGI-58 may contribute to the development of non-alcoholic fatty liver disease in patients with insulin resistance,” *Scandinavian Journal of Gastroenterology*, vol. 43, no. 8, p. 1018, 2008.

[61] V. Schoenborn, I. M. Heid, C. Vollmert, A. Lingenhel, T. D. Adams, P. N. Hopkins, T. Illig, R. Zimmermann, R. Zechner, and S. C. Hunt, “The ATGL gene is associated with free fatty acids, triglycerides, and type 2 diabetes,” *Diabetes*, vol. 55, pp. 1270–1275, 2006.

[62] P. J. Randle, P. B. Garland, C. N. Hales, and E. A. Newsholme, “The glucose fatty-acid cycle. Its role in insulin sensitivity and the metabolic disturbances of diabetes mellitus,” *The Lancet*, vol. 281, no. 7285, pp. 785–789, Apr. 1963.

[63] L. Hue and H. Taegtmeyer, “The Randle cycle revisited: a new head for an old hat,” *American Journal of Physiology, Endocrinology and Metabolism*, vol. 297, no. 3, pp. E578–E591, Sep. 2009.

[64] Z. Lei, D. V Huhman, and L. W. Sumner, “Mass spectrometry strategies in metabolomics,” *The Journal of Biological Chemistry*, vol. 286, no. 29, pp. 25435–25442, Jul. 2011.

[65] J. J. Ramsden, “Metabolomics and metabonomics,” in *Bioinformatics: An Introduction*, Springer, 2004, pp. 221–226.

[66] L. Pauling, A. B. Robinson, R. O. Y. Teranishit, and P. Cary, “Quantitative analysis of urine vapor and breath by gas-liquid partition chromatography,” *Proceedings of the National Academy of Sciences*, vol. 68, no. 10, pp. 2374–2376, 1971.

[67] K. Dettmer, P. A. Aronov, and B. D. Hammock, “Mass spectrometry - based metabolomics,” *Mass Spectrometry Reviews*, vol. 26, no. 1, pp. 51–78, 2007.

[68] E. J. Want, A. Nordström, H. Morita, and G. Siuzdak, “From exogenous to endogenous: The inevitable imprint of mass spectrometry in metabolomics,” *Journal of Proteome Research*, vol. 6, no. 2, pp. 459–468, Feb. 2007.

[69] J. L. Griffin, “Understanding mouse models of disease through metabolomics,” *Current Opinion in Chemical Biology*, vol. 10, no. 4, pp. 309–315, Aug. 2006.

[70] D. S. Wishart, D. Tzur, C. Knox, R. Eisner, A. C. Guo, N. Young, D. Cheng, K. Jewell, D. Arndt, S. Sawhney, C. Fung, L. Nikolai, M. Lewis, M.-A. Coutouly, I. Forsythe, P. Tang, S. Shrivastava, K. Jeroncic, P. Stothard, G. Amegbey, D. Block, D. D. Hau, J. Wagner, J. Miniaci, M. Clements, M. Gebremedhin, N. Guo, Y. Zhang, G. E. Duggan, G. D. Macinnis, A. M. Weljie, R. Dowlatabadi, F. Bamforth, D. Clive, R. Greiner, L. Li, T. Marrie, B. D. Sykes, H. J. Vogel, and L. Querengesser, “HMDB: the human metabolome database,” *Nucleic Acids Research*, vol. 35, no. Database issue, pp. D521–D526, Jan. 2007.

[71] P. W.-N. Lee, P. N. Wahjudi, J. Xu, and V. L. Go, “Tracer-based metabolomics: concepts and practices,” *Clinical Biochemistry*, vol. 43, pp. 1269–1277, Dec. 2010.

[72] M. Rühl, B. Rupp, K. Nöh, W. Wiechert, U. Sauer, and N. Zamboni, “Collisional fragmentation of central carbon metabolites in LC-MS/MS increases precision of ^{13}C metabolic flux analysis,” *Biotechnology and Bioengineering*, vol. 109, no. 3, pp. 763–771, Mar. 2012.

[73] A. Vella and R. a Rizza, “Application of isotopic techniques using constant specific activity or enrichment to the study of carbohydrate metabolism,” *Diabetes*, vol. 58, pp. 2168–2174, Oct. 2009.

[74] H. N. Moseley, “Correcting for the effects of natural abundance in stable isotope resolved metabolomics experiments involving ultra-high resolution mass spectrometry,” *BioMed Central Bioinformatics*, vol. 11, no. 139, Jan. 2010.

[75] I. Bang, *Ein verfahren zur Mikrobestimmung von Blutbestandteilen*. CWK Gleerup, 1913.

[76] R. Guthrie and A. Susi, “A simple phenylalanine method for detecting phenylketonuria in large populations of newborn infants,” *Pediatrics*, vol. 32, no. 3, pp. 338–343, 1963.

[77] T. N. T. Tran, P. J. De Vries, L. P. Hoang, G. T. Phan, H. Q. Le, B. Q. Tran, C. M. T. Vo, N. V Nguyen, P. A. Kager, and N. Nagelkerke, “Enzyme-linked immunoassay for dengue virus IgM and IgG antibodies in serum and filter paper blood,” *BioMed Central Infectious Diseases*, vol. 6, no. 1, p. 13, 2006.

[78] L. F. Hofman, T. P. Foley, J. J. Henry, and E. W. Naylor, “The use of filter paper-dried blood spots for thyroid-antibody screening in adults,” *Journal of Laboratory and Clinical Medicine*, vol. 144, no. 6, pp. 307–312, 2004.

[79] I. Lewensohn-Fuchs, P. Osterwall, M. Forsgren, and G. Malm, “Detection of herpes simplex virus DNA in dried blood spots making a retrospective diagnosis possible,” *Journal of clinical virology: the official publication of the Pan American Society for Clinical Virology*, vol. 26, no. 1, p. 39, 2003.

[80] W. Stevens, L. Erasmus, M. Moloi, T. Taleng, and S. Sarang, “Performance of a novel human immunodeficiency virus (HIV) type 1 total nucleic acid-based real-time PCR assay using whole blood and dried

blood spots for diagnosis of HIV in infants," *Journal of Clinical Microbiology*, vol. 46, no. 12, pp. 3941–3945, 2008.

[81] T. W. McDade, S. Williams, and J. J. Snodgrass, "What a drop can do: dried blood spots as a minimally invasive method for integrating biomarkers into population-based research," *Demography*, vol. 44, no. 4, pp. 899–925, Nov. 2007.

[82] B. G. Keevil, "The analysis of dried blood spot samples using liquid chromatography tandem mass spectrometry," *Clinical Biochemistry*, vol. 44, no. 1, pp. 110–8, Jan. 2011.

[83] T. C. Dainty, E. S. Richmond, I. Davies, and M. P. Blackwell, "Dried blood spot bioanalysis: an evaluation of techniques and opportunities for reduction and refinement in mouse and juvenile rat toxicokinetic studies," *International Journal of Toxicology*, vol. 31, no. 1, pp. 4–13, 2012.

[84] W. Li and F. L. S. Tse, "Dried blood spot sampling in combination with LC-MS/MS for quantitative analysis of small molecules," *Biomedical Chromatography*, vol. 24, no. 1, pp. 49–65, Jan. 2010.

[85] K. Diehl, R. Hull, D. Morton, R. Pfister, Y. Rabemampianina, D. Smith, J. Vidal, and C. Van De Vorstenbosch, "A good practice guide to the administration of substances and removal of blood, including routes and volumes," *Journal of Applied Toxicology*, vol. 21, no. 1, pp. 15–23, 2001.

[86] D. Brooks, P. Black, M. Arcangeli, T. Aoki, and D. Wilmore, "The heated dorsal hand vein: an alternative arterial sampling site," *Journal of Parenteral and Enteral Nutrition*, vol. 13, no. 1, pp. 102–105, Jan. 1989.

[87] N. Abumrad, D. Rabin, M. Diamond, and W. Lacy, "Use of a heated superficial hand vein as an alternative site for the measurement of amino acid concentrations and for the study of glucose and alanine kinetics in man," *Metabolism*, vol. 30, no. 9, pp. 936–940, 1981.

[88] T. S. McIntosh, H. M. Davis, and D. E. Matthews, "A liquid chromatography-mass spectrometry method to measure stable isotopic tracer enrichments of glycerol and glucose in human serum," *Analytical Biochemistry*, vol. 300, no. 2, pp. 163–169, Jan. 2002.

[89] R. E. Ardrey, *Liquid chromatography-mass spectrometry: An introduction*. 2003.

[90] W. Niessen and A. Tinke, "Liquid chromatography-mass spectrometry - General principles and instrumentation," *Journal of Chromatography A*, vol. 703, pp. 37–57, 1995.

[91] W. M. A. Niessen, "Progress in liquid chromatography-mass spectrometry instrumentation and its impact on high-throughput screening," *Journal of Chromatography A*, vol. 1000, pp. 413–436, Jun. 2003.

[92] C. Herbert and R. Johnstone, *Mass spectrometry basics*. 2002.

[93] L. Anderson, "Quantitative mass spectrometric multiple reaction monitoring assays for major plasma proteins," *Molecular & Cellular Proteomics*, vol. 5, pp. 573–588, 2006.

[94] N. R. Kitteringham, R. E. Jenkins, C. S. Lane, V. L. Elliott, and B. K. Park, "Multiple reaction monitoring for quantitative biomarker analysis in proteomics and metabolomics," *Journal of Chromatography B*, vol. 877, pp. 1229–1239, May 2009.

[95] J. Gross, *Mass spectrometry: a textbook*. 2004.

[96] M. Katajamaa and M. Oresic, "Data processing for mass spectrometry-based metabolomics," *Journal of Chromatography A*, vol. 1158, no. 1–2, pp. 318–328, Jul. 2007.

[97] F. T. Peters, O. H. Drummer, and F. Musshoff, "Validation of new methods," *Forensic Science International*, vol. 165, pp. 216–224, Jan. 2007.

[98] S. M. R. Wille, F. T. Peters, V. Fazio, and N. Samyn, “Practical aspects concerning validation and quality control for forensic and clinical bioanalytical quantitative methods,” *Accreditation and Quality Assurance*, vol. 16, pp. 279–292, Apr. 2011.

[99] US Food and Drug Administration, “Guidance for industry - Bioanalytical method validation,” no. May. pp. 1–22, 2001.

[100] W. Chai, V. Piskarev, and A. M. Lawson, “Negative-ion electrospray mass spectrometry of neutral underivatized oligosaccharides,” *Analytical Chemistry*, vol. 73, no. 3, pp. 651–657, 2001.

[101] V. F. Taylor, R. E. March, H. P. Longerich, and C. J. Stadey, “A mass spectrometric study of glucose, sucrose, and fructose using an inductively coupled plasma and electrospray ionization,” *International Journal of Mass Spectrometry*, vol. 243, no. 1, pp. 71–84, May 2005.

[102] A. Van Eeckhaut, K. Lanckmans, S. Sarre, I. Smolders, and Y. Michotte, “Validation of bioanalytical LC-MS/MS assays: evaluation of matrix effects,” *Journal of Chromatography B*, vol. 877, no. 23, pp. 2198–207, Aug. 2009.

[103] R. Houghton, C. Horro Pita, I. Ward, and R. Macarthur, “Generic approach to validation of small-molecule LC-MS/MS biomarker assays.,” *Bioanalysis*, vol. 1, no. 8, pp. 1365–74, Nov. 2009.

[104] I. Viegas, V. M. Mendes, S. Leston, I. Jarak, R. a Carvalho, M. Â. Pardal, B. Manadas, and J. G. Jones, “Analysis of glucose metabolism in farmed European sea bass (Dicentrarchus labrax L.) using deuterated water,” *Comparative Biochemistry and Physiology. Part A*, vol. 160, no. 3, pp. 341–7, Nov. 2011.

[105] L. A. Alves, J. B. Almeida, and M. Giulietti, “Solubility of D -glucose in water and ethanol / water mixtures,” *J. Chem. Eng. Data*, vol. 52, pp. 2166–2170, 2007.

[106] W. Liu, Y. Hou, W. Wu, and S. Ren, “Solubility of glucose in ionic liquid+ antisolvent mixtures,” *Industrial & Engineering Chemistry Research*, vol. 50, pp. 6952–6956, 2011.

[107] H. S. Kim, R. Pani, S. H. Ha, Y.-M. Koo, and Y. G. Yingling, “The role of hydrogen bonding in water-mediated glucose solubility in ionic liquids,” *Journal of Molecular Liquids*, vol. 166, pp. 25–30, Feb. 2012.

[108] L. Kupiainen, J. Ahola, and J. Tanskanen, “Kinetics of glucose decomposition in formic acid,” *Chemical Engineering Research and Design*, vol. 89, pp. 2706–2713, Dec. 2011.

[109] T. H. van Dijk, T. S. Boer, R. Havinga, F. Stellaard, F. Kuipers, and D.-J. Reijngoud, “Quantification of hepatic carbohydrate metabolism in conscious mice using serial blood and urine spots,” *Analytical Biochemistry*, vol. 322, no. 1, pp. 1–13, Nov. 2003.

[110] Z. Gong, G. Tian, Q. Huang, Y. Wang, and Q. Ge, “Quantification of total hexose on dry blood spot by tandem mass spectrometry,” *Clinical Biochemistry*, vol. 45, pp. 1673–1677, Dec. 2012.

[111] T. Mauriala and N. Chauret, “A strategy for identification of drug metabolites from dried blood spots using tripleâ€ quadrupole/linear ion trap hybrid mass spectrometry,” *Rapid Communications in Mass Spectrometry*, vol. 19, pp. 1984–1992, 2005.

[112] W. Buckley, S. N. Huckis, and G. K. Eigendorf, “Calculation of stable isotope enrichment for tracer kinetic procedures,” *Biological Mass Spectrometry*, vol. 12, no. 1, pp. 1–5, 1985.

[113] S. Bansal and A. DeStefano, “Key elements of bioanalytical method validation for small molecules,” *The American Association of Pharmaceutical Scientists Journal*, vol. 9, no. 1, pp. E109–E114, Jan. 2007.

[114] WADA Laboratory Commitee, “WADA Technical Document – Identification criteria for qualitative assays incorporating column chromatography and mass spectrometry.” pp. 1–9, 2010.

[115] National Association of Testing Authorities, “Guidelines for the validation and verification of quantitative and qualitative test methods,” no. August 2004. pp. 1–32, 2012.

[116] G. Shabir, “Validation of high-performance liquid chromatography methods for pharmaceutical analysis: Understanding the differences and similarities between validation requirements of the US Food and Drug Administration, the US Pharmacopeia and the International Conf,” *Journal of Chromatography A*, vol. 987, pp. 57–66, 2003.

[117] J. Miller and J. Miller, *Statistics and chemometrics for analytical chemistry*. 2005.

[118] H. Karnes, G. Shiu, and V. Shah, “Validation of bioanalytical methods,” *Pharmaceutical Research*, vol. 8, no. 4, 1991.

[119] M. Mulholland and D. B. Hibbert, “Linearity and the limitations of least squares calibration,” *Journal of Chromatography A*, vol. 762, pp. 73–82, Feb. 1997.

[120] L. Brüggemann, W. Quapp, and R. Wennrich, “Test for non-linearity concerning linear calibrated chemical measurements,” *Accreditation and Quality Assurance*, vol. 11, pp. 625–631, Oct. 2006.

[121] J. Van Loco, M. Elskens, C. Croux, and H. Beernaert, “Linearity of calibration curves: use and misuse of the correlation coefficient,” *Accreditation and Quality Assurance*, vol. 7, no. 7, pp. 281–285, Jul. 2002.

[122] J. M. Andrade and M. P. Gómez-Carracedo, “Notes on the use of Mandel’s test to check for nonlinearity in laboratory calibrations,” *Analytical Methods*, vol. 5, no. 5, p. 1145, 2013.

[123] A. M. Almeida, M. M. Castel-Branco, and A. C. Falcão, “Linear regression for calibration lines revisited: weighting schemes for bioanalytical methods,” *Journal of Chromatography B*, vol. 774, pp. 215–222, Jul. 2002.

[124] K. Danzer and L. Currie, “Guidelines for calibration in analytical chemistry-Part I. Fundamentals and single component calibration (IUPAC Recommendations 1998),” *Pure and Applied Chemistry*, vol. 70, no. 4, pp. 993–1014, 1998.

[125] C. Mansilha, A. Melo, H. Rebelo, I. M. P. L. V. O. Ferreira, O. Pinho, V. Domingues, C. Pinho, and P. Gameiro, “Quantification of endocrine disruptors and pesticides in water by gas chromatography-tandem mass spectrometry. Method validation using weighted linear regression schemes,” *Journal of Chromatography A*, vol. 1217, no. 43, pp. 6681–91, Oct. 2010.

[126] P. Araujo, “Key aspects of analytical method validation and linearity evaluation,” *Journal of Chromatography B*, vol. 877, pp. 2224–2234, Aug. 2009.

[127] Committee for Medical Products for Human Use, “Guideline on bioanalytical method validation,” 2012.

[128] M. Thompson, S. Ellison, and R. Wood, “Harmonized guidelines for single-laboratory validation of methods of analysis (IUPAC Technical Report),” *Pure and Applied Chemistry*, vol. 74, no. 5, pp. 835–855, 2002.

[129] M. Natrella, “NIST/SEMATECH e-handbook of statistical methods,” *http://www.itl.nist.gov/div898/handbook/*, 2010. .

[130] A. Maroto, J. Riu, R. Boqué, and F. X. Rius, “Estimating uncertainties of analytical results using information from the validation process,” *Analytica Chimica Acta*, vol. 391, pp. 173–185, 1999.

[131] A. Maroto, R. Boqué, J. Riu, and F. Xavier Rius, “Estimation of measurement uncertainty by using regression techniques and spiked samples,” *Analytica Chimica Acta*, vol. 446, pp. 131–143, Nov. 2001.

[132] W. Lindner and I. W. Wainer, “Requirements for initial assay validation and publication in J. Chromatography B,” *Journal of Chromatography B*, vol. 707, no. 1–2, p. 1, 1998.

[133] F. T. Peters and H. H. Maurer, “Bioanalytical method validation and its implications for forensic and clinical toxicology - A review,” *Accreditation and Quality Assurance*, vol. 7, no. 11, pp. 441–449, Nov. 2002.

[134] F. T. Peters, “Stability of analytes in biosamples - an important issue in clinical and forensic toxicology?,” *Analytical and Bioanalytical Chemistry*, vol. 388, no. 7, pp. 1505–19, Aug. 2007.

[135] N. M. Faber, “The limit of detection is not the analyte level for deciding between ‘detected’ and ‘not detected’,” *Accreditation and Quality Assurance*, vol. 13, no. 4, pp. 277–278, 2008.

[136] R. King, R. Bonfiglio, C. Fernandez-Metzler, C. Miller-Stein, and T. Olah, “Mechanistic investigation of ionization suppression in electrospray ionization,” *Journal of the American Society for Mass Spectrometry*, vol. 11, no. 11, pp. 942–950, 2000.

[137] J. L. Sterner, M. V Johnston, G. R. Nicol, and D. P. Ridge, “Signal suppression in electrospray ionization Fourier transform mass spectrometry of multi-component samples,” *Journal of Mass Spectrometry*, vol. 35, no. 3, pp. 385–391, 2000.

[138] R. Bonfiglio, R. C. King, T. V Olah, and K. Merkle, “The effects of sample preparation methods on the variability of the electrospray ionization response for model drug compounds,” *Rapid Communications in Mass Spectrometry*, vol. 13, no. 12, pp. 1175–1185, 1999.

[139] S. Wang, M. Cyronak, and E. Yang, “Does a stable isotopically labeled internal standard always correct analyte response?: A matrix effect study on a LC/MS/MS method for the determination of carvedilol enantiomers in human plasma,” *Journal of Pharmaceutical and Biomedical Analysis*, vol. 43, no. 2, pp. 701–707, 2007.

[140] World Health Organization, “Definition, diagnosis and classification of diabetes mellitus and its complications. Part 1: diagnosis and classification of diabetes mellitus. Report of a WHO Consultation,” 1998.

[141] A. J. Hoy, C. R. Bruce, S. M. Turpin, A. J. Morris, M. a Febbraio, and M. J. Watt, “Adipose triglyceride lipase-null mice are resistant to high-fat diet-induced insulin resistance despite reduced energy expenditure and ectopic lipid accumulation,” *Endocrinology*, vol. 152, no. 1, pp. 48–58, Jan. 2011.

[142] B. R. Jones, G. a Schultz, J. a Eckstein, and B. L. Ackermann, “Surrogate matrix and surrogate analyte approaches for definitive quantitation of endogenous biomolecules,” *Bioanalysis*, vol. 4, no. 19, pp. 2343–56, Oct. 2012.

[143] X. Chen, N. Iqbal, and G. Boden, “The effects of free fatty acids on gluconeogenesis and glycogenolysis in normal subjects,” *The Journal of Clinical Investigation*, vol. 103, no. 3, pp. 365–372, Feb. 1999.

[144] P. R. Haddad and P. E. Jackson, “Ion Chromatography: Principles and Applications,” in *Elsevier Science B.V.*, 2003, pp. 1–12.